Premoli Silva, I., Haggerty, J., Rack, F., et al., 1993
Proceedings of the Ocean Drilling Program, Initial Reports, Vol. 144

5. SITE 873[1]

Shipboard Scientific Party[2]

HOLE 873A

Date occupied: 7 June 1992

Date departed: 9 June 1992

Time on hole: 2 days, 16 hr, 48 min

Position: 11°53.796′N, 16°55.188′E

Bottom felt (rig floor, m; drill-pipe measurement): 1346.0

Distance between rig floor and sea level (m): 11.0

Water depth (drill-pipe measurement from sea level, m): 1335.0

Total depth (rig floor, m): 1578.3

Penetration (m): 232.3

Number of cores (including cores with no recovery): 21

Total length of cored section (m): 178.00

Total core recovered (m): 35.73

Core recovery (%): 20

Oldest sediment cored:
Depth (mbsf): 175.1
Nature: ferruginous clay and claystone
Age: Campanian or older

Hard rock:
Depth (mbsf): 232.3
Nature: Volcanic breccia with graded beds
Measured velocity (km/s): 4.4-4.5

HOLE 873B

Date occupied: 10 June 1992

Date departed: 12 June 1992

Time on hole: 11 hr, 15 min

Position: 11°53.838′N, 164°55.230′E

Bottom felt (rig floor, m; drill-pipe measurement): 1345.0

Distance between rig floor and sea level (m): 11.0

Water depth (drill-pipe measurement from sea level, m): 1334.0

Total depth (rig floor, m): 1414.0

Penetration (m): 69.00

Number of cores (including cores with no recovery): 10

Total length of cored section (m): 69.00

Total core recovered (m): 53.83

Core recovery (%): 78

Oldest sediment cored:
Depth (mbsf): 68.39
Nature: packstone, and grainstone
Age: Maastrichtian

Principal results: A local pre-site seismic survey of Wodejebato Guyot was conducted to determine the location of Site 873. The *JOIDES Resolution* approached the guyot from the southwest, and a seismic profile was shot across the entire width of the guyot. Profiling continued past the northeast flank of the guyot, and then the ship reversed direction to survey from the east-northeast. An expendable sonobuoy was deployed on the approach from the basin to the northeastern edge of the guyot; the seismic experiment was conducted in conjunction with the seismic profiling. Coring at Site 873 began on 7 June 1992 and was completed on 11 June after 4.4 days. Upon completion of the drilling, a logging program was undertaken that included the geophysical and geochemical tool strings, and the Formation MicroScanner (FMS) tool.

Site 873 (proposed Site Syl-2A) is located at 11°53.84′N, 164°55.20′E, in 1334 m water depth, on the southern central summit of Wodejebato (Sylvania) Guyot, in the Ralik Chain of the northern Marshall Islands. The objectives at this location were (1) to relate the acoustic stratigraphy of the pelagic cap to its depositional and diagenetic history; (2) to date the interface between the pelagic cap and the underlying platform; (3) to establish the characteristics of the platform carbonate facies and facies changes with time; (4) to examine the diagenesis of the platform limestones; (5) to determine the age and cause of platform drowning, and the emergence and subsidence history of the platform limestone relative to sea level; (6) to establish the age and paleolatitude of the volcanic edifice; and (7) to compare the stratigraphy and facies of Wodejebato Guyot with its living sibling Pikinni (Bikini) Atoll.

Two holes were drilled at Site 873; Hole 873B was located 100 m to the northeast of Hole 873A. Hole 873A was spudded using the rotary core barrel (RCB). After washing through the pelagic cap, cores were recovered from 54.3 to 232.3 mbsf total depth (TD). Recovery in Hole 873A averaged 20.1%. This hole was logged with the aid of the conical side entry sub (CSES). Logging ended after 36 hr. The use of the CSES was a very time-consuming operation, but it produced good logs in otherwise unsuitable hole conditions. The FMS, geophysical, and geochemical tools produced good data, with the exception of the sonic velocity log; this data was marginal as the result of hole rugosity. The recovered material included a manganese crust and a manganese-encrusted, phosphatized limestone conglomerate from 54.3 to 59.8 mbsf; platform limestones, from about 69.3 to 155.9 mbsf; clay and claystone, from 155.9 to 174 mbsf; altered basalt, from 175.1 to 204.3 mbsf, and volcanic breccia, from 204.3 to 232.2 mbsf.

The second hole (Hole 873B) was cored with the advanced hydraulic piston corer (APC) through the pelagic cap to 58 mbsf, where refusal occurred at the boundary between lower Miocene and middle Eocene sediments. This hole was deepened by the motor driven core barrel (MDCB) method to 69 mbsf in an attempt to recover the upper, poorly cemented platform sediments. Recovery of this material in Hole 873A was 2.4%. The MDCB method yielded a 39.1% recovery for the 11 m cored, although the rate of coring was six times slower than the coring rate in the same interval using the RCB in Hole 873A. Total recovery in Hole 873B averaged 78%.

The oozes in the APC cores in Hole 873B were winnowed and very soupy, similar to the sediments recovered from the pelagic cap at Limalok and Lo-En guyots (Sites 871 and 872, respectively). Excess water at the

[1] Premoli Silva, I., Haggerty, J., Rack, F., et al., 1993. *Proc. ODP, Init. Repts.,* 144: College Station, TX (Ocean Drilling Program).
[2] Shipboard Scientific Party is as given in the list of participants preceding the contents.

top of the cores was removed with a "piglet" (a small weight with a filter hole through the center) that was inserted into the core liner while the core was upright within the core barrel on the rig floor.

Six lithologic units were recognized at Site 873 using a combination of visual core descriptions, augmented with smear slide and thin section data, and downhole logging data. The age of these units was based on the identification of calcareous nannofossils and planktonic foraminifers in the pelagic cap; and larger benthic foraminifers and macrofossils in the platform limestones. The recognized units are, from top to bottom:

Unit I (0–54.0 mbsf) consists of nannofossil foraminifer ooze and foraminifer ooze of Pleistocene to early Miocene age. The average carbonate content in Unit I is >97%. Sediment composition allowed the division of Unit I into two subunits. Subunit IA (0–29.0 mbsf) is comprised of light gray nannofossil foraminifer ooze of Pleistocene to latest Miocene age; Subunit IB (29.0–54.3 mbsf) is comprised of very pale brown, mainly homogeneous foraminifer ooze with medium sand texture of middle to early Miocene age; it is well sorted and winnowed. The transition between the two subunits is marked by a disconformity spanning most of the late and late middle Miocene. Minor disconformities occur within the remainder of the middle Miocene and in the early Miocene.

Unit II (54.0–58.0 mbsf) consists of manganese-oxide-encrusted, phosphatized limestone conglomerate of middle Eocene to late Paleocene age.

Unit III (58.0–151.5 mbsf) consists of a sequence of very pale brown to gray platform carbonates of mainly Maastrichtian to possibly late Campanian age. The average carbonate content in Unit III is 98% with slightly lower values (94%) in the lower portion of the platform. The limestones in Unit III include predominantly skeletal packstone and grainstone as well as mudstone, wackestone, floatstone, and rudstone. Components include common to abundant radiolitid rudists, abundant larger foraminifers (*Asterorbis, Sulcoperculina,* and miliolids, with *Omphalocyclus* in the upper part and *Dicyclina* in the lower part), common red algae (corallinaceans and subordinate squamariaceans) and mollusk molds, and rare caprinid rudists fragments. The porosity is predominantly moldic, interparticle, and vuggy; the porosity is estimated to reach 25%–30% and rarely <10%. The majority of the carbonate platform sequence is represented in the FMS data as 0- to 30-cm alternations in resistivity, which are interpreted to be variations in grain size and cementation porosity.

Unit III is divided into two subunits on the basis of depositional texture, variations in skeletal constituents, color, and organic carbon and pyrite content. The occurrence of woody material (total organic carbon up to 2.4%) and pyrite characterize Subunit IIIB; both components decrease in abundance upward and are missing in overlying Subunit IIIA. The FMS and other logging data indicate that (1) the uppermost portion of Subunit IIIA consists of 15 m of high-porosity facies beneath the manganese crust; (2) at 118 mbsf, the contact between the gray-colored limestone of Subunit IIIB and the overlying tan-colored limestone of Subunit IIIA is a well-cemented surface coinciding with a peak in uranium concentration; and (3) the base of Subunit IIIB is a well-cemented layer that directly overlies clay at 151.5 mbsf.

Unit IV (155.9–175.1 mbsf) consists of dark red ferruginous clay to olive claystone of indeterminate age, possibly late Campanian at the top. The unit is essentially carbonate free. The upper portion of the interval has red to pinkish gray mottles, followed downward by dusky red claystone containing white veins and patches of zeolites that mimic the shape of vesicles.

Unit V (175.1–204.3 mbsf) consists of altered basalt of indeterminate age. Differentiated, olivine-poor alkali basalt and hawaiite are observed in at least eight flow units. Magnetic measurements were undertaken on a few discrete samples. The inclination obtained is positive (+17° to +27°) with some indications, to be confirmed by shore-based study, that this positive inclination represents a reversed magnetization acquired at a low latitude (~9° to 14°S) in the Southern Hemisphere. The data obtained through the downhole magnetometer supports the idea that the magnetization of the basalt is of reversed polarity with respect to the present field.

Unit VI (204.3–232.3 mbsf) consists of olive gray volcanic breccia of indeterminate age. The volcanic breccia is poorly sorted with angular to subangular clasts in a dusky red to dark gray green matrix of fine sand and clay. The matrix was originally composed of glass shards and broken fragments of glassy basalt, which are now extensively altered to clay. The volcanic breccia exhibits rare low-angle cross laminations and numerous intervals that fine upward.

BACKGROUND AND OBJECTIVES

Introduction

Wodejebato Guyot (formerly Sylvania Guyot) is located 44 km northwest of Pikinni Atoll (formerly Bikini Atoll), in the Ralik Chain in the northern Marshall Islands (Fig. 1). Wodejebato Guyot is the sibling edifice to the living atoll Pikinni; the sibling relationship is drawn on the basis of both bathymetric features sharing the same volcanic pedestal. The two edifices are connected by a volcanic ridge at a water depth of approximately 1500 m.

Operation Crossroads (Emery et al., 1954) was the first detailed geologic and geophysical investigation of the Marshall Islands area. Holes were drilled into the coralline sand islands of Pikinni Atoll as well as Anewetak Atoll. The oldest shallow-water carbonates recovered from Pikinni Atoll were early Eocene to Oligocene in age (Cole, 1954; Emery et al., 1954); no basalt was recovered in the 780-m penetration into the atoll. Schlanger (1963) predicted that the depth to volcanic basement was 1300 to 1600 m, based on a comparison between the stratigraphic formations of Anewetak and Pikinni atolls.

In the Marshall Islands area, the association of atolls with adjoining guyots is prevalent. The geologic relationship between atoll and guyot siblings has not been extensively investigated. This expedition will provide the first extensive data set to compare the Cenozoic record of Pikinni Atoll with the drowned sibling Wodejebato Guyot. This guyot is interpreted to have the typical guyot pattern of (1) pelagic cap, (2) reef rims, and (3) gullied lower slopes consisting of debris flows. The geologic interpretation of this guyot is based on dredged hauls, side-scan imagery, and seismic lines.

During the 1988 site survey cruise by the *Moana Wave* (MW8805), manganese-coated vesicular basalt, hyaloclastite, breccia, and moderately to well-lithified pelagic sediment were recovered from the talus slopes that flank Wodejebato Guyot. Planktonic foraminifers in the matrix of the breccia constrain the age of volcanism at Wodejebato Guyot to Eocene or older. In one sample, the lower Tertiary matrix contains clasts of pelagic sediment with poorly preserved Late Cretaceous planktonic foraminifers. The only identifiable species is *Globotruncana bulloides,* which is associated with the elongated species of *Heterohelix* in the absence of *Rugoglobigerina.* This association suggests that these lithoclasts are late Santonian to earliest Campanian in age. The Late Cretaceous and early Tertiary faunas are mixed at the edges of the clasts, suggesting erosion and redeposition of poorly consolidated Late Cretaceous pelagic sediment in early Tertiary time. Rounded basalt pebbles in several dredged conglomerates indicate subaerial erosion of the volcanic edifice (Lincoln et al., in press).

A dredge from the slope break on the south side of Wodejebato Guyot was successful in recovering almost 300 lb of manganese-encrusted limestones (Lincoln et al., in press). Several of these large limestone samples were coarse-grained, poorly sorted, shallow-bank deposits that contained larger foraminifers, calcareous algae, coral fragments, echinoid debris, bryozoan fragments, and molluscan debris. The larger foraminifer assemblage was dominated by *Sulcoperculina vermunti* with minor numbers of *S. obesa* and *S. globosa.* Species of *Asterorbis,* similar to *A. havanensis* and *A. cubensis,* were also abundant in these rocks. Premoli Silva (1986) assigned an age of Campanian to Maastrichtian to the Nauru Basin shallow-water fossil assemblages that contained these genera. Specimens of a primitive *Orbitoides,* possibly *O. tissoti,* were also present; the biostratigraphic range of these primitive orbitoids is from early to middle Campanian, probably slightly older than the *Sulcoperculina-Asterorbis* assemblage. Moreover, several poorly preserved shell fragments and whole specimens of radiolitids and caprinids rudists were recovered in the dredge haul. The Caprinidae contain a form (*Coalcomana* or *Caprinuloidea*) that indicates an Albian age; this age determination is also

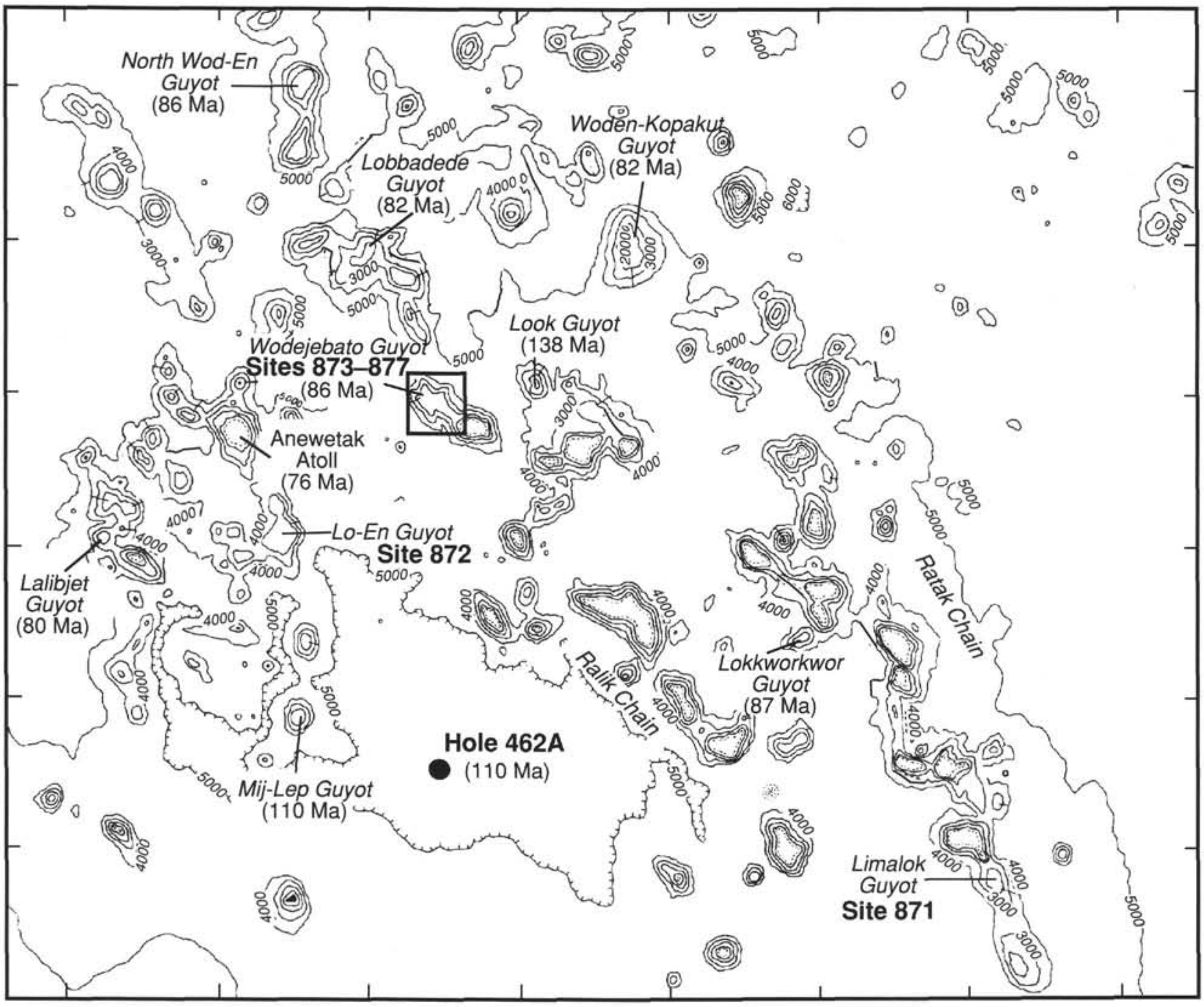

Figure 1. Bathymetry around the Marshall Islands. Contour interval is 1000 m, and the ages shown in parentheses are radiometric dates of basalts collected over a number of different surveys. Radiometric ages from Davis et al. (1989) and Pringle (1992). Figure revised from Hein et al. (1990). The location of Wodejebato Guyot and Sites 873–877 are indicated.

supported by the associated presence of the mytilid pelecypod, *Chondrodonta* (Lincoln et al., in press).

Although dredging operations on Wodejebato Guyot never recovered basalt that was suitable for radiometric dating, the fossil evidence yields a minimum age for the edifice and indicates that Wodejebato Guyot reached the photic zone before or during Aptian or early Albian time. This implies that Wodejebato Guyot underwent the same geological evolution as many other edifices in the Pacific and specifically in the Marshall Islands area. Duncan and Clague (1985) suggested that the Marshall Islands formed when the region passed over one or more hotspots during the Cretaceous. Reheating of underlying Jurassic lithosphere during this period of volcanism resulted in crustal thinning and uplift. In the Marshall region, this volcanism led to the formation and uplifting of several guyots to the photic zone apparently during mid or Late Cretaceous times. This interpretation is supported by radiometric ages of dredged basalts from other guyots in the Marshall Islands, which cluster around 110 and 82 Ma (Lincoln et al., in press). Thus, Wodejebato Guyot, an Aptian-Albian volcanic edifice, subsided along with its thermally maturing lithosphere and an Albian rudist reef complex developed on top of the edifice.

Based on the thermal subsidence model proposed by Detrick and Crough (1978), Lincoln et al. (in press) calculated that the edifice beneath Wodejebato Guyot should have subsided nearly 600 m between middle Albian and Campanian time, which is the age assigned to the sediment containing larger foraminifers. If reef growth was continuous during this time interval, Wodejebato Guyot should now be capped by at least 600 m of reef; however, the seismic profiles from Wodejebato Guyot reveal a reef cap that is <200 m thick.

SeaMARC II side-scan imagery of Wodejebato Guyot (Schlanger and Duennebier, unpubl. data, 1988) is interpreted according to the classical features of a drowned atoll: the white central pelagic cap, the black exposed reef rims, and the radial gullies formed by debris flows that cover the lower slopes. The seismic lines show that the drowned atoll is ringed by a perimeter ridge that is interpreted to be Cretaceous reef. These data are also used to suggest the presence of a thin pelagic cap, back reef, and lagoonal sediments.

A seismic line recorded during Leg 144 shows a seismic character similar to that seen on the site survey line from the *Moana Wave* cruise. These profiles illustrate the existence of two perimeter ridges along the northeastern rim of the guyot. The reflector marking the bottom of the platform shallows from a maximum of about 2.1 s two-way traveltime (TWT), along the southern flank of the guyot, to a minimum of 1.88 s TWT, near the center of the profile; it deepens again to 2.08 s TWT, beneath the perimeter ridges and the northeastern rim of the guyot.

Drilling plans for Wodejebato Guyot included two first-priority proposed sites; both sites were located on the central summit region. One proposed site (Syl-1) was planned to penetrate 50 m into basement by means of the rotary core barrel (RCB), to core through approximately 80 m of pelagic cap and 120 m of carbonate platform (interpreted as a lagoonal section). A second or possibly third hole at the site was to be dedicated to advanced hydraulic piston coring (APC) of the pelagic cap. The second proposed site (Syl-2A) was planned to double APC core approximately 90 m of pelagic cap and then to use the extended core barrel (XCB) to core across the contact into 110 m of lagoonal carbonate platform. A second-priority proposed site (Syl-4) was also listed for RCB coring 200 m of "reef" limestone along the outer perimeter ridge or upper flank of the guyot with the aid of a mini hard-rock guide base.

The original intention of scheduling pelagic cap and paired lagoonal drill sites during Leg 144 was (1) to provide material for high-resolution stratigraphic and paleoceanographic studies of Neogene to Cretaceous pelagic sections, and (2) to recover information pertaining to earlier sea-level changes based on facies changes within the shallow-water carbonate platforms.

Wodejebato Guyot was the third guyot to be drilled on Leg 144. Experience from drilling the pelagic cap at two previous guyots demonstrated that the ooze comprising these caps was not cohesive and, therefore, was very soupy. In the lagoonal section of Limalok Guyot, core recovery was only 3.5%, or exceedingly low. This low recovery in the lagoonal sections was also typical of the results from other atoll and guyot drilling during Leg 143. Because of the dramatic low recovery in the lagoonal section at Limalok Guyot, the proposal to drill two lagoonal sites on Wodejebato Guyot to obtain information about sea-level history was viewed with some skepticism.

The basic drilling objectives planned for the two proposed lagoonal sites on Wodejebato Guyot were (1) to recover pelagic sediments for high-resolution stratigraphy, (2) to document the age and duration of the carbonate platform, and (3) to recover the igneous basement. It was noted that on the seismic lines the pelagic cap is thicker at proposed Site Syl-2A than at proposed Site Syl-1. In addition, at Site Syl-2A the acoustic basement reflector is shallower than at Site Syl-1, and a deep, discontinuous reflector beneath the acoustic basement also shallows significantly. Therefore, the objectives of these two proposed sites were combined at Site 873 (near Site Syl-2A), at which the deep, discontinuous reflector is shallowest, reaching a local minimum of 2.05 s TWT.

Site 873

The specific objectives of Site 873 were (1) to relate the acoustic stratigraphy of the pelagic cap to its depositional and diagenetic history; (2) to date the interface between the pelagic cap and the underlying platform; (3) to establish the characteristics of the shallow-water facies and changes with time in the lagoonal setting; (4) to examine the diagenesis of the platform limestones; (5) to determine the age and cause of platform drowning, emergence, and subsidence history of the platform limestone relative to sea level; (6) to establish the age and paleolatitude of the volcanic edifice; (7) to study the geochemical relationships between basalts and the DUPAL/SOPITA anomaly; and (8) to compare the stratigraphy and facies of Wodejebato Guyot with its living sibling, Pikinni Atoll.

Drilling at Site 873, in the central portion of Wodejebato Guyot, recovered the pelagic cap and carbonate platform as well as the igneous edifice. The primary objectives of this site can be addressed by the preliminary shipboard studies and additional shore-based studies. Core recovery with the RCB in the upper 34 m of the platform sediments in Hole 873A was low (2.5%), and in Hole 873B, core recovery using the motor driven core barrel (MDCB) was 39.1% in the upper 11 m of the carbonate platform. This poor recovery will hamper the extent and certainty with which the sea-level history can be deciphered at this location.

OPERATIONS

Site 872 to Site 873

The *JOIDES Resolution* left Site 872 and sailed northeast to Wodejebato (Sylvania) Guyot in the Republic of the Marshall Islands; the transit speed was only about 10.3 kt as a consequence of opposing winds and currents. Speed was reduced at 2230L (L = local time) on 6 June 1992 to stream the 200-in.^{3} water gun as the vessel approached Wodejebato Guyot from the southwest. A seismic profile, shot across the entire width of the guyot, passed through proposed Sites Syl-2A, Syl-1, and Syl-4. Profiling continued past the northeast flank of the guyot, and then the ship reversed direction to survey from the east-northeast to the location of Site Syl-2A. A sonobuoy experiment was conducted over the eastern edge of the guyot. A positioning beacon was dropped on the second crossing of Site Syl-2A at 0545L on 7 June 1992. The profile continued for about 2¼ nmi before the gear was recovered and the vessel took station on the beacon. Site 873 was occupied by 0800L on 6 June 1992. Total steaming distance, including survey, was 193 nmi.

Site 873—Wodejebato Guyot

Wodejebato Guyot is the sibling feature to the emergent Pikinni (Bikini) Atoll, as they have a relationship similar to the one previously described for Lo-En Guyot and Anewetak Atoll (see "Operations" section, "Site 872" chapter, this volume). Site 873 was situated only about 22 nmi from the atoll.

Hole 873A

A higher priority RCB hole into acoustic basement was drilled first; a second hole for APC cores was then completed through the pelagic cap. No mud-line core was taken in the first hole; the depth-corrected (from Matthews tables) precision-depth-recorder (PDR) reading was 1348 m below the driller's datum, or 1337 m below sea level. The weight indicator and heave compensator indicated contact with the seafloor slightly shallower than 1348 m. At Hole 873B, the drill-pipe measurement showed the seafloor to be at 1345.0 m below the dual-elevator stool (DES) on the rig floor, or 1334 m below sea level.

The pelagic cap was drilled in about 45 min to 53.4 mbsf, where the first real resistance was encountered by the bit. The "wash" core barrel then was recovered and continuous RCB coring began. The first four cores (to 88.3 mbsf) were cut in poorly cemented limestone that crumbled upon contact with the bit. The rate of penetration (ROP) was approximately 40 m/hr, and average core recovery was 2.5% for the uppermost 34 m (Table 1). The limestone then became better indurated and recovery increased to about 16% in the denser limestone. Near 156 mbsf, the limestone gave way to 20–25 m of clay and altered volcanic material. The ROP and core recovery improved, but the first signs of hole problems also occurred.

Basalt was encountered in Core 144-873A-14R at 175 mbsf. Circulating pressure was abnormally high following retrieval of Core 144-873A-14R, indicating a partially plugged bit. The bit deplugger was attached to an inner core barrel and pumped to the bit. Normal circulating pressure was regained upon retrieval of the deplugger and coring operations continued. The bottom-hole assembly (BHA) began sticking and "packing off" after Core 144-873A-15R, and the core barrel for Core 144-873A-16R was pulled with no core recovery after some extremely slow penetration. A "wiper trip" was made up to 164 mbsf (above the clay) and then back to total depth. The hole seemed clean except for a minor bridge around 187 mbsf. As an added

Table 1. Coring summary, Site 873.

Core no.	Date (June 1992)	Time (Z)	Depth (mbsf)	Cored (m)	Recovered (m)	Recovery (%)
144-873A-						
1R	7	0155	54.3–59.8	5.5	0.20	3.6
2R	7	0245	59.8–69.3	9.5	0.04	0.4
3R	7	0345	69.3–78.7	9.4	0.15	1.6
4R	7	0435	78.7–88.3	9.6	0.40	4.2
5R	7	0545	88.3–98.0	9.7	1.03	10.6
6R	7	0710	98.0–107.6	9.6	1.15	12.0
7R	7	0820	107.6–117.3	9.7	1.90	19.6
8R	7	0950	117.3–126.9	9.6	1.49	15.5
9R	7	1100	126.9–136.6	9.7	2.33	24.0
10R	7	1220	136.6–146.2	9.6	1.30	13.5
11R	7	1410	146.2–155.9	9.7	2.31	23.8
12R	7	1540	155.9–165.5	9.6	5.54	57.7
13R	7	1825	165.5–175.1	9.6	6.53	68.0
14R	7	2130	175.1–177.4	2.3	0.21	9.1
15R	8	0310	177.4–184.9	7.5	0.82	10.9
16R	8	0520	184.9–193.8	8.9	0.00	0.0
17R	8	0940	193.8–203.0	9.2	0.49	5.3
18R	8	1225	203.0–212.2	9.2	1.44	15.6
19R	8	1820	212.2–221.7	9.5	4.62	48.6
20R	8	2355	221.7–228.2	6.5	0.78	12.0
21R	9	0340	228.2–232.3	4.1	3.00	73.2
Coring totals				178.0	35.73	20.1
144-873B-						
1H	10	2325	0.0–6.5	6.5	6.59	101.0
2H	11	0005	6.5–16.0	9.5	8.30	87.3
3H	11	0055	16.0–25.5	9.5	9.92	104.0
4H	11	0130	25.5–35.0	9.5	7.96	83.8
5H	11	0155	35.0–44.5	9.5	8.70	91.6
6H	11	0230	44.5–54.0	9.5	8.05	84.7
7H	11	0355	54.0–58.0	4.0	0.01	0.3
8N	11	0610	58.0–62.5	4.5	2.17	48.2
9N	11	0810	62.5–67.0	4.5	1.05	23.3
10N	11	0945	67.0–69.0	2.0	1.08	54.0
Coring totals				69.0	53.83	78.0

precaution, in case a piece of basalt core had fouled the bit throat, support bearing, or float valve, a core breaker was pumped into place on a core barrel.

Coring resumed in basalt and volcanic breccia; the ROP occasionally fell below 1 m/hr. Core recovery varied from poor to good (Table 1); poor recovery was related to jamming of the core catcher with basalt. Coring ended on 9 June 1992 at 232.3 mbsf.

Hole 873A was logged to obtain a clearer understanding of (1) the nature of the unconformity between the pelagic cover and the underlying manganese and phosphatic hardground, (2) the thickness and characteristics of the limestone lithologic units, and (3) the downhole position of the contacts between limestone and clay and between clay and basalt. A wiper trip was made to prepare the hole for logging. The pipe was raised to the top of the limestone section at 56 mbsf and run back to total depth. No particular resistance was encountered, except for some drag beginning about 15 m off the bottom, and the presence of about 6 m of fill at total depth. The hole was swept with viscous mud and the bit was released without incident before the pipe was raised to 65 mbsf.

When the logging sheaves were rigged, the FMS tool was assembled. Last-minute checks revealed mechanical problems with the contact pad mechanism; therefore, the backup FMS tool was used for logging in Hole 873A. The tool was run to the end of the drill string, but it descended only 4 m into open hole before it came to a stop on a ledge or bridge. Repeated attempts were unsuccessful in moving the tool past the obstruction. The pipe was located high in the limestone section; therefore, it was thought that a few meters of additional pipe might allow the tool to bypass the ledge. After the logging tool was recovered, one additional joint of drill pipe was added to the string. Again the tool, which weighs only about 150 lb in water, was stopped by an impediment in the hole—this time only 1 m beyond the pipe.

With three logs to run and the condition of the hole questionable, the conical side-entry sub (CSES) was rigged so that the drill string could be used to deliver the logging tools deep into the hole. After the tool string had been recovered and the sheaves rigged down, about 4 hr was required to remove the upper guide-horn assembly, incorporate the CSES into the string, reave the logging cable through the various sheaves, and introduce the logging tool through the CSES.

The logging tool and drill string were run into the hole together, and the tool was successfully emplaced just 3 m above total depth. A successful log was recorded up from that depth to the top of the limestone section. The FMS tool was then replaced by the geophysical tool string. The heavier tool found its way past the ledges in the upper hole and reached 224 mbsf without the aid of the drill string. Another satisfactory log was recorded, but the quality of the sonic velocity log was marginal because of hole rugosity. The final log string was the geochemical combination, which came to a stop on a ledge about 45 m below the pipe. The logging tool was pulled inside the drill string, and the pipe was tripped to total depth to put the geochemical tool in position for a full log, which was then run without incident.

The full suite of logs was successful for the entire limestone and volcanic section of the hole (Table 2), but over 33 hr was devoted to the logging effort. When the CSES and logging tools were secured, the upper guide horn (UGH) was replaced and the rig was returned to tripping configuration. The BHA was on deck at 0500L, 11 June 1992, ending Hole 873A.

Hole 873B

The primary purpose of Hole 873B was to core with the APC the pelagic cap that had been bypassed by the RCB operation in Hole 873A. Because the upper 35 m of the platform limestone was poorly recovered in Hole 873A, the special subs required for the MDCB were incorporated into the APC/XCB BHA to provide the option of high-speed diamond coring in the uppermost platform limestones.

The new hole was spudded at 1015L on 11 June 1992, and recovery in the first core fixed the seafloor depth at 1345 m. Again, the foraminifer ooze was winnowed and very soupy, similar to the sediments recovered from the pelagic caps at Limalok and Lo-En guyots, Sites 871 and 872, respectively. Excess water at the top of the cores was removed with a "piglet" that was inserted into the core liner while the core was upright within the core barrel on the rig floor (see the "Operations" section, in "Site 872" chapter, this volume, for details of "piglet" usage).

Core 144-873B-7H, from 54 mbsf, indicated that the core barrel had undergone an incomplete stroke; the impact shook the rig. The impact also sheared the pin on the retrieving tool and required an extra wireline trip to replace the pin. On the second attempt, the coring winch operator was unable to engage the receiving cup of the inner barrel, apparently because the "crush bushing" was fouling the cup. Repeated attempts to "spud" the bushing to the bottom of the cup resulted in another sheared pin and a third wireline trip. The barrel was engaged and recovered, only to reveal that the impact had shattered the plastic core liner into small pieces and that the core was lost. Two small flakes of manganese crust in the core catcher confirmed that the contact with the limestone was reached.

The "shoulder" of the APC hole was drilled until the bit found limestone 4 m beyond the core point of Core 144-873B-7H. The hole was flushed with mud while the MDCB coring system was being assembled.

The MDCB was used to deepen Hole 873B in an attempt to recover the upper poorly cemented platform sediments. Recovery of this material in Hole 873A was 2.4%; the MDCB method, which was used from 58 to 69 mbsf (Cores 144-873B-8N to -10N), yielded a recovery rate of 39.1%, even though all three cores eventually jammed. The high rate of recovery did have a disadvantage; six times the length of time was needed to core the 11-m interval with the MDCB system than with the RCB.

Coring ended because of time limitations. The drill string was recovered, and at 0100L on 12 June 1992, the ship departed Site 873

Table 2. Well-log data recorded from Hole 873A.

Log type	Depth (mbsf)
Natural gamma ray	51–225
Sonic	51–225
Neutron porosity (AmBe neutron source)	51–225
Lithodensity (Ce gamma-ray source)	51–225
Resistivity	51–225
*Aluminum clay (Ca neutron source)	0–225
*Gamma-ray spectrometry	0–225
Formation MicroScanner	51–225

Notes: Log data assume that the seafloor is at 1335.0 m, with all logs correlated and depths shifted to the gamma-ray log from the geochemical tool string.
*These logs were recorded in pipe from 0 to 51 mbsf.

with seismic gear streamed for a preliminary survey to determine the position of Site 874, which lay only about 6 nmi to the north-northeast.

UNDERWAY AND SITE GEOPHYSICS

Introduction

Wodejebato Guyot lies northwest of Pikinni Atoll in the northernmost portion of the Ralik Chain in the Marshall Islands (Fig. 1). An accurate magnetic anomaly estimate of the age of the Pacific Plate beneath these edifices is not possible because this portion of the plate is part of the Jurassic Quiet Zone. Extrapolation of the magnetic anomalies identified in the southern Marshall Islands (Nakanishi et al., 1992) northwest to Wodejebato Guyot results in a plate age estimate of >160 Ma.

Early observations on the surface and subsurface structure of Pikinni Atoll and Wodejebato Guyot come from Operation Crossroads (Emery et al., 1954). The deepest of four holes drilled into the summit of Pikinni Atoll penetrated 780 m of shallow-water reef sediments of early Eocene to Oligocene age (Cole, 1954; Emery et al., 1954). None of the holes encountered basalt. Schlanger (1963), by comparing the stratigraphy of this guyot with that of Anewetak Atoll (formerly Eniwetok Atoll) to the west where volcanic basement was drilled, inferred that the basement depth of Pikinni Atoll lay between 1300 and 1600 m.

Wodejebato Guyot lies approximately 74 km northwest of Pikinni Atoll (Fig. 2). A volcanic ridge 20 km long and at a depth of ~1500 m connects the two edifices. The summit of Wodejebato Guyot is about 43 km long; it increases in width from <12 km in the southeast to >25 km in the northwest. Four lobes project from the edifice and, along with the volcanic spur attaching Wodejebato Guyot to Pikinni Atoll, give the guyot a distinct "starfish" appearance. The regional gradient divides the flanks of the guyot into a steep upper slope (~20° to 24°), which gives way to a more gently inclined lower slope (~7°). In general, the transition depth between the upper and lower slopes is around 2500 m.

Site Survey—*Moana Wave* Cruises MW8805 and MW9009

Much of the site survey work on Wodejebato Guyot was performed during a 1988 *Moana Wave* Cruise (MW8805; S.O. Schlanger and F. Duennebier, unpubl. data, 1988). Data collected during this cruise included SeaMARC II side-scan sonar images and swath map bathymetry, digital single-channel seismic records, 3.5-kHz echo-sounder profiles, gravity and magnetic measurements, and dredge samples. A 1990 *Moana Wave* cruise (MW9009) collected additional six-channel seismic data across the summit (D.D. Bergersen and W.H.F. Smith, unpubl. data, 1990). These data proved invaluable, both for interpreting the subsurface structure of Wodejebato Guyot and for selecting the lagoon and initial perimeter ridge sites. The bathymetric map in Figure 2 shows the seismic coverage across Wodejebato Guyot.

Radiometric ages of basalt samples from various guyots in the Marshall Islands illustrate the complicated history of volcanism in this area (Fig. 1). Many of the edifice ages are transposed within apparently well-defined island chains (e.g., Woden-Kopakut and Lokkworkwor guyots in the Ratak Chain; Davis et al., 1989). At present, only one episode of constructional volcanism across each edifice is recorded by these radiometric ages. Lincoln et al. (in press) used the limestones recovered from dredge hauls in the Marshall Islands to propose a more detailed history of volcanism and reef growth. One of the guyots used to construct this history was Wodejebato Guyot. Rock dredge (RD) 50 from Cruise MW8805 recovered an assemblage of mid-Cretaceous rudists in a matrix composed of Late Cretaceous shallow-water organisms. This suggests two potentially distinct periods of reef growth across Wodejebato's summit: (1) an Albian growth stage as evidenced by the rudists, and (2) a Campanian to Maastrichtian growth stage as evidenced by the larger foraminifers in the matrix. Radiometric dating of a basalt sample collected along the north flank of Wodejebato Guyot during the Mid-Pacific Expedition (Hamilton and Rex, 1959) places the latest stage of volcanism at ~86 Ma (Pringle, 1992). Thus, although the fossil assemblage in the limestone shows that this edifice existed during the mid-Cretaceous, the basalt date reveals an episode of volcanism at least ~20 m.y. later.

Bergersen (in press) analyzes in detail the surface and subsurface structure of Wodejebato Guyot using the side-scan sonar, bathymetric, and seismic data collected across this edifice. The side-scan data (Fig. 3) show a high-backscatter band inset slightly from the upper slope of the guyot (marked by high-backscatter channels). This high-backscatter band extends around the perimeter of the summit, similar to what is seen on Limalok Guyot to the southeast. Along the southern flank, a low-backscatter terrace separates the high-backscatter band from the guyot flank. Dredge samples from the slopes below and above the terrace (RD49 and RD50 from Cruise MW8805) are basalt and platform limestone, respectively. Consequently, the inner high-backscatter band represents areas where the carbonate complex capping this edifice crops out from the overlying pelagic sediments. Seismic data show that horizontal reflectors visible across the summit (presumably lagoonal sediments) truncate against a perimeter ridge present along all flanks except the south side. Along the south flank, a down-dropped block of presumed lagoonal sediments forms the terrace visible in the side-scan images (Fig. 4). Apparently, faulting and erosion may have removed the perimeter ridge along the southern flank. Along the north flank of the guyot, a second perimeter ridge lies seaward of the more continuous inner ridge (Fig. 3). This seaward or outer ridge broadens and becomes more distinct across the relatively wide and flat regions of the lobes projecting from the edifice. Dredge hauls along the slopes of these lobes recovered only basalt.

Figure 4 illustrates a seismic profile across the summit. This six-channel line was used to correlate reflectors in the single-channel profiles and to locate Site 873. A layer of pelagic sediment covers the carbonate platform; hence, the summit appears fairly featureless in the side-scan images. The pelagic sediments thin toward the edge of the summit, reaching a maximum thickness of 100 m near the center (assuming a velocity of 1550 m/s). Bergersen (in press) identified two major lagoonal sediment units. The lowermost unit (L2) is 0.16 s TWT thick and constitutes the majority of carbonate sediment deposited on this guyot. Within this unit, horizontal reflectors define subunits that onlap a basement high. Overlying the lower limestone unit are a series of closely spaced reflectors (L1), possibly representing either a sequence of diagenetic horizons or a packet of sediments deposited shortly before the carbonate complex drowned. The reflector marked "basement" in Figure 4 marks the bottom of the carbonate platform. Dredge RD49 suggests that a volcanic sequence lies below this reflector, but the "deep reflector" shown in Figure 4 suggests a potential change in the character of the basement. The basement reflector extends almost into the pelagic sediments near the center of the profile (Fig. 4) and can be traced in other profiles to represent two

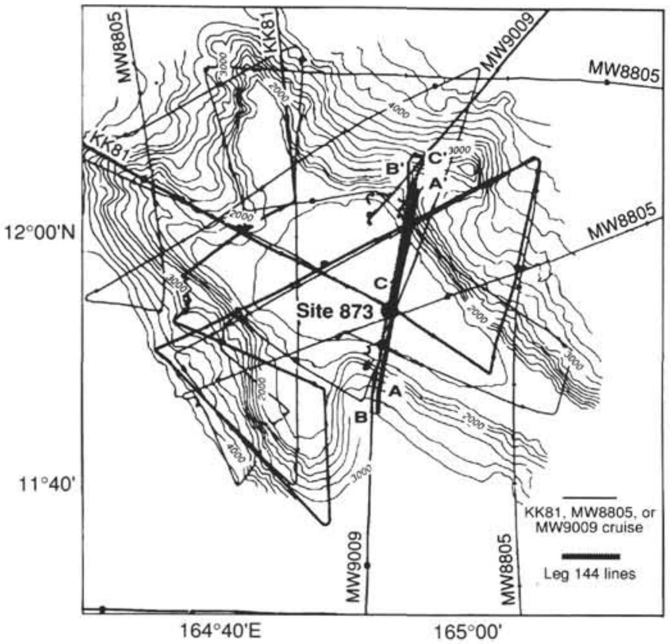

Figure 2. Contoured SeaMARC II bathymetry over Wodejebato Guyot. Contour interval is 200 m. The ship tracks shown in this figure represent the seismic coverage across this guyot. Profile A–A′ was collected during a 1990 *Moana Wave* cruise (MW9009), and Profiles B–B′ and C–C′ were collected during Leg 144.

peaks located on the northern half of the summit (Fig. 5). From the age data and geophysical information, Bergersen (in press) provided an overview of the geologic evolution of Wodejebato Guyot, proposing that much of the guyot morphology formed subsequent to the uplift associated with the Late Cretaceous volcanic event. Combining the geophysical observations with those of Lincoln et al. (in press), the proposed geologic evolution of Wodejebato Guyot included:

1. Formation of the edifice in the mid-Cretaceous, possibly in the vicinity of the MacDonald Hotspot (Lincoln et al., in press). As the underlying plate cooled and subsided away from the hotspot, a carbonate platform established itself on top of the summit. At some point in its history, the rates of subsidence and sea-level rise surpassed the rate of carbonate accumulation, and the developing atoll drowned (Lincoln et al., in press).
2. Uplift of the plate (and edifice), possibly as it passed over the Rurutu Hotspot (Lincoln et al., in press), in the Late Cretaceous, resulted in restricted volcanism across the edifice and extensive erosion of the mid-Cretaceous carbonate platform.
3. Recolonization of the existing veneer of platform sediments by a Late Cretaceous carbonate platform as the plate cooled and subsided. An acoustically massive carbonate bank rim bounded horizontally deposited lagoon sediments. The paired carbonate bank ridges along the northern flank of Wodejebato Guyot suggest that more than one reef-building episode occurred during this last stage of uplift.
4. Removal of a portion of the southern flank, including the carbonate bank ridge, after full atoll development by a large-scale submarine landslide, comparable with those observed along the Hawaiian Islands by Moore et al. (1989). Smaller scale faults continue to erode blocks of basement and lagoon sediments, one of which forms the terrace along the southern flank.

Site Survey—Leg 144

The *JOIDES Resolution* approached Wodejebato (Sylvania) Guyot from the southwest and was slowed at 2230L on 6 June to stream the geophysical gear. A magnetometer, seismic streamer, 200-in.[3] water gun, and the 3.5- and 12-kHz echo sounders were used to collect geophysical data at a ship speed of about 6 kt. A seismic profile, shot across the entire width of the summit, passed through proposed Sites Syl-2A, Syl-1, and Syl-4. Data acquisition continued past the northeast flank of the guyot, at which time the ship turned and reversed direction to survey from the east-northeast to the location of Site Syl-2A. An expendable sonobuoy was deployed on the approach from the basin to the northeastern edge of the guyot, in about 1400 m of water (Fig. 2).

The site location was chosen on the Cruise MW9009 profile, at the point where the deep reflector (as noted in Fig. 4) is shallowest. The 3.5-kHz echo-sounder record was used to monitor the thickness of the pelagic cap and the topography of the underlying platform. The seismic profiles were also monitored to identify acoustic basement and the shallowest location of the deep reflector. When the seismic character resembled that of the location chosen on the Cruise MW9009 profile, a positioning beacon was dropped. This occurred at 0552L (or 1852Z) on 7 June near the location of Site Syl-2A. The seismic profiling continued for about 4 km before the gear was recovered and the vessel took station on the beacon. Site 873 was situated only about 40 km from Pikinni Atoll.

The seismic line recorded during this survey shows a character similar to that seen on the site survey line (Figs. 4, 6, and 7). These profiles show the existence of two perimeter ridges along the northeastern rim of the guyot. The reflector marking the bottom of the platform shallows from a maximum two-way traveltime of approximately 2.10 s along the southern flank of the guyot to a minimum of 1.88 s TWT near the center of the profile and deepens again to 2.08 s TWT beneath the perimeter ridges and the northeastern rim of the guyot. The deep reflector beneath acoustic basement reaches a local minimum two-way traveltime of 2.05 s at Site 873.

The sonobuoy experiment produced a moderately strong signal, but no refractions were visible on the real time record. Preliminary processing has not significantly improved the record. Shore-based analysis of the refraction data will be necessary to produce information about the velocity structure of Wodejebato Guyot.

LITHOSTRATIGRAPHY

Lithologic units were identified by color, carbonate and clay content, fossil and particle constituents, lithification, sedimentary structures, and log characteristics. The six major lithologies identified at this site are (1) light gray to white nannofossil foraminifer ooze (Unit I: Hole 873B, 0–54.0 mbsf); (2) manganese-encrusted, phosphatized, limestone conglomerate with mixed pelagic and neritic components (Unit II: Hole 873A, 54.3–59.84 mbsf; Hole 873B, 54.0–58.14 mbsf); (3) algal-rudist-foraminifer limestone (Unit III: Hole 873A, 69.3–151.5 mbsf; Hole 873B, 58.14–68.39 mbsf); (4) ferruginous clay and claystone (Unit IV: Hole 873A, 151.5–175.1 mbsf); (5) basalt (Unit V: Hole 873A, 175.1–204.3 mbsf); and (6) volcanic breccia (Unit IV: Hole 873A, 204.3–237.7 mbsf). The lithologic units and subunits are summarized in Table 3 and Figure 8; they are also described below.

Unit I

Intervals: Core 144-873B-1H through -6H
Depth: 0–54.0 mbsf
Age: Pleistocene to early Miocene

Unit I is comprised of light gray (10YR 7/2) nannofossil foraminifer ooze that grades into very pale brown (10YR 7/3) homogeneous foraminifer ooze downhole. The carbonate content of the sediment averages 97.1% (see "Organic Geochemistry" section, this chapter). Unit I is divided into two subunits based on a decrease in the abundance of nannofossils, changes in texture (grain size and

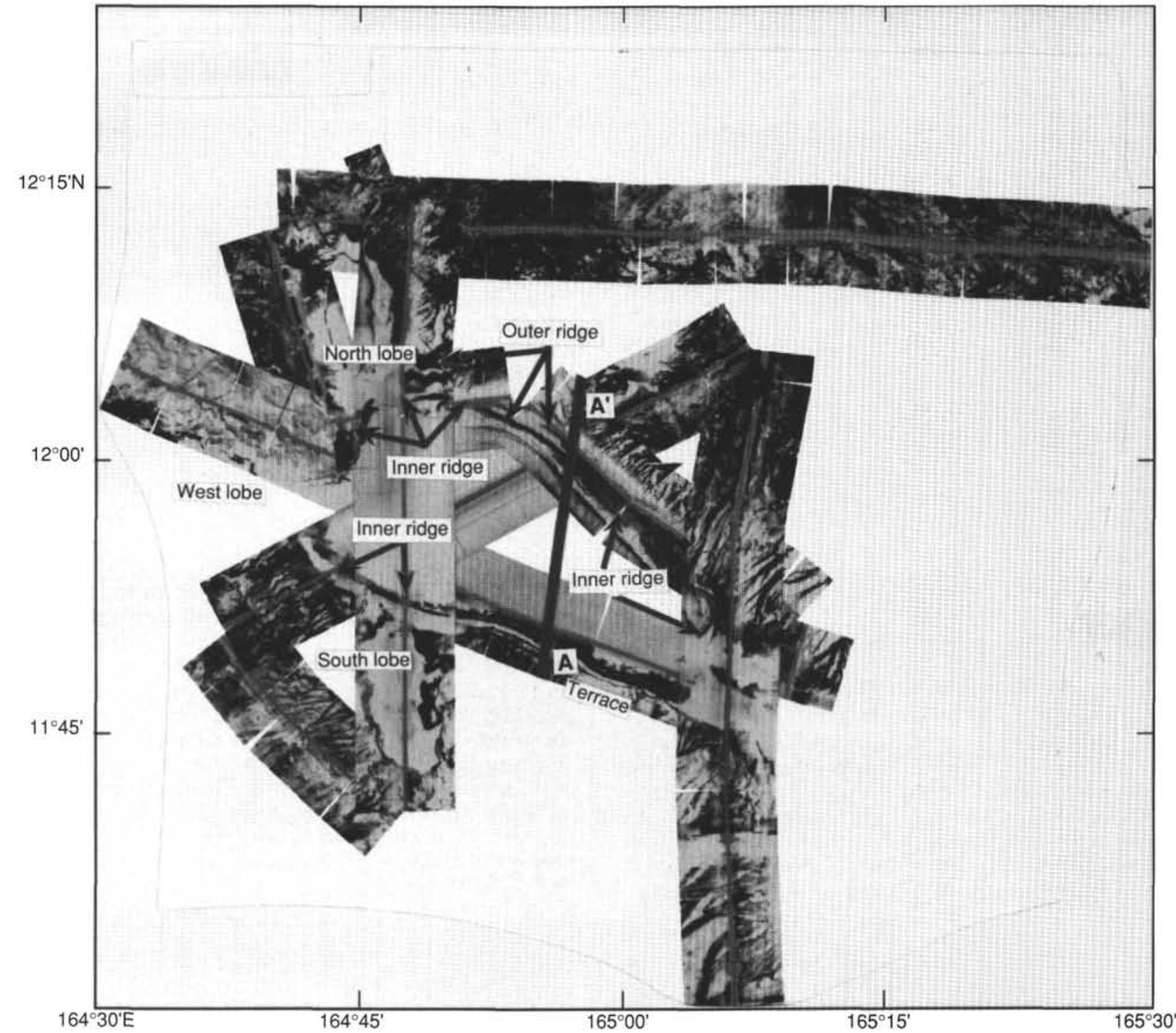

Figure 3. SeaMARC II side-scan images over Wodejebato Guyot collected on Cruise MW8805. In this image, dark tones represent high backscatter features, and light-gray to white tones represent low backscatter features. The ridge (dark band) represents areas where carbonate sediments crop out from the overlying pelagic sediments. Line A–A′ marks the location of the Cruise MW9009 six-channel profile.

sorting), and a change in the color of the sediments from light gray to very pale brown.

Subunit IA

Intervals: Core 144-873B-1H to Section 144-873B-4H-3, 82 cm
Depth: 0–29.0 mbsf
Age: Pleistocene to late Miocene

Subunit IA is a light gray (10YR 7/2) nannofossil foraminifer ooze with a fine- to medium-sand texture. Nannofossil abundance, as estimated from the smear slides, is 30%–40% in Subunit IA, with foraminifers comprising the remainder. Clay and zeolites occur in trace amounts throughout the subunit. Locally intercalated with the light gray ooze are bands of white (10YR 8/2) nannofossil foraminifer ooze. These color bands are several centimeters to tens of centimeters thick and have variably diffuse and sharp boundaries with the surrounding light gray ooze. This banding is apparent throughout Cores 144-873B-1H to -3H. Another color variation consists of gray (10YR 6/1) irregular bands and circular mottles (1–3 cm) that may be the result of burrowing. Both gray mottles and white banding are found in Intervals 144-873B-1H-1, 59–119 cm, and -3H-3, 35–100 cm, and again in Interval 144-873B-4H-1, 40–86 cm (Fig. 9); the top of this last interval is sharper than the previous two and coincides with a hiatus spanning parts of the middle and late Miocene, based on the calcareous nannofossils and planktonic foraminifers present in these samples (see "Biostratigraphy" section, this chapter). Black, sand-sized grains are both disseminated throughout Subunit IA and are concentrated in occasional vague gray bands, reaching a maximum concentration in Interval 144-873B-2H-2, 37–50 cm. These dark grains appear to be a mixture of manganese oxide micronodules and foraminifers stained by manganese and iron oxides.

Subunit IB

Interval: Section 144-873B-4H-3, 82 cm, to Core 144-873B-6H
Depth: 29.0–54.0 mbsf
Age: middle Miocene to early Miocene

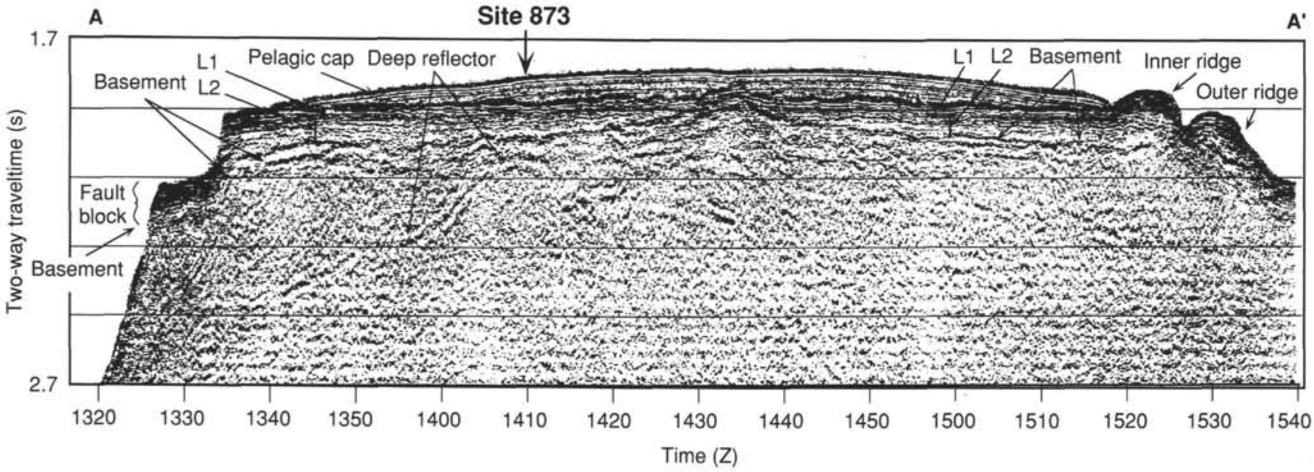

Figure 4. Migrated six-channel seismic profile (A–A′) from which Site 873 (on Wodejebato Guyot) was selected. An arrow marks the location of Site 873 directly above the local high in the deep reflector. The basement reflector (L1) marked on this profile represents the bottom of the carbonate complex. The deep reflector (L2) suggests a change in the character of the basement.

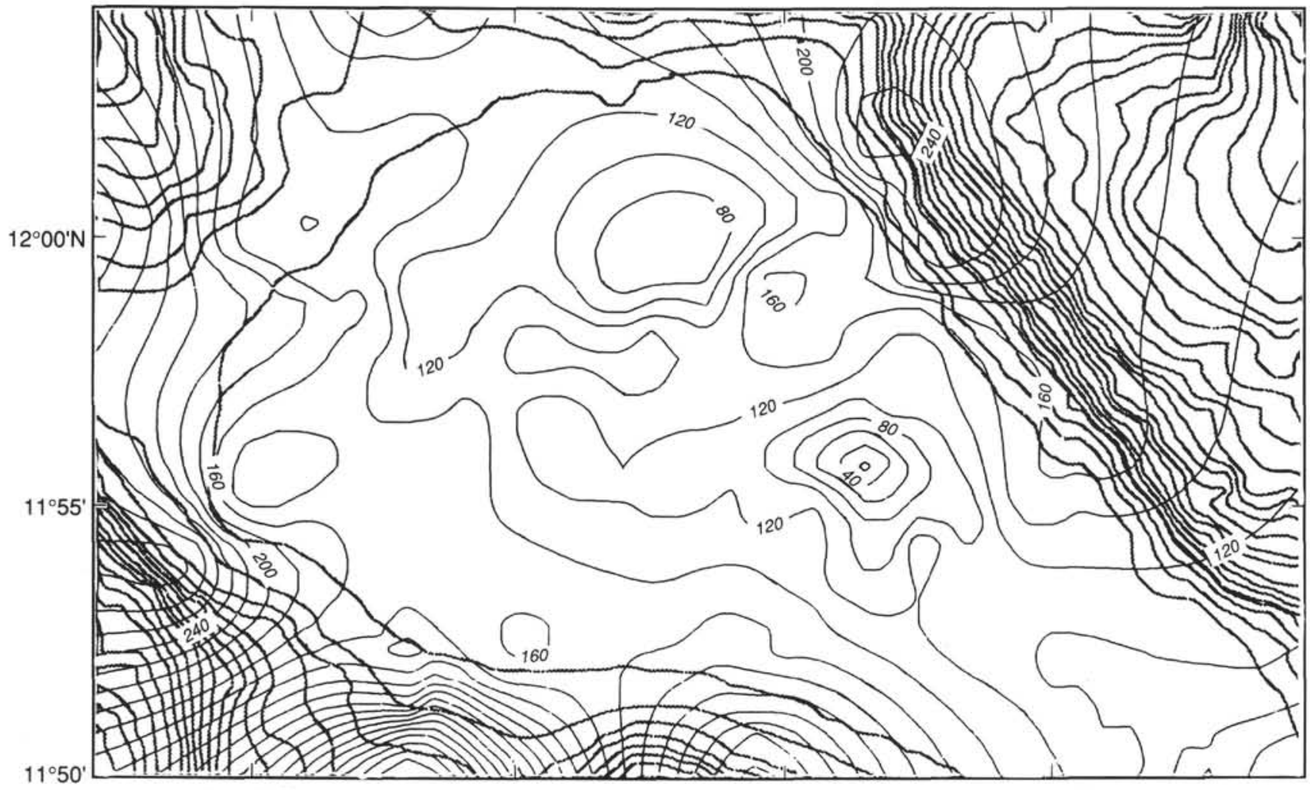

Figure 5. Isopach map of carbonate thickness on Wodejebato Guyot. As the interface between the pelagic cap and the underlying carbonate complex is essentially a horizontal reflector, changes in thickness of the carbonate sediments represent changes in the topography of the basement. Consequently, this figure is a map of basement topography. Contour intervals in meters.

Subunit IB is comprised of very pale brown (10YR 7/3), mainly homogeneous foraminifer ooze with medium-sand texture that is well sorted and winnowed. Subunit IB is dominated by planktonic foraminifers (95%); nannofossils are a very minor component (<5%) throughout most of the subunit, but they can reach abundances of up to 15% at the top of Subunit IB. The boundary between Subunits IA and IB is defined by a decrease in the abundance of nannofossils from 40% at Section 144-873B-4H-2, 70 cm, to 10% at Section 144-873B-4H-3, 110 cm, and the change in overall color from light gray to very pale brown at Section 144-873B-4H-3, 82 cm. This boundary may be gradational over at least two sections, with the first very pale brown foraminifers appearing in Section 144-873B-4H-2. There are local patches (nearly circular) and irregular bands of gray (10YR 6/1) foraminifer ooze near the top of Subunit IB (e.g., Section 144-873B-4H-4); these may be the result of bioturbation (Fig. 9). Small (0.5–1.0 cm), circular, very pale brown (10YR 8/3) mottles occur in Section

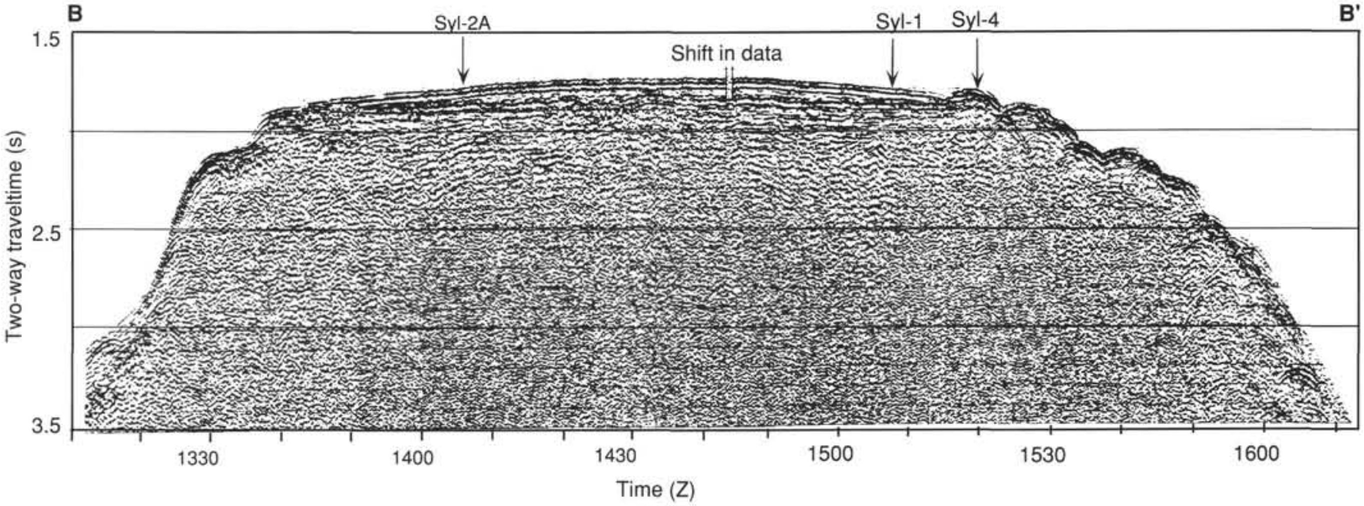

Figure 6. Single-channel seismic profile (B–B′) collected during Leg 144 across Wodejebato Guyot. Acoustic basement deepens away from the center of the summit, with a concomitant thickening of platform sediments. Profile B–B′ location shown in Figure 2; location of Site 873 is near 1408Z.

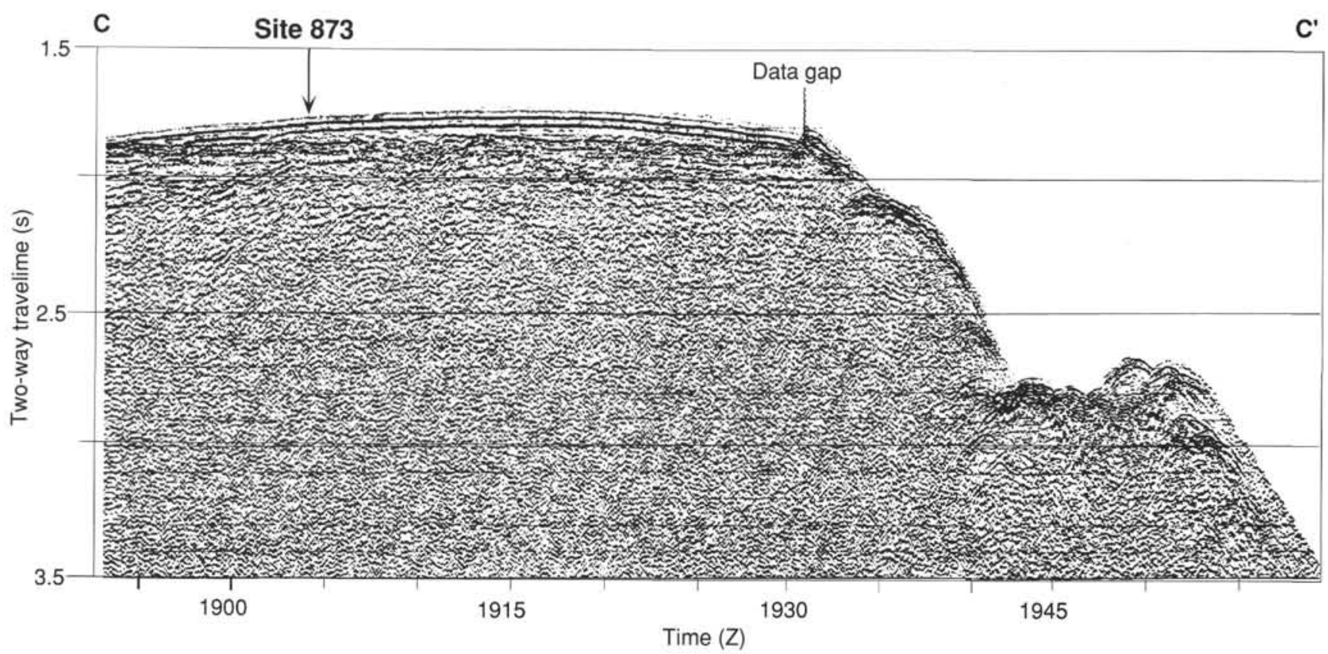

Figure 7. Single-channel seismic profile (C–C′) collected during Leg 144 on the return line to drop the beacon. Profile C–C′ location shown in Figure 2; location of Site 873 is at 1852Z.

144-873B-5H-4; these may also be evidence of bioturbation (Fig. 9). Small (fine sand-sized), black, opaque grains are dispersed throughout the lower portion of Subunit IB. The occurrence of these black grains coincides with a change in overall color of the subunit to pale brown (10YR 6/3) at Section 144-873B-6H-4, 30 cm.

Unit II

Interval: Hole 873A, Core 144-873A-1R to Interval 144-873A-2R, 0–4 cm; Hole 873B, Core 144-873B-7H to Section 144-873B-8N-1, 14 cm
Depth: Hole 873A, 54.3–59.8 mbsf; Hole 873B, 54.0–58.14 mbsf
Age: middle Eocene to late Paleocene

Unit II at Site 873 consists of a layer of rubble between Units I and III that contains manganese-coated pieces (cobble-sized and larger?) of limestone conglomerate with platform carbonate lithoclasts and large bioclasts in a pelagic limestone matrix.

In Hole 873A, Unit II is comprised of manganese-coated pieces of phosphatized limestone conglomerate with planktonic foraminifer limestone matrix (Fig. 10). Clasts within pieces of the conglomerate recovered in Cores 144-873A-1R and -2R include (1) lithoclasts (up to 1.5 cm) of skeletal grainstone with large benthic foraminifers, rudist fragments, and other platform skeletal debris; and (2) bioclasts, mainly rudist (radiolitid) fragments, as well as one shark tooth (Fig. 11). Cobbles of this unit, as well as clasts contained within the conglomerate, are coated with manganese crusts of varying thicknesses.

The outermost manganese crust on some pieces reaches 1.5 cm thick and is very spongy, with laminated fingers that enclose either pores or white planktonic foraminifer limestone. Fractures within this external manganese crust are filled with planktonic foraminifer lime-

Table 3. Lithostratigraphic summary, Site 873.

Unit/subunit	Cores	Depth (mbsf)	Age	Description
Subunit IA	144-873B-1H to -4H-3, 82 cm	0.0–29.0	Pleistocene to late Miocene?	Nannofossil foraminifer ooze.
Subunit IB	144-873B-4H-3, 82 cm, to -6H	29.0–54.0	middle Miocene to early Miocene	Foraminifer ooze.
Unit II	144-873A-1R to -2R-1, 4 cm	54.3–59.8	middle Eocene to late Paleocene	Manganese-encrusted, phosphatized, limestone conglomerate with mixed pelagic and neritic components.
	144-873B-7H to -8N-1, 14 cm	54.0–58.14		
Subunit IIIA	144-873A-3R to 8R-1, 76 cm	69.3–118.06	Maastrichtian	Very pale brown skeletal packstone and grainstone with radiolitid rudists, miliolid and large benthic foraminifers, and red algae; minor mudstone and wackestone.
	144-873B-8N-1, 14 cm, to -10N	58.14–68.39		
Subunit IIIB	144-873A-8R-1, 76 cm, to -11R	118.06–151.5	Maastrichtian to Campanian	Gray skeletal wackestone, packstone, and grainstone with abundant dasycladacean algae and pyrite.
Unit IV	144-873A-12R to -13R	151.5–175.1	Indeterminate	Ferruginous clay and claystone.
Unit V	144-873A-14R to -18R-1, 133 cm	175.1–204.33	Indeterminate	Altered basalt.
Unit VI	144-873A-18-1, 133 cm, to -21R	204.33–232.3	Indeterminate	Volcanic breccia with graded beds.

stone. At least three generations of pelagic sediments, ranging in age from the late Paleocene to the middle Eocene, have been identified (see "Biostratigraphy" section, this chapter). Some clasts within the conglomerate have manganese crusts and thin manganese "dendrites" extending into the enclosing matrix (Fig. 12). The crusts on the enclosed pebbles probably formed during reworking and before being redeposited; the dendrites probably formed after redeposition.

Powdered samples of yellow limestone from Core 144-873A-1R test positive for phosphate when mixed with HNO_3 and NH_4MoO_4. Phosphate has generally replaced the conglomerate, but locally it is selective. For example, one 10-mm lithoclast in Core 144-873A-1R is surrounded by concentric phosphate banding extending 4 mm into the matrix, yet it remains unreplaced despite a 10% moldic porosity in the lithoclast; bioclasts within the lithoclast are heavily phosphatized as well.

In Hole 873B, Unit II was recovered in two cores. Two pebbles of manganese crust were recovered in Core 144-873B-7H; these pebbles were encrusted with small patches of white pelagic chalk dated as early Miocene (see "Biostratigraphy" section, this chapter). Interval 144-873B-8N-1, 0–14 cm, consists of a mixture of planktonic foraminifer limestone and rudist skeletal grainstone that is encrusted with up to 3 cm of manganese crust comprised almost entirely of branching dendrites with finely laminated, submillimeter scale, hemispheric segments. The planktonic foraminifer limestone is cemented to manganese crusts in lenses up to 5 mm thick, in borings and interparticle pores within the rudist skeletal grainstone, and apparently intermixed with neritic components without sharp boundaries, although usually within domains that may be a kind of filling.

The thickness of Unit II was determined by the ODP convention of hanging core recovery at the top of the drilled interval. In Hole 873A, the top of the unit is based on 25-cm total recovery in Core 144-873A-1R, hung at a depth of 54.3 mbsf; the base is defined by 4-cm total recovery from Core 144-873A-2R, hung at a depth of 59.8 mbsf. The single piece recovered in the latter core could have caved from the previous drilled interval. In Hole 873B, the top of the unit is based on 2-cm-sized pieces (total recovery) from Core 144-873B-7H, hung at a depth of 54.0 mbsf; the base is defined by Interval 144-873B-8N-1, 0–14 cm (in contact with the underlying unit), recovered from 58.0–58.14 mbsf. Unit II could be as thin as 29 cm or could be significantly thicker than 4 m. Downhole logging results do not help constrain the boundaries of this unit; this differs from the logging results at Site 871 (Limalok Guyot), in which the manganese-encrusted, phosphatized surface of the carbonate platform was well defined by uranium enrichment apparent in the gamma-ray logs (see "Downhole Measurements and Seismic Stratigraphy" section, this chapter).

Unit III

Interval: Hole 873A, Cores 144-873A-3R to -11R; Hole 873B, Section 144-873B-8N-1, 14 cm, to Core 144-873B-10N
Depth: Hole 873A, 69.3–151.5 mbsf; Hole 873B, 58.14–68.39 mbsf
Age: Hole 873A, Maastrichtian to Campanian; Hole 873B, Maastrichtian

Unit III is comprised of white (10YR 8/1), very pale brown (10YR 7/3 and 10YR 8/3), and gray (e.g., 2.5Y 6/0 and 10YR 5/1) platform carbonates, 93.36 m thick. Limestones in Unit III are dominated by packstone and grainstone, but they also include mudstone, wackestone, floatstone, and rudstone. Components include abundant benthic foraminifers (mostly larger foraminifers and miliolids), common algae (e.g., corallinaceans and dasycladaceans), common molluscan molds (bivalves and gastropods), common to abundant radiolitid rudists, mostly fragmented, and rare caprinid rudist fragments. Several upward-coarsening and upward-fining intervals, 0.5–0.7 m thick, have been identified in Unit III. All cores recovered from Unit III at Site 873 are shown in Figure 13.

Two subunits are recognized in Unit III on the basis of depositional texture, variations in skeletal constituents, color, and organic-carbon and pyrite content. The two subunits are most readily distinguished on the basis of color.

Subunit IIIA

Intervals: Hole 873A, Core 144-873A-3R to Section 144-873A-8R-1, 76 cm; Hole 873B, Section 144-873B-8N-1, 14 cm, to Core 144-873B-10N
Depth: Hole 873A, 69.3–118.06 mbsf; Hole 873B, 58.14–68.39 mbsf
Age: Hole 873A, Maastrichtian; 873B, Maastrichtian

Subunit IIIA consists of 59.92 m of very pale brown (10YR 7/3) platform limestone dominated by skeletal packstone and grainstone with some intervals of wackestone. Petrographic analysis shows that benthic foraminifers are abundant and include miliolids and orbitoids. Nearly whole and fragmented radiolitid rudists are abundant throughout most of Subunit IIIA; none of the small (<3 cm) rudists are thought to be in growth position (Figs. 14–15). Other molluscan fragments (bivalve and gastropod) are abundant as molds throughout the subunit (Fig. 16). Red algae fragments and small rhodoliths are locally abundant or common. Bioturbation is evident in several intervals throughout the subunit (e.g., Interval 144-873A-6R-1, 75–79 cm; Fig. 17). Average carbonate content in Subunit IIIA is 97.9% and total-organic-carbon (TOC) content is 0.20% (see "Organic Geochemistry" section, this chapter).

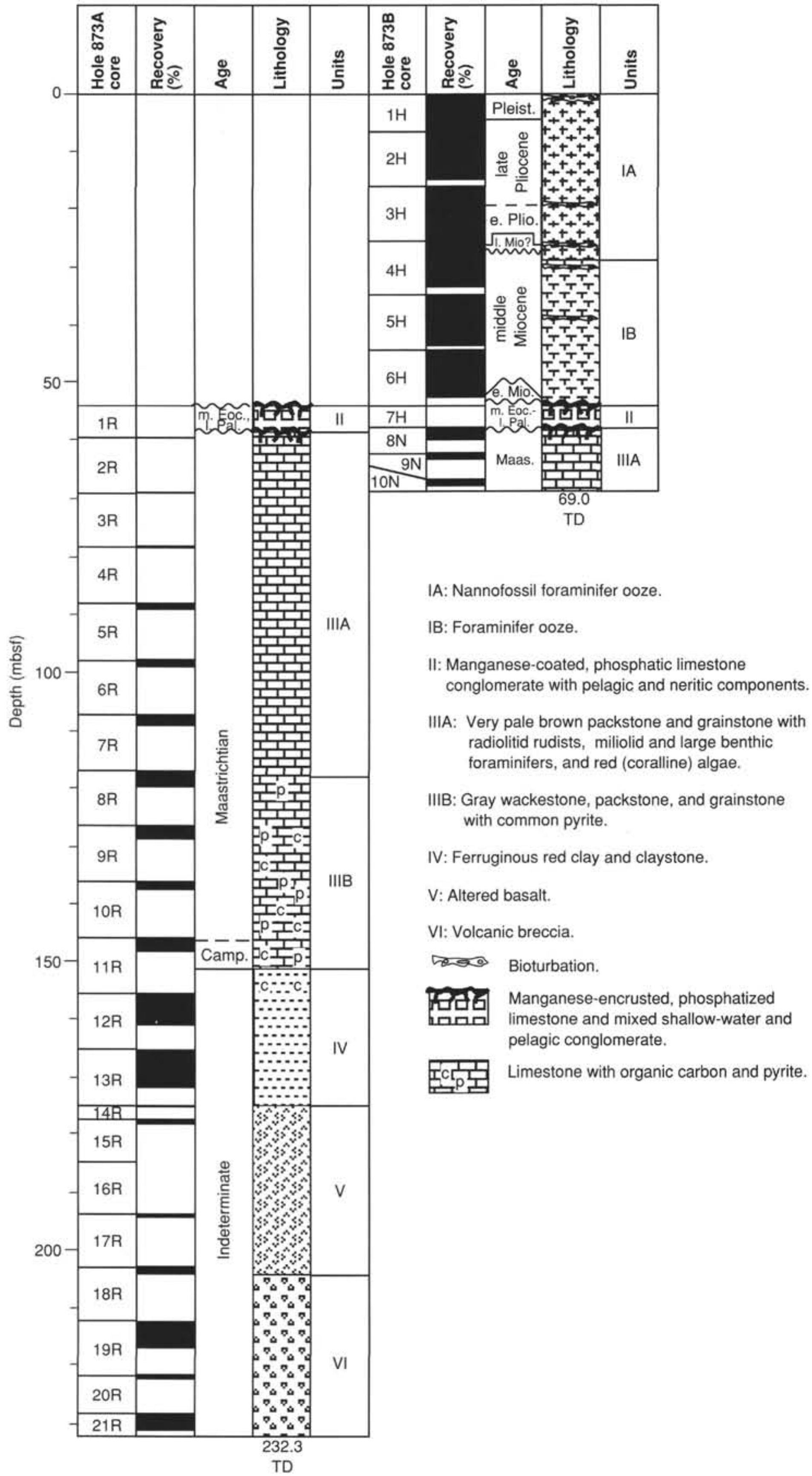

Figure 8. Lithostratigraphic summary of Site 873. TD = total depth.

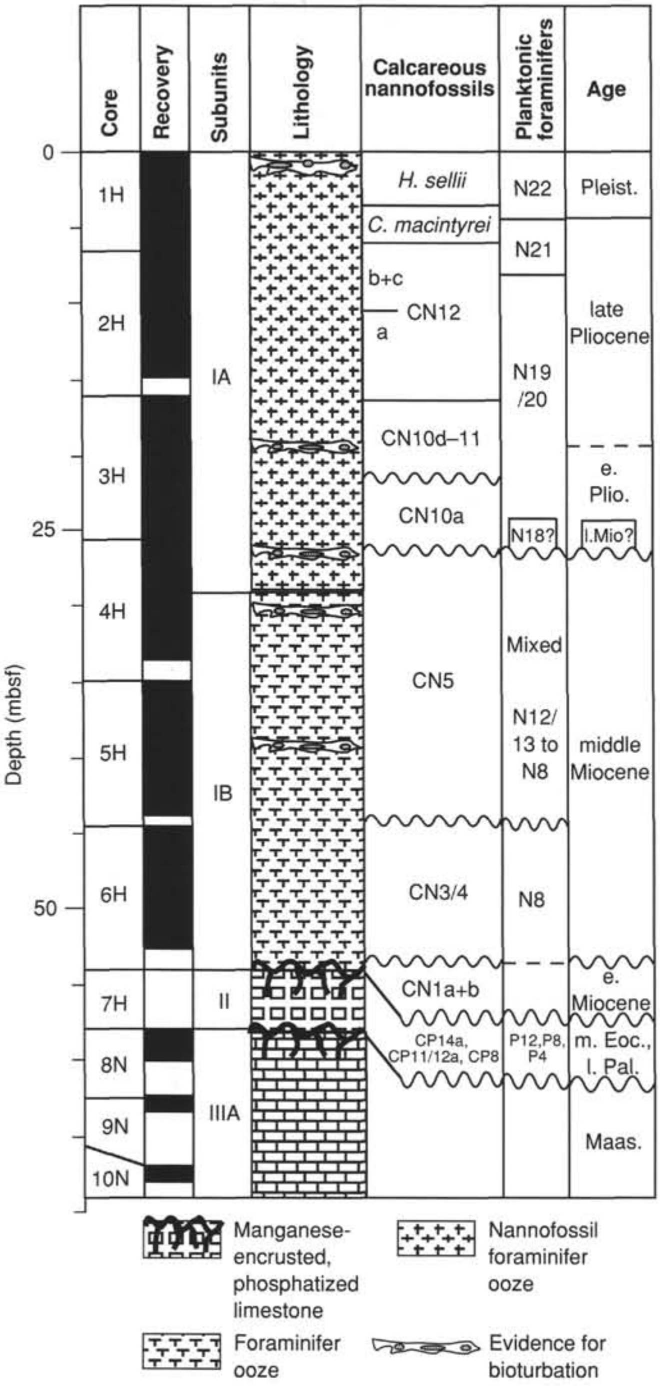

Figure 9. Detailed correlation of lithostratigraphy and biostratigraphy in the pelagic cap, Hole 873B.

Because of the overall low recovery (average 11.7% throughout the carbonate platform in Hole 873A; see "Operations" section, this chapter), we did not divide Subunit IIIA into smaller lithologic units. However, division of this subunit may be justified following shore-based studies and detailed correlation with the results of downhole logging. Significant variations in texture and composition within Subunit IIIA are discussed in detail below.

In Hole 873B, 5.23 m of algal skeletal grainstone and rudstone were recovered from between 58.14 and 69.0 mbsf (Cores 144-873B-8N through -10N). The moldic (primarily after molluscan debris), interparticle, and vuggy porosity in this interval reaches 25%–30% and rarely falls below 10% (except for some small, highly cemented patches). Most cement consists of small- to medium-crystalline, bladed, calcite crystals lining the moldic and vuggy pores; pervasive intergranular and mold-filling cements are generally absent. Although the uppermost 10–15 m of Subunit IIIA were not recovered in Hole 873A, we assume the lithologies are the same as those recovered at Hole 873B. Downhole logs from Hole 873A indicate a bulk density of only 1.5 g/cm^3 in this interval, compared with 2.1–2.2 g/cm^3 for underlying intervals (see "Downhole Measurements and Seismic Stratigraphy" section, this chapter); this result is consistent with the high porosity of Subunit IIIA in Hole 873B.

Three distinct lithologies are recognized in the 5.23 m of Subunit IIIA recovered at Hole 873B (Figs. 13 and 18):

1. Interval 144-873B-8N-1, 14–88 cm, consists of algal rudist rudstone with a skeletal grainstone matrix. Algal, coral, and rudist fragments range from 2 to 5 cm in size and the matrix is fine-sand size. Fragments of radiolitid rudist, though large, are not quite whole, nor are they in a growth position. Red algae encrust extensively, especially the radiolites, but they also occur as broken fragments and as 0.3-cm rhodoliths (Fig. 14).

2. Sections 144-873B-8N-1, 88 cm, to Section -9N-1, 135 cm, consists of a fine to very fine (1/16-1/4 mm), very pale brown (10YR 7/3 to 10YR 8/4) skeletal grainstone with pale brown (10YR 8/3), 1- to 2-cm mottles throughout. Grains are mostly well rounded and sorted. Coralline algal fragments, rudist fragments, and gastropods are few to rare in this interval. Pale brown mottles are related to increased cementation. Although these mottles are suggestive of bioturbation, no direct evidence, such as burrow linings or encrustations, was observed (Fig. 19).

3. Section 144-873B-9N-2, 9 cm, to Core 144-873B-10N consist of very pale brown to light yellowish-brown (10YR 7/3 to 10YR 6/4) algal skeletal grainstone that grades from coarse-sand-size at the base to medium-sand-size at the top of the interval. Poorly developed cross-lamination is apparent in several pieces of core within this interval (e.g., Interval 144-873B-10N-1, 112–115 cm). This facies has high moldic porosity after molluscan fragments (Fig. 20).

In Hole 873A, four beds in Subunit IIIA, 0.5–1.0 m thick, coarsen upward (Fig. 21). Interval 144-873A-5R-1, 23–78 cm, consists of white (10YR 8/2), pinkish white (7.5YR 8/2), and light gray (10YR 7/2), upward-coarsening foraminifer wackestones with conspicuous mottling at the base as a result of bioturbation (Fig. 17). Interval 144-873A-6R-1, 93–130 cm, coarsens upward from skeletal wackestone at the base to skeletal packstone at the top. Major components include gastropods, bivalves, and miliolids; the gastropods are mostly low-spired forms and the bivalves include rare radiolitid rudists. Interval 144-873A-7R-1, 0–90 cm, is a third upward-coarsening sequence that consists of fine-grained foraminifer peloid packstone at the base and bivalve-rudist packstone and grainstone near the top. Interval 144-873A-7R-1, 99–138 cm, consists of floatstone and rudstone rich in radiolitid rudists with wackestone and packstone matrix. The matrix coarsens upward through the interval; it contains miliolid foraminifers, fragments of red algae, lithoclasts, small gastropods, and coral molds. A rudist cluster of about 10 specimens, with individual diameters between 0.5 and 1.5 cm, is found in Interval 144-873A-7R-1, 106–114 cm (Fig. 15).

At the base of Subunit IIIA in Hole 873A, there are two beds, nearly 1 m thick, that fine upward (Fig. 21). Section 144-873B-7R-2 consists of upward-fining grainstone and packstone rich in radiolitid rudist, red algae (corallinacean), and bivalve fragments. Benthic foraminifers (miliolids and orbitoids) are also common. The porosity is moldic, intergranular, and locally vuggy. A second upward-fining interval is located in Interval 144-873B-8R-1, 9–76 cm. This interval consists of floatstone to rudstone, rich in rudist fragments at the base, but grading up into very-fine-sand to silt grainstones. The fine grainstones have been bioturbated.

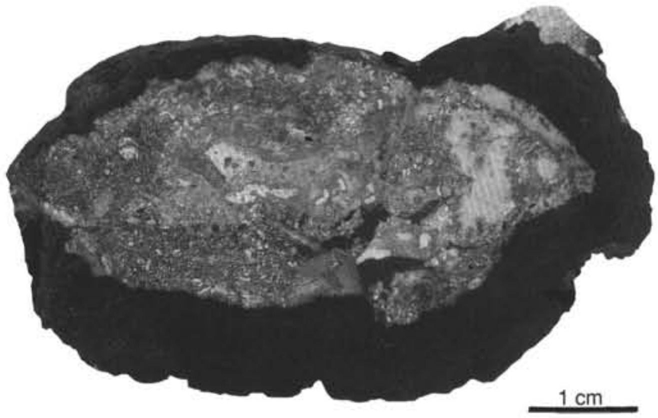

Figure 10. Close-up core photograph of manganese-encrusted, phosphatized limestone conglomerate (Interval 144-873B-2R-1, 0–4 cm).

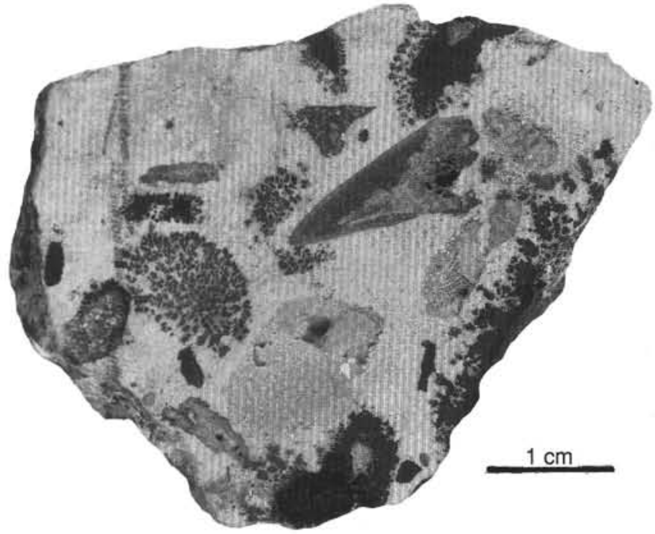

Figure 11. Close-up core photograph of manganese-encrusted, phosphatized limestone conglomerate containing a shark tooth (Interval 144-873A-1R-1, 21–25 cm).

A single 9-cm cylinder in Interval 144-873A-7R-1, 90–99 cm, consists of pale brown, coarse-grained packstone that is unlike any adjacent lithology, but which is similar to the lithology in Section 144-873A-7R-2 (Fig. 13). This isolated piece is a reminder that, because of the low recovery, it is probable that some of the upward-coarsening and upward-fining intervals identified in core recovered from Hole 873A may not consist of continuous recovery but, rather, could be samples from two or three distinct facies that appear gradational. Nearly all of the upward-fining and upward-coarsening intervals identified in Figure 21 also correspond with changes to either open-marine fauna (high diversity) or more restricted marine faunas (low diversity) (see "Biostratigraphy" section, this chapter).

Subunit IIIB

Interval: Sections 144-873A-8R-1, 76 cm, to Core 144-873A-11R
Depth: 118.06–151.5 mbsf
Age: Maastrichtian to Campanian

Subunit IIIB consists of mainly gray wackestone, packstone, and grainstone. The most distinctive features of Subunit IIIB are its light gray to gray color, abundance of disseminated pyrite, pyritization of many constituent grains, and locally abundant woody organic debris (average TOC content is 0.43%, up to 3% locally; see "Organic Chemistry" section, this chapter). The gray to black color is related to pyrite content and indicates either depositional or postdepositional sulfate reduction. The most distinctive faunal changes from Subunit IIIA to Subunit IIIB are the decreased overall diversity and the increased abundance of dasycladacean algae. Rare, poorly preserved, caprinid rudist fragments are also present in Subunit IIIB. As is the case with Subunit IIIA, several distinctive facies changes and gradations can be recognized within Subunit IIIB; these are shown in Figure 22 and are discussed below.

The top of Subunit IIIB (Sections 144-873B-8R-1, 76 cm, to -8R-2, 23 cm; Fig. 23) consists of mostly light gray to gray mudstone, wackestone, and packstone with common miliolids, bivalve fragments (few rudist fragments), gastropod molds, dasycladacean algae (often as molds), and numerous gray to black, pellet-shaped and subangular grains; many of the shell fragments are blackened. Several of the fine-grained rocks have brown flakes deposited in thin laminae. Pyrite is common as disseminated grains and as partial or complete replacement of components, especially foraminifers.

Two intervals within Subunit IIIB suggest that some of this lithology did not undergo sulfate reduction. Interval 144-873A-9R-1, 0–11 cm, consists of two pieces of very pale brown skeletal grainstone with coarse, shell-rich laminae alternating with 1-cm-thick, finer grained beds. These pieces look very much like Subunit IIIA, although they are thought to be too large to have caved from higher in the section. Interval 144-873A-10R-1, 56–64 cm (one cylinder), is a light brownish gray, fine-grained, well-sorted rudist foraminifer grainstone that appears to have a 1-cm-thick layer at the top that is more brown than gray; this may be a zone of postdepositional oxidation.

Subunit IIIB has several intervals that appear to grade upward to either finer or coarser textures (Fig. 22). The uppermost graded sequence, Interval 144-873A-9R-1, 0–98 cm, varies from gray miliolid-rich mudstone/wackestone at the base to oxidized, medium- to coarse-sand grainstones at the top (see previous paragraph). Dasycladacean algae are abundant throughout the interval; radiolitid rudist fragments and large benthic foraminifers are common. A few caprinid rudist fragments were also found in this section (e.g., Interval 144-873A-9R-1, 15–18 cm). Miliolids and gastropods increase in abundance toward the base.

The next two graded sequences fine upward in Intervals 144-873A-9R-2, 0–39 cm, and -9R-2, 39–132 cm. The first graded interval consists of a gray peloid packstone with common dasycladacean algae, common brown flakes of organic matter, few miliolids, and few larger foraminifers at the base, wackestones in the center, and mudstone with *Terquemella* packstone burrow fill at the top. The next graded interval consists of coral-gastropod rudstone at the base grading through packstone/grainstone in the middle, and then to bioturbated wackestone at the top. Caprinid shell fragments were also found at the base of this interval.

Grading trends in Cores 144-873A-10R and -11R are not as clear as others discussed above. Core 144-873A-10R consists of bivalve foraminifer wackestones at the base, which may grade up into rudist foraminifer grainstones at the top. In this core, some alternation occurs between fine and very fine bivalve algal packstone and coarser rudist foraminifer grainstone. Section 144-873A-11R-1, 0–97 cm, consists of skeletal grainstones that grade upward to a maximum coarseness (coarse sand) between 21 and 34 cm. This coarse interval is then overlain by medium-sand bivalve foraminifer grainstones; it is not clear whether this interval coarsens upward and then fines, or whether we have sampled more than one trend within the drilled interval. The lowermost graded interval is in Interval 144-873A-11R-2, 79–146 cm, in which coarse peloidal grainstones with fecal pellets, red algae, larger foraminifers, miliolids, molluscan fragments, and echinoderm debris grade upward into finer peloidal grainstones with molluscan debris (including radiolitid and caprinid rudists), gastro-

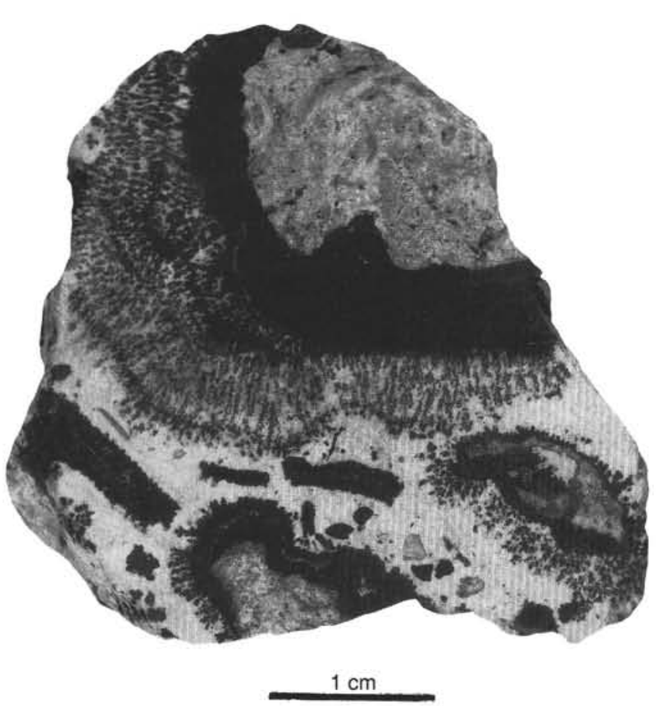

Figure 12. Close-up core photograph of manganese dendrites growing into pelagic limestone matrix that contains manganese-encrusted platform limestone clasts (Interval 144-873A-1R-1, 16–21 cm).

pods, benthic foraminifers, encrusting foraminifers, and encrusting red algae.

Sections 144-873A-11R-1, 97 cm, to -11R-2, 23 cm, contain packstone and grainstone in which black to brown flakes of organic matter are abundant. In several pieces within this interval, patches of carbonate-rich material are enclosed by wispy patches of organic-rich material (Fig. 24). In addition, the carbonate-rich patches contain fragments of organic matter. Pyrite is abundant in several pieces. Analyses of TOC content within this interval range from 1.26% to 2.44% (see "Organic Geochemistry" section, this chapter). The base of this organic-rich interval is a dark gray, pyrite-rich clayey chalk that is only 65.7% $CaCO_3$ by weight; smear slide visual estimates indicate that 40% of the grains may be clay. Nannofossils in this clay provide a Campanian age (see "Biostratigraphy" section, this chapter).

The base of Subunit IIIB consists of rhodolith packstone (Interval 144-873A-11R-2, 140–146 cm) and a well-cemented peloidal grainstone cobble embedded in red clays at the top of Section 144-873A-12R-1. The rhodoliths are nucleated on corals. The grainstone consists of well-sorted, well-rounded grains that may have been fecal pellets; most are now coated with micrite and have been replaced. One radiolitid fragment and a 2-mm rhodolith were found in the grainstone. It is not entirely certain whether this grainstone is the basal limestone in Subunit IIIB or whether it was caved from some higher interval. Results from the FMS indicate that a 20-cm bed with high resistivity lies immediately above the clays; high resistivity is consistent with the near-zero porosity of the grainstone (see "Downhole Measurements and Seismic Stratigraphy" section, this chapter).

Unit IV

Interval: Core 144-873A-12R to Core 144-873A-14R
Depth: 151.5–175.1 mbsf
Age: indeterminate

Unit IV consists of 19.2 m of ferruginous clay and claystone first recovered at the top of Section 144-873A-12R from a depth of 155.6 m. The top of Unit IV is recorded in the downhole logs at a depth of 151.5 mbsf as a sharp increase in thorium and aluminum, a sharp decrease in resistivity, and a sudden increase in borehole diameter. No evidence is present of a gradational contact with the overlying limestones: gamma and chemical logs do not show gradually increasing thorium or aluminum levels that might be expected if clay were reworked into the overlying limestone (see "Downhole Measurements and Seismic Stratigraphy" section, this chapter). Based on these logging results, we place the top of Unit IV at 151.5 mbsf.

From Sections 144-873A-12R-1, 0 cm, to -12R-2, 23 cm, Unit IV is a dark red (10R 3/6) ferruginous clay. The unit becomes olive (5Y 5/4) with dark red (10R 3/4), pale red (10R 6/4), and pinkish gray (5YR 7/2) mottles in Interval 144-873A-12R-2, 23–88 cm; the red clay is soft and the olive is more indurated (claystone). Beneath this interval, Unit IV has a marbled appearance that looks like anastomosing veins separating distinct, indurated blocks of claystone (Fig. 25). The blocks are generally weak red (10R 4/4) and the "veins" are dusky red (10R 3/4). This fractured claystone continues until Section 144-873A-13R-2, 100 cm. Beneath the fractured claystone interval, white patches of zeolites are common to few; these patches are in the shape of vesicles and may reflect the original texture of highly altered basalt (Fig. 26). One interval within the unit (Interval 144-873A-13R-3, 97–120 cm) might be more appropriately described as highly altered basalt rather than as claystone, based on degree of induration and apparent remnant fabric.

Unit V

Interval: Core 144-873A-15R to Section 144-873A-18R-1, 133 cm
Depth: 175.1–204.33 mbsf
Age: indeterminate

Unit V consists of altered alkalic basalt that is discussed in the "Igneous Petrology" section (this chapter).

Unit VI

Interval: Section 144-873A-18R-1, 133 cm, to Core 144-873A-21R
Depth: 204.33–232.3 mbsf
Age: indeterminate

Unit VI is comprised of poorly sorted, olive gray (5Y 5/2) volcanic breccia (Fig. 27) with angular to subangular clasts (from several millimeters to 1.5 cm in diameter) in a fine-sand to clay size matrix that is dusky red (10R 3/4) and of indeterminate composition in Sections 144-873B-19R-1, 0 cm, to -19R-3, 68 cm. Below this depth, the matrix is dark gray green (10Y 4/1). Numerous intervals throughout the unit fine upward (e.g., Intervals 144-873A-19R-1, 0–29 cm, and -19R-1, 141–193 cm) and at least one displays low-angle cross laminations (Interval 144-873A-19R-1, 80–83 cm). Clasts at the base of graded beds are about 1 cm in diameter, and they fine to a few millimeters. The breccia is clast supported. Some clasts are rounded and well sorted (e.g., Interval 144-873A-19R-2, 75–95 cm); however, this is the exception rather than the rule. Several clasts appear to be highly altered, vesicular basalt (e.g., Interval 144-873A-19R-3, 0–78 cm). About 10% of the vesicles in the clasts (Interval 144-873A-19R-3, 75–101 cm) are filled by soft, white zeolites. Thin-section analyses indicate that angular, moderately well-preserved glass shards are abundant in the lower, dark gray green portion of the breccia (see "Igneous Petrology" section, this chapter).

Preliminary Interpretation of Depositional History

The depositional history of Site 873 on Wodejebato Guyot began with some form of phreatomagmatic eruption relatively close to the drill site; this eruption was the source for the relatively well-preserved

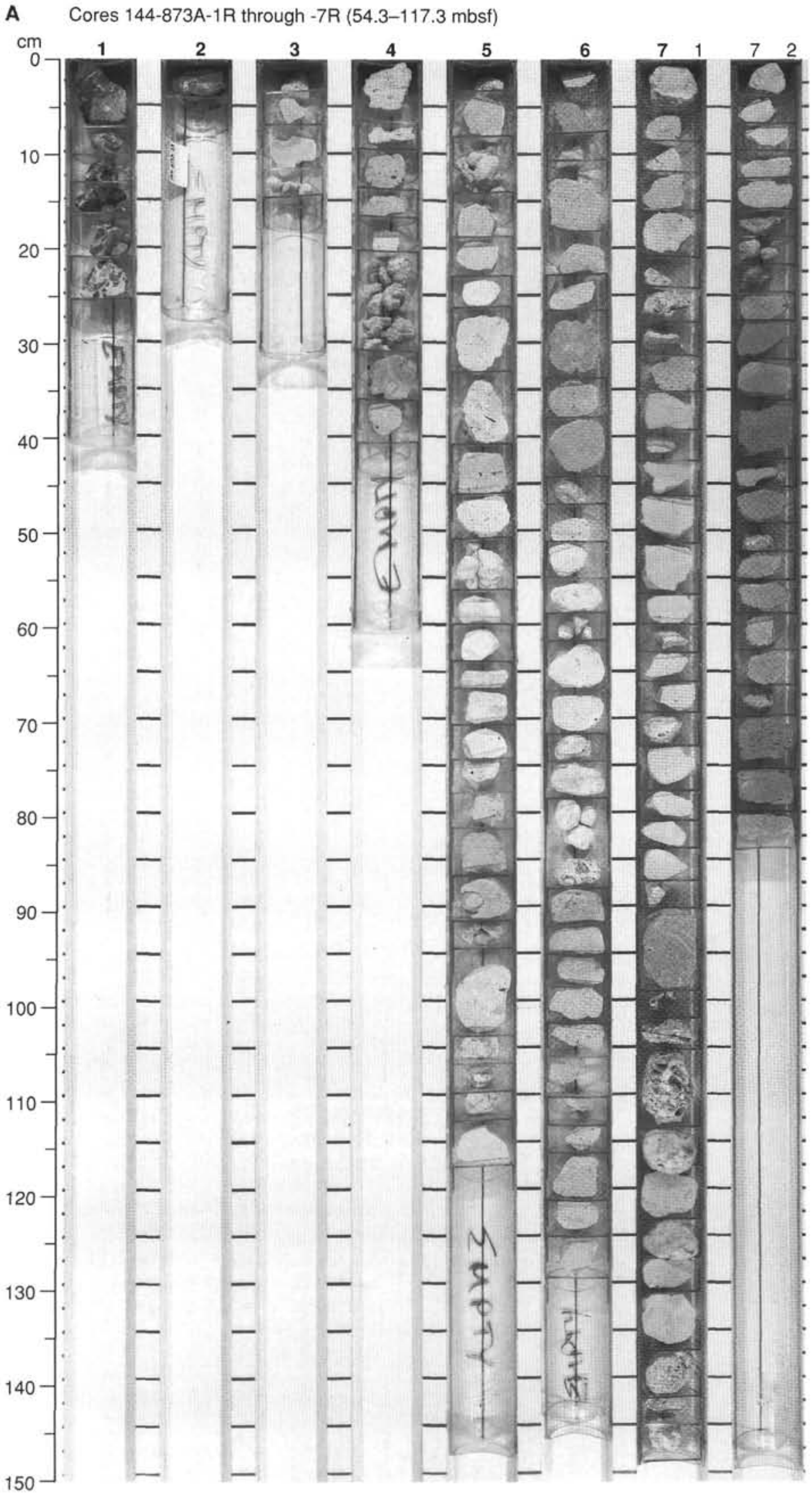

Figure 13. Composite photographs of Unit III from Holes 873A (**A** and **B**) and 873B (**C**).

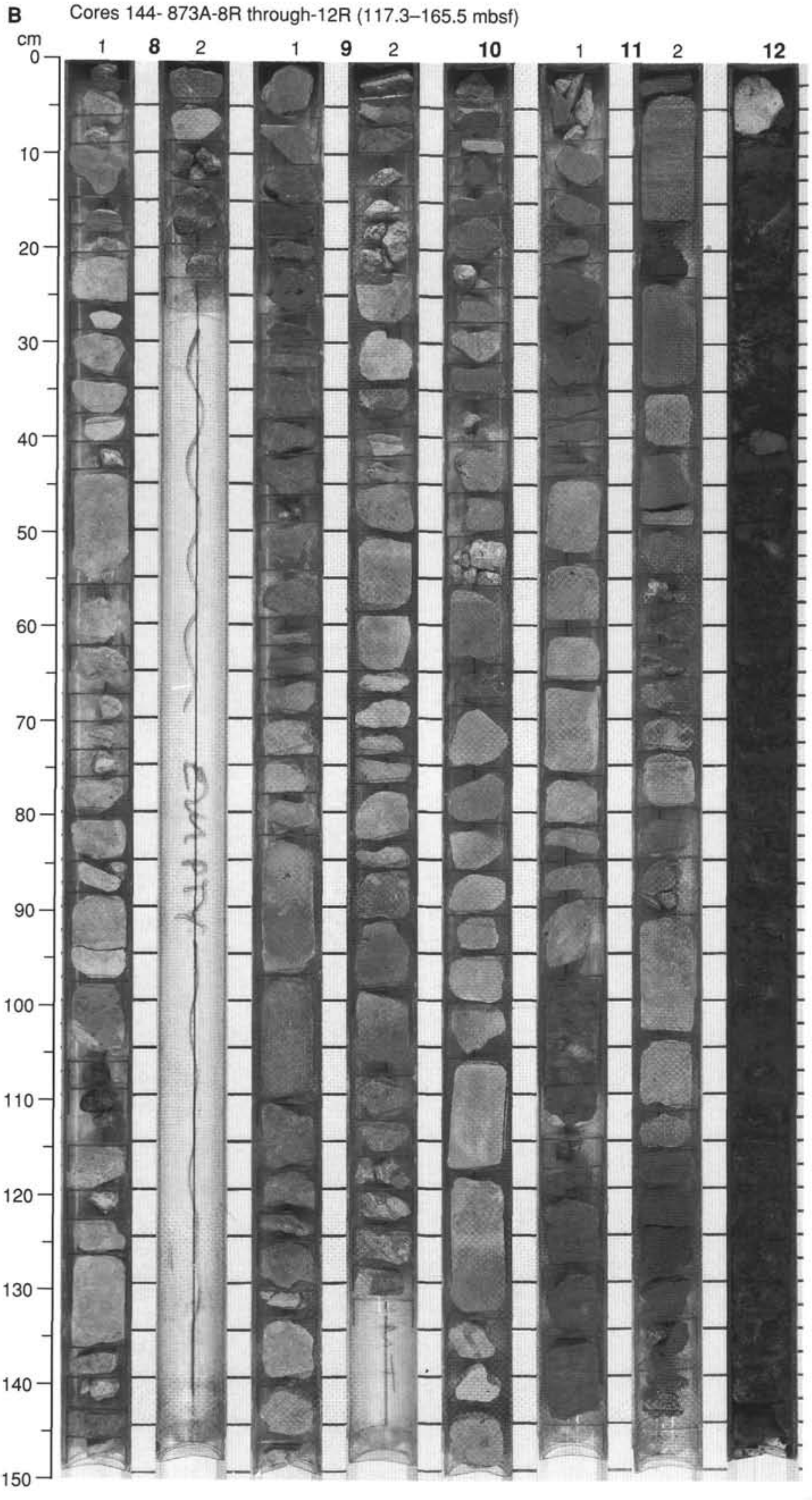

Figure 13 (continued).

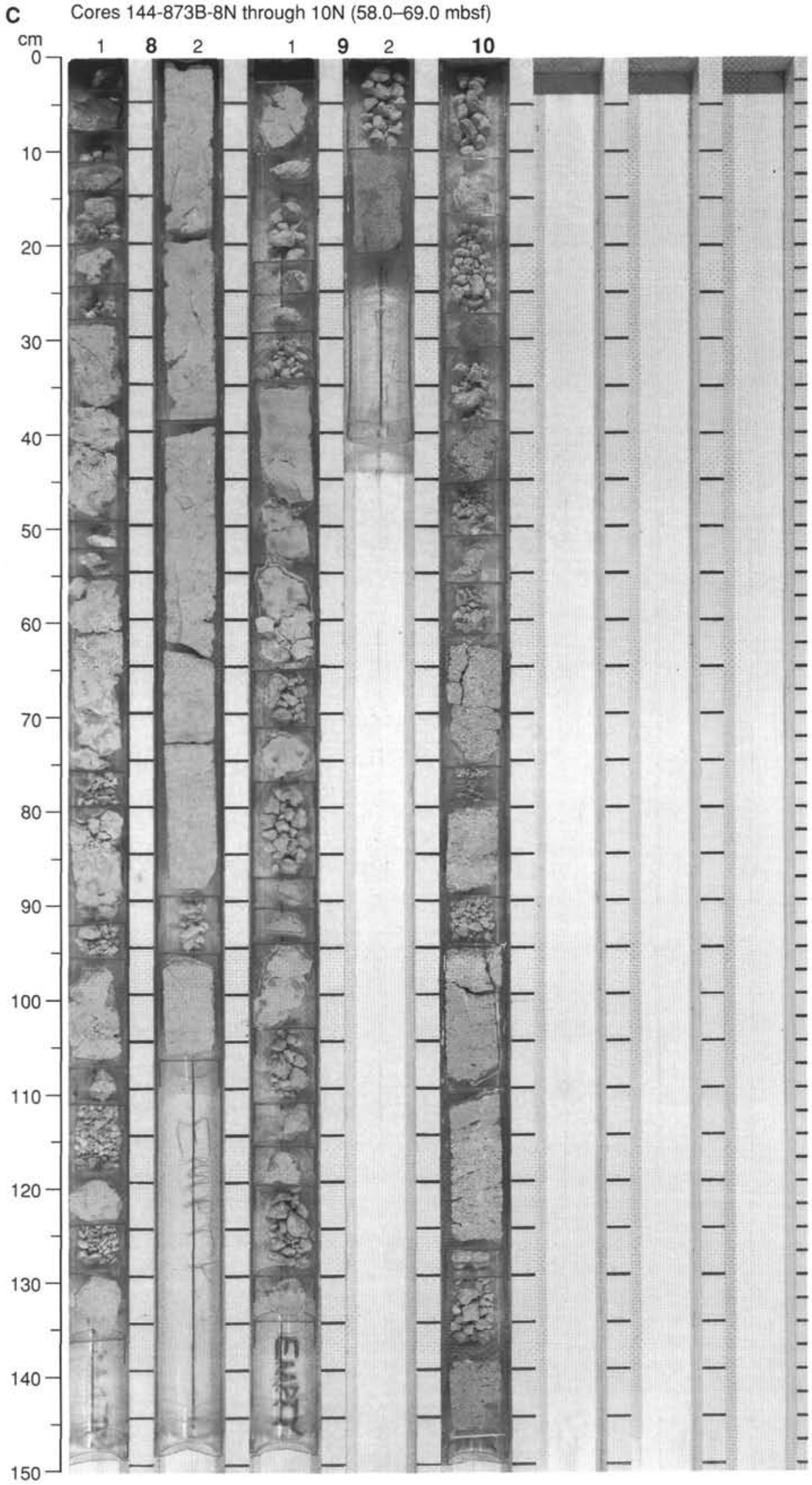

Figure 13 (continued).

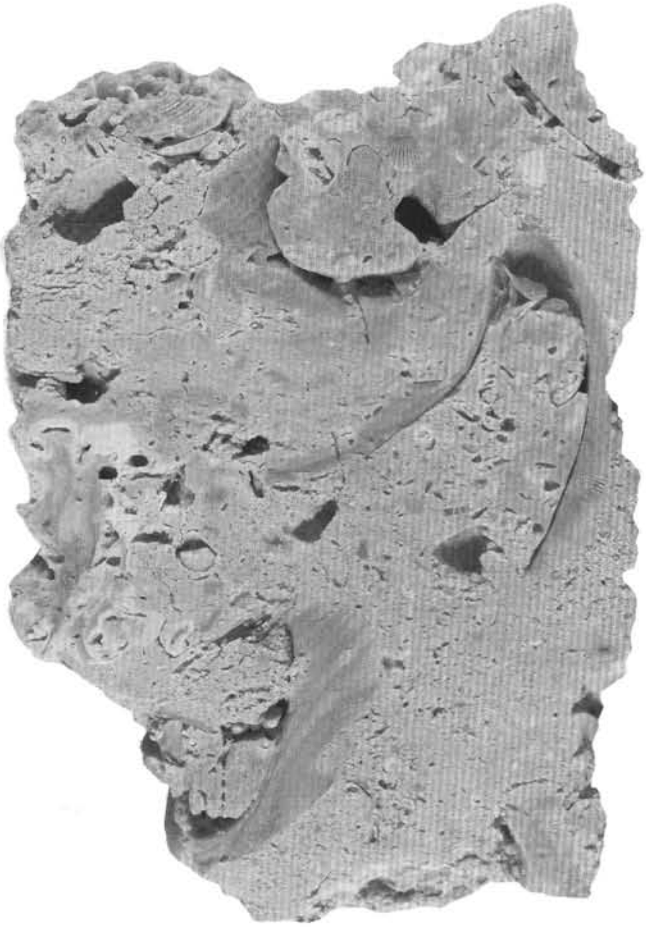

1 cm

Figure 14. Close-up core photograph of whole and fragmented radiolitid rudists, some encrusted by red algae (Interval 144-873B-8N-1, 43–50 cm). Also note molds of other bivalve mollusks.

1 cm

Figure 15. Close-up photograph of a cluster of small radiolitid rudists (Interval 144-873A-7R-1, 106–113 cm).

glass shards found in the matrix of Unit VI. Numerous graded beds and local cross-bedding suggest these glass shards and basalt fragments were transported a short distance and deposited in water. The top of this hyaloclastic deposit (Sections 144-873A-18R-1, 133 cm, to -19R-3, 68 cm), where the matrix is dusky red, weathered in an oxic environment for an indeterminate interval as the overlying alkalic basalts in Unit V were erupted. The basalts of Unit V represent the waning phase of volcanism at Site 873.

The contact between the basalt of Unit V and the clays and claystone of Unit IV was not recovered. However, a downhole change in color from dark red to lighter shades of red and olive, a downhole increase in induration, the wide variation in magnetic susceptibility (see "Paleomagnetism" section, this chapter), and the remnant basaltic fabric recognized in the lower portion of the claystone interval (all discussed in the description of Unit IV, above) suggest that Unit IV is a subaerial weathering profile of one or more basalt flows.

The contact between Units IV and III is sharp with no evidence of clay reworking (see discussions of Subunit IIIB and Unit IV, above). Submergence in a low-energy (lagoonal) environment or rapid burial are both consistent with incomplete erosion of the clays and the lack of reworked clay in the overlying limestone. The deepest limestones recovered from above the clay have a normal shallow-marine fauna and are mostly grainstones, with at least one graded interval (Sections 144-873A-11R-2, 82 cm, to -12R-1, 7 cm); it is unlikely that the initial carbonates were deposited in a protected, restricted lagoon. Rather, the environment during initial transgression was a shallow platform with open-marine circulation. Therefore, it is more likely that preservation of the red clays and lack of reworking are the result of rapid burial.

The platform carbonate sequence (Unit III) records the submergence of a volcanic island and the growth and demise of a Maastrichtian carbonate platform or atoll. The presence of woody organic matter near the base of Subunit IIIB implies that a vegetated island, possibly the remnant of a central volcanic cone, was close to Site 873 during the initial stages of carbonate deposition. As the volcanic edifice continued to subside, its size diminished until it was completely submerged; this island drowning is recorded by an upward decrease in woody matter through Subunit IIIB and its virtual absence in Subunit IIIA.

The abundance of bioturbated packstone, wackestone, and some mudstone intercalated with grainstone in Subunit IIIB is consistent with deposition in a shallow lagoon that was periodically affected by storms, changing current patterns, or short-term relative sea-level changes. The fauna in intervals with mostly grainstone (e.g., Interval 144-873A-10R-1, 10–95 cm) tend to be characteristic of normal marine conditions, that is, high diversity, including echinoderm debris, corallinacean algae, rudists debris, and larger foraminifers such as *Sulcoperculina* and Orbitoididae. Faunas in mudstone, wackestone, and some packstone intervals are characteristic of a more restricted environment with lower diversity (see also "Biostratigraphy" section, this chapter).

Despite the gray to black color of Subunit IIIB, the total organic carbon content is relatively low (although it is higher than Subunit IIIA). This low TOC, common evidence for bioturbation, and

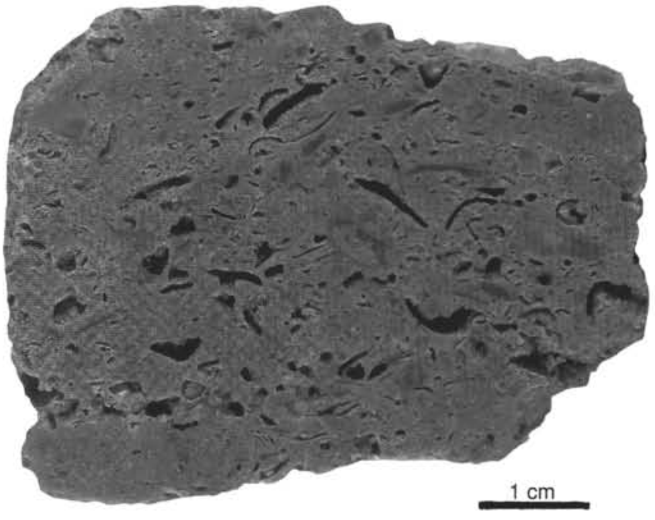

Figure 16. Close-up core photograph of the moldic porosity (after mollusks) that is common throughout Unit III (Interval 144-873A-7R-2, 70–75 cm).

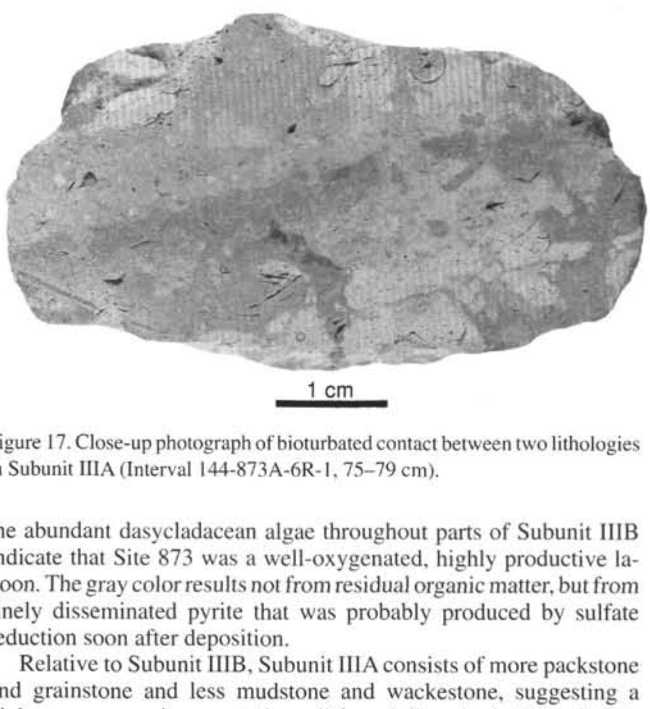

Figure 17. Close-up photograph of bioturbated contact between two lithologies in Subunit IIIA (Interval 144-873A-6R-1, 75–79 cm).

the abundant dasycladacean algae throughout parts of Subunit IIIB indicate that Site 873 was a well-oxygenated, highly productive lagoon. The gray color results not from residual organic matter, but from finely disseminated pyrite that was probably produced by sulfate reduction soon after deposition.

Relative to Subunit IIIB, Subunit IIIA consists of more packstone and grainstone and less mudstone and wackestone, suggesting a higher energy environment. Overall faunal diversity in Subunit IIIA is higher than in Subunit IIIB, indicating more open-marine conditions. Colonies of small radiolitid rudists recovered in Subunit IIIA also attest to open-marine conditions. A lack of woody material could indicate that the central volcanic island was completely submerged by the time Subunit IIIA was deposited.

Subunit IIIA is capped by 75 cm (recovery) of algal rudist rudstone underlain by at least 4.5 m (recovery) of coarse to fine grainstones (Cores 144-873B-8N to -10N). This algal rudstone is the only evidence of bioherm proximity recovered at Site 873. Whether this near-reef facies signifies a small inner platform/lagoon patch reef near Site 873 or whether it is related to the final deepening and drowning of the Maastrichtian-age platform is uncertain.

Wodejebato Guyot did not simply subside quietly into the pelagic realm. Unit II is a mixed neritic and pelagic limestone conglomerate with a complex history. The surface of the carbonate platform was repeatedly reworked by bioturbation and/or some other unidentified submarine erosion process during late Paleocene to middle Eocene time. During and after reworking, lithoclasts of neritic and pelagic origin were coated by manganese crusts. The final product is at least 30 cm, and perhaps up to 4 m, of manganese-coated rubble that overlies the guyot.

Pelagic sedimentation began in early Miocene time and was interrupted by a number of disconformities with hiatuses of varying lengths (see "Sedimentation Rates" section, this chapter). The longest hiatus (parts of late and middle Miocene) is associated with the lithologic boundary between foraminifer sand (Subunit IA) and nannofossil foraminifer ooze (Subunit IB). The gradations in color and nannofossil abundance used to define the lithologic boundary begin near the position associated with the hiatus. This disconformity also correlates with a 0.5-m-thick zone of apparent bioturbation in Interval 144-873B-4H-1, 40–86 cm (Fig. 9).

Preliminary Interpretation of Postdepositional History

The most pervasive diagenetic feature is the development of leached intervals in which porosity is commonly moldic, solution-enlarged interparticle, or vuggy (Figs. 14, 16, 17, 19, 20, and 23). Secondary porosity is variably reduced by the precipitation of pore-lining calcite cements (Figs. 23 and 28).

Subunit IIIA contains two intervals that may be the result of subaerial weathering. Open spaces in Interval 144-873A-5R-1, 23–78 cm, are primarily tubular pores (1.0–0.3 mm) that may be (1) burrows, (2) tiny tubular fenestrae caused by escaping fluids, or (3) molds of rootlets; these tubes are Y-shaped and narrow downward. All open space is generally stained yellow to red. The overall porosity (3%) is moderately reduced by geopetal sediment infilling or by drusy, laminated, asymmetric calcite crusts. Gray, 1-cm-thick laminations near the base of this section (Interval 144-873A-5R-1, 64–70 cm) are bored and seemingly disrupted. Interval 144-873A-5R-1, 51–64 cm, appears to be chalky.

Interval 114-873A-7R-1, 138–150 cm, consists of wackestone with tubular pores, 1 mm in diameter, that are probably burrows; however, some with a Y shape may be plant rootlets. Interval 114-873A-7R-1, 138–142 cm, has an irregular surface punctured by tubular pores that may be bores or may be solution features. The pores are filled with yellow silty material. Below this surface, cavities are filled with white sediment.

BIOSTRATIGRAPHY

Introduction

Two holes were drilled at Site 873 on central Wodejebato Guyot with the aim of recovering the pelagic cap and drilling the lagoonal limestone deposited during the platform stage of this seamount.

The pelagic cap consists of Neogene sediments (lower Miocene to Pleistocene) that have been influenced by winnowing or erosion, especially in the Miocene section. As a consequence, an upper lithology of nannofossil foraminifer ooze and a lower lithology of foraminifer ooze can be differentiated in the pelagic cap. Biostratigraphy for the pelagic sediments relies on planktonic foraminifers and calcareous nannofossils. The same fossil groups also provide biostratigraphic information for the manganese crusts and the conglomerate on top of the platform carbonates.

Biostratigraphic analysis of the Upper Cretaceous platform carbonate sequence relies mainly on larger foraminifers (Fig. 29). Paleoenvironmental information is provided by analysis of thin-section samples and by the occurrence and abundance of siliceous microfossils and palynomorphs.

The APC coring system delivered greater than 80% recovery in the pelagic oozes (Cores 144-873B-1H to -6H). A problem that

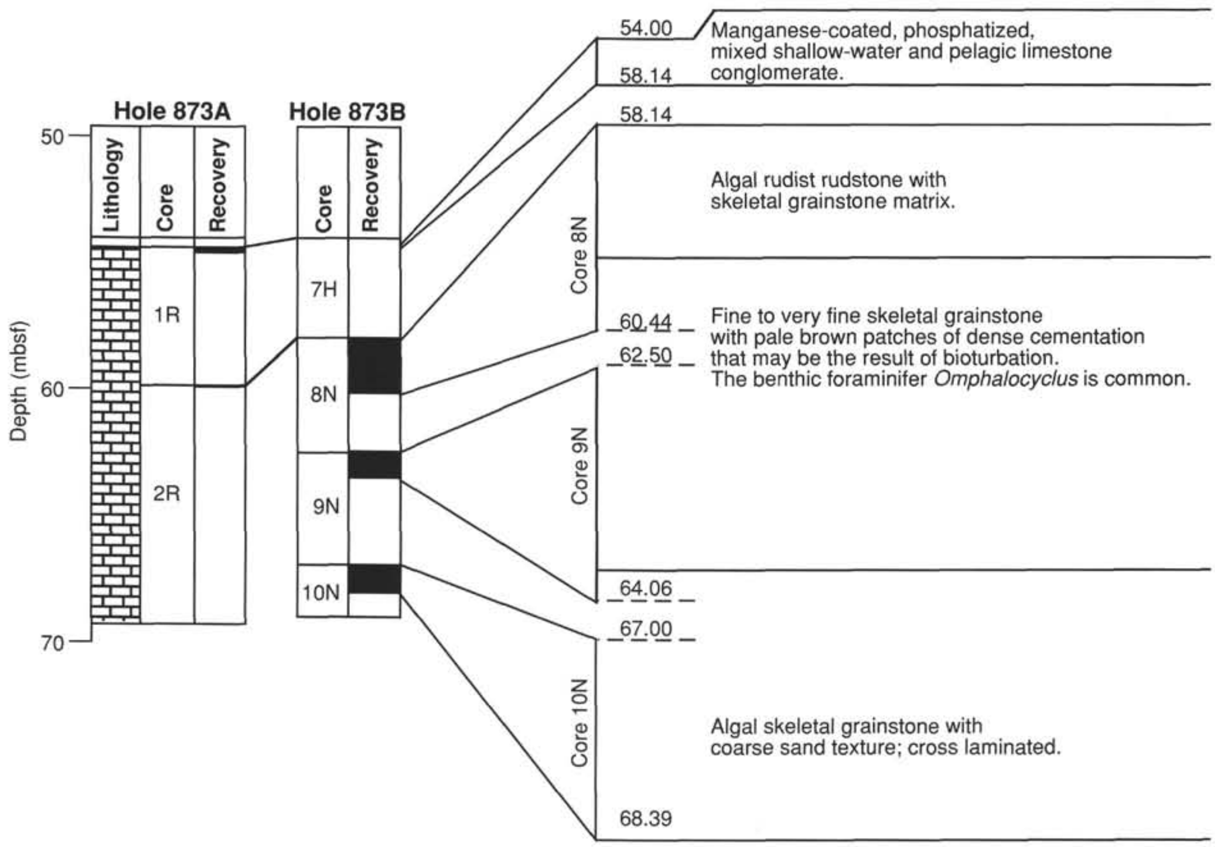

Figure 18. Lithostratigraphic detail of Subunit IIIA in Hole 873B.

affected biostratigraphy was the caving-in of the borehole in the loose sandy and watery sediment; this led to downhole contamination at the top of many cores. There was poor recovery in Core 144-873B-7H because the core barrel struck the ooze/platform limestone boundary and manganese crust. A thin veneer of chalk adhered to fragments of the manganese crust.

Because of the relatively low recovery of the shallow-water carbonates using the RCB in Hole 873A (0.4%–25%), the top of the limestone sequence in Hole 873B was cored using the motor driven core barrel (MDCB). This technique improved recovery to approximately 39%.

Calcareous Nannofossils

Calcareous nannofossils were examined in sediments of the pelagic cap, from within manganese crusts, and from selected horizons within the platform carbonate sequence. The pelagic cap sequence (Hole 873B) was studied from smear slides of core-catcher samples and supplemented by examination of one sample per section. Samples from the platform carbonate sequence were studied from smear slides of raw sediments and differentially settled concentrates. The internal stratigraphies of the manganese crusts were examined during analyses of thin-section samples.

Pelagic Cap (Hole 873B)

The occurrence of *Helicosphaera sellii* without *Calcidiscus macintyrei* in Samples 144-873B-1H-1, 5–6 cm, through -1H-3, 50–51 cm (0.05–3.07 mbsf), identifies the *H. sellii* Zone of early Pleistocene age. The presence of this zone within the top 5 cm of the core would imply that the middle and upper Pleistocene (the last ~1.3 m.y.) are missing at Site 873. However, specimens of *Emiliania huxleyi* (indicator of the late middle and late Pleistocene) occur as downhole contaminants in several intervals (e.g., Sample 144-873B-2H-1, 5–6 cm; 1.24 mbsf). Thus, the upper part of the Pleistocene probably is present at this site but was not recovered.

The interval from Samples 144-873B-1H-4, 5–6 cm, through -1H-4, 50–51 cm (4.02–4.47 mbsf), is assigned to the *Calcidiscus macintyrei* Zone based on the presence of *C. macintyrei* and *H. sellii* without any discoasters. The first stratigraphic appearance of *Gephyrocapsa oceanica* (s.l.) in Sample 144-873B-1H-4, 5–6 cm, marks the Pleistocene/Pliocene boundary.

The interval from Samples 144-873B-1H-4, 100–101 cm, through -2H-1, 100–101 cm (5.0–7.5 mbsf), contains *Discoaster brouweri* and *Discoaster triradiatus* without *Discoaster pentaradiatus,* indicating Subzone CN12d of late Pliocene age. Samples 144-873B-2H-2, 52–53 cm, through -2H-3, 52–53 cm (8.52–9.91 mbsf), contain *Discoaster brouweri* and *Discoaster pentaradiatus* without *Discoaster surculus, Discoaster tamalis,* or *Reticulofenestra pseudoumbilica,* indicating the *Discoaster pentaradiatus* Subzone (CN12c) of late Pliocene age (Fig. 30).

The interval from Samples 144-873B-2H-4, 52–53 cm, through -3H-1, 50–51 cm (11.38–16.5 mbsf), contains *Discoaster tamalis* without *Reticulofenestra pseudoumbilica*, indicating Subzone CN12a of late Pliocene age. Many of the discoasters in this interval are significantly overgrown, making identification difficult. Interestingly enough, the basal sample contains *Sphenolithus abies* without *R. pseudoumbilica*. Berggren et al. (1985) note that the interval containing *Sphenolithus abies* without *R. pseudoumbilica* spans approximately 30 k.y. at the very base of the subzone.

Samples 144-873B-3H-2, 50–51 cm, through -3H-4, 50–51 cm (17.56–20.56 mbsf), contain both *Reticulofenestra pseudoumbilica* and *Sphenolithus* spp. but lacks *Amaurolithus* spp. This is normally indicative of Zone CN11 of late early to early late Pliocene age.

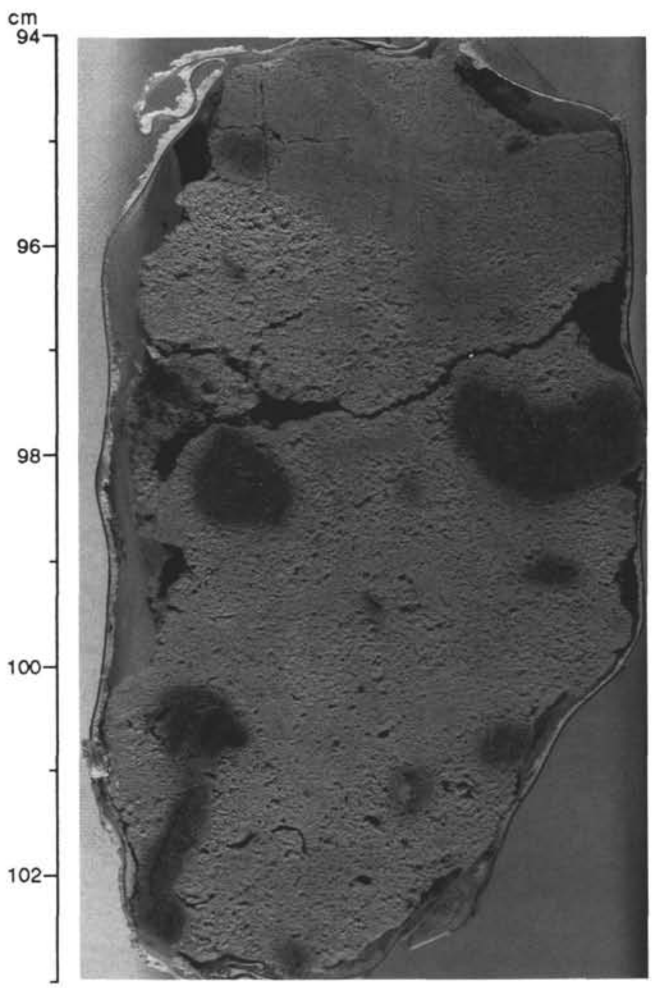

Figure 19. Close-up core photograph of well-cemented mottles that may provide evidence for bioturbation (Interval 144-873B-9N-1, 94–103 cm). The remainder of the limestone is a fine grainstone with high porosity.

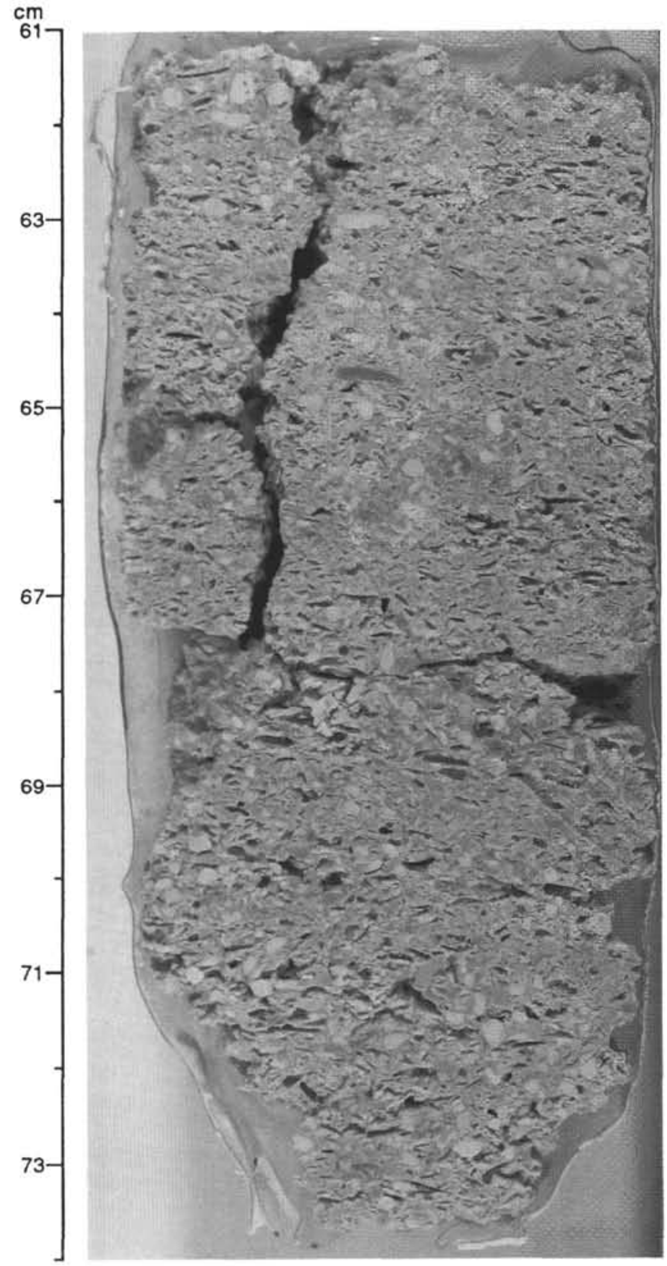

Figure 20. Close-up core photograph of algal molluscan grainstone with high moldic porosity (Interval 144-873B-10N-1, 61–74 cm).

However, preservation in this interval is poor, with significant overgrowth of the discoasters and dissolution of other taxa. Thus, the absence of the amauroliths may be diagenetic. The presence of common *Discoaster asymmetricus* restricts the lower biostratigraphic limit of this interval to Subzone CN10d. Therefore, this interval is assigned to the combined Zone CN10d–11.

The interval from Samples 144-873B-3H-5, 50–51 cm, through -3H-CC (22.06–25.48 mbsf), is assigned tentatively to Subzone CN10a based on the questionable occurrence of *Triquetrorhabdulus rugosus* in the upper sample. Poor preservation prohibits positive identification at this time. *Discoaster quinqueramus* is absent throughout the interval, indicating that it cannot be older than Zone CN10.

A significant disconformity, with a hiatus of at least 5.2 m.y., occurs between the base of Core 144-873B-3H and Sample 144-873B-4H-1, 5–6 cm. Samples in Core 144-873B-4H through Sample 144-873B-5H-6, 48–49 cm (25.5–41.48 mbsf), contain *Discoaster exilis, Cyclicargolithus floridanus,* and *Discoaster moorei* without *Catinaster coalitus* or *Sphenolithus heteromorphus.* This association of taxa identifies Zone CN5 of middle Miocene age. Division of this interval into subzones is hampered by poor preservation with significant overgrowth of the discoasters. A few horizons, such as Sample 144-873B-5H-1, 10–11 cm, contain identifiable *Discoaster kugleri.* Thus, at least part of this interval is assignable to Subzone CN5b. However, in most cases the assignment of subzone is premature at this point, and the entire interval has been designated merely as Zone CN5.

Section 144-873B-5H-CC through Core 144-873B-6H (41.92–51.82 mbsf) are assigned to the combined Zone CN3/4 (middle Miocene) based on the occurrence of *Sphenolithus heteromorphus.* The occurrence of *Discoaster exilis* throughout most of this interval implies the presence of Zone CN4, although preservation makes identification of this species difficult near the base of Core 144-873B-6H.

Core 144-873B-7H (54.0–54.02 mbsf) recovered only two small fragments of a manganese crust. Nannofossil chalk adhering to the presumed upper surface of the larger of the two fragments yields *Sphenolithus delphix, Sphenolithus conicus, Cyclicargolithus abisectus, Cyclicargolithus floridanus,* and *Triquetrorhabdulus carinatus* without *Sphenolithus heteromorphus, Discoaster druggii, Dictyococcites bisectus,* or *Sphenolithus ciperoensis.* This species association identifies Subzone CN1a+b of earliest Miocene age. Drilling complications throw doubt on whether a full 4 m were really drilled for Core

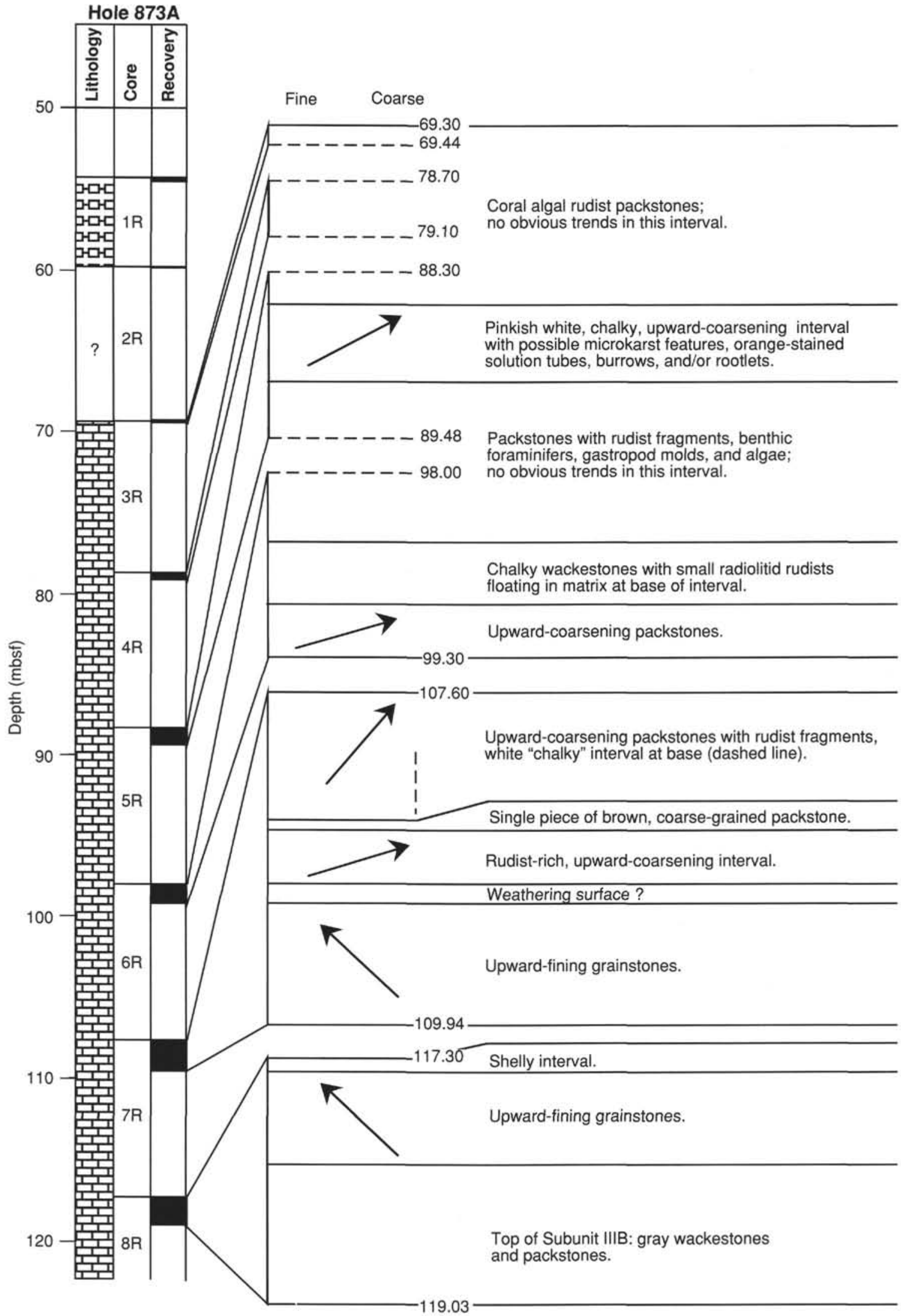

Figure 21. Lithostratigraphic detail of Subunit IIIA in Hole 873A. Plot conventions as in Figure 8.

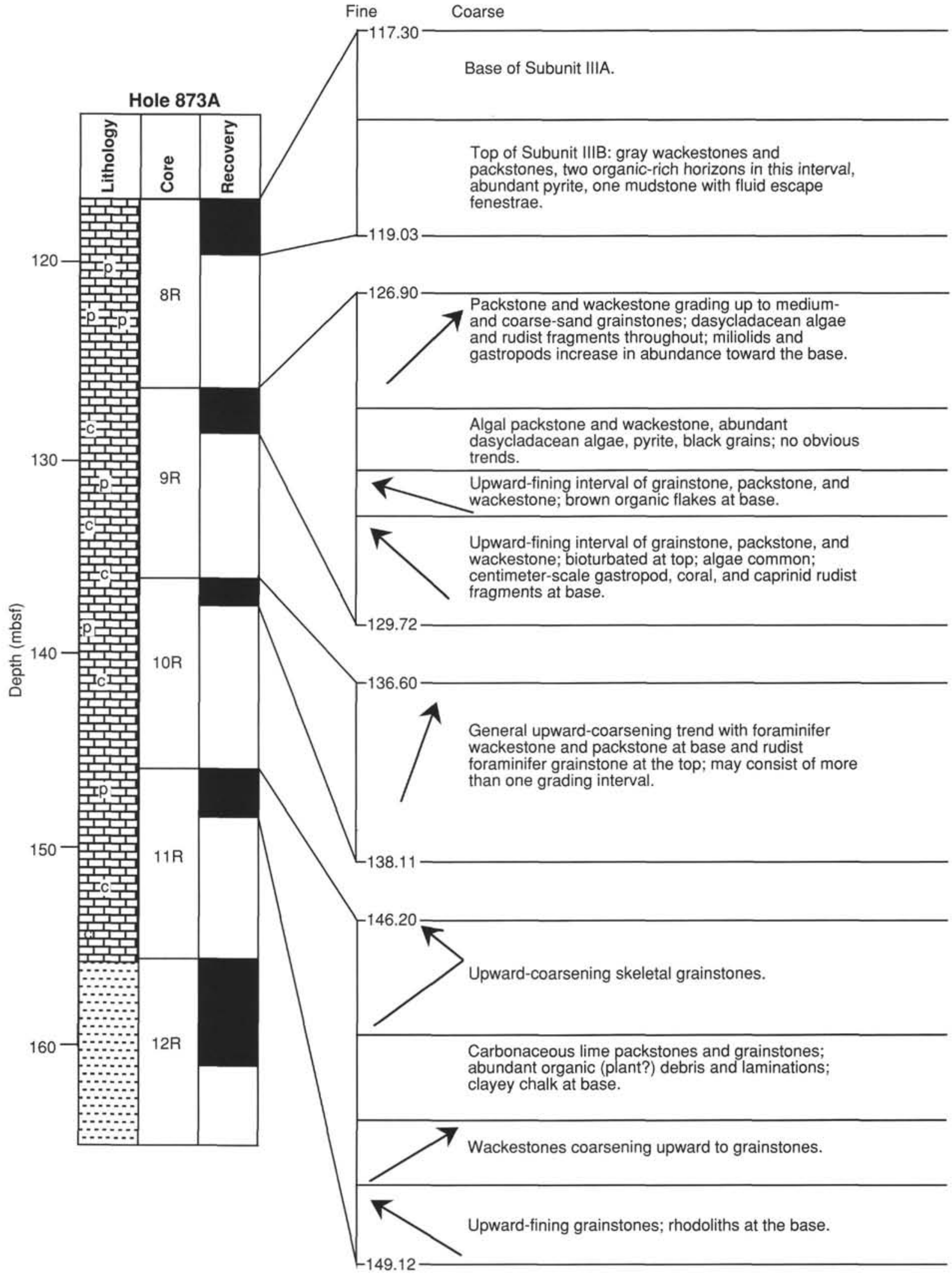

Figure 22. Lithostratigraphic detail of Subunit IIIB in Hole 873A. Plot conventions as in Figure 8.

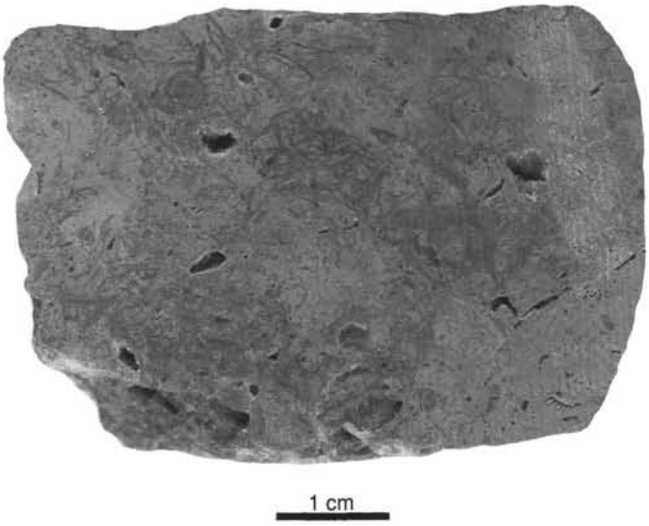

Figure 23. Close-up core photograph of a gray molluscan wackestone typical of Subunit IIIB (Interval 144-873A-8R-1, 81–85 cm). Note the cement-filled molluscan molds and cement-lined vugs.

144-873B-7H. If the recovered manganese and chalk represents the complete stratigraphic section, then a disconformity with a hiatus of at least 5.9 m.y. separates the base of Core 144-873B-6H from the nannofossil chalk in Core 144-873B-7H.

Manganese-oxide-coated, Phosphatized Limestone Conglomerate

The top 20 cm of Section 144-873A-1R-1 (54.3–54.5 mbsf) contains four fragments of manganese crusts. Pelagic limestone encrusted by manganese contains material of at least three distinct ages: late middle Eocene, early Eocene, and late Paleocene.

The upper middle Eocene pelagic limestone contains *Reticulofenestra umbilica, Reticulofenestra dictyoda, Dictyococcites bisectus, Discoaster bifax, Discoaster barbadiensis, Chiasmolithus nitidus, Chiasmolithus grandis,* and *Chiasmolithus titus.* This assemblage indicates the *Discoaster bifax* Subzone (CP14a). This assemblage occurs in the upper part of the crust.

The upper lower Eocene assemblage includes *Discoaster kuepperi, Discoaster lodoensis, Discoaster septemradiatus, Camplyosphaera dela, Sphenolithus radians, Reticulofenestra dictyoda, Lophodolithus mocholoporus,* and *Rhabdosphaera scabrosa.* This association of species indicates Zone CP11 or Subzone CP12a. One questionable specimen of *Discoaster sublodoensis* was observed. If verified by further examination, this would narrow the assignment to Subzone CP12a (early Eocene).

The upper Paleocene assemblage includes *Fasciculithus tympaniformis* (s.s.), *Fasciculithus* sp. cf. *F. clinatus, Discoaster multiradiatus, Toweius eminens,* and *Sphenolithus primus,* indicating Zone CP8.

Sample 144-873B-8N-1, 4–8 cm, consists of a manganese crust underlain by a complex mixture of platform debris and pelagic limestone. The latter contains well-preserved nannofossils including *Reticulofenestra dictyoda, Reticulofenestra umbilica, Discoaster barbadiensis, Discoaster strictus, Discoaster bifax, Chiasmolithus titus, Chiasmolithus nitidus,* and *Chiasmolithus grandis.* This assemblage is diagnostic of Subzone CP14a of late middle Eocene age. The pelagic limestone containing this assemblage is intimately associated with the upper part of the manganese crust and is penetrated by manganese dendrites.

Black Claystone

A 5- to 7-cm-thick, black, calcareous claystone horizon in Sample 144-873A-11R-2, 17–23 cm, contains a very sparse, well-preserved

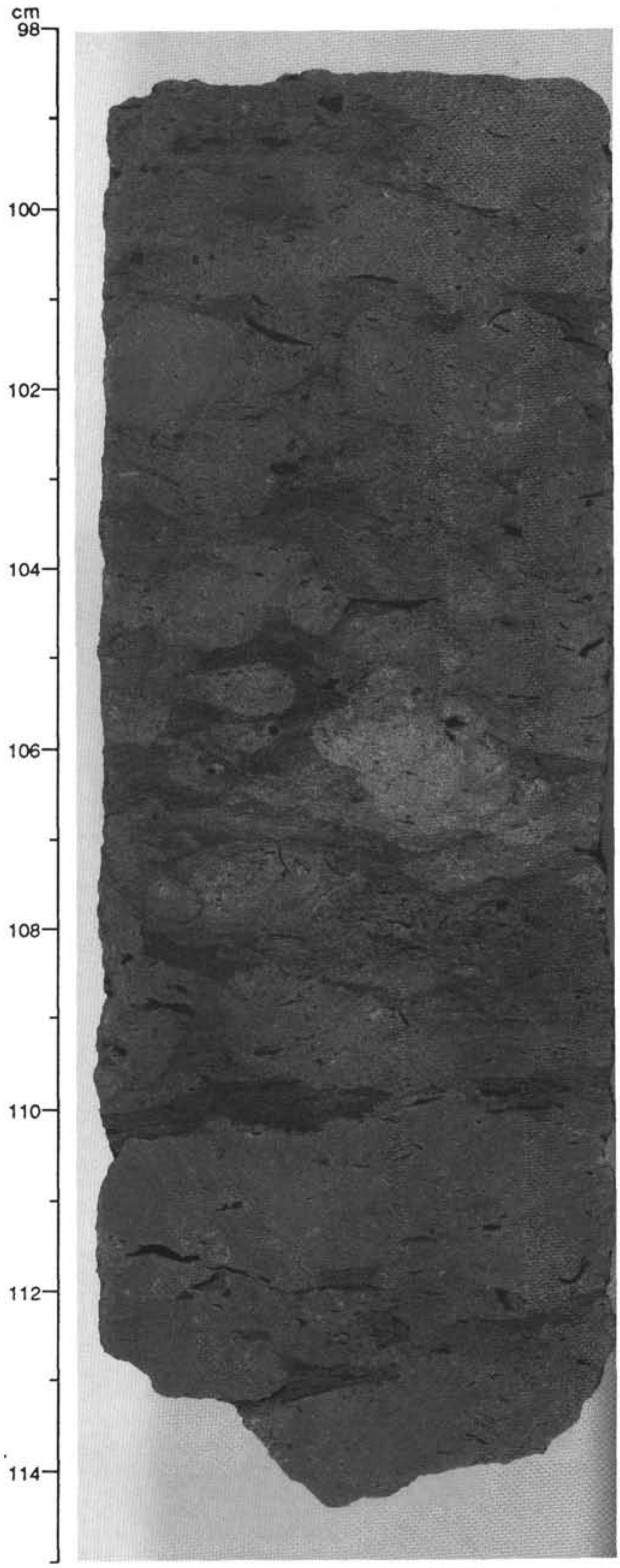

Figure 24. Close-up core photograph of packstone/grainstone with organic-rich laminae from near the base of Subunit IIIB (Interval 144-873A-11R-1, 98–115 cm).

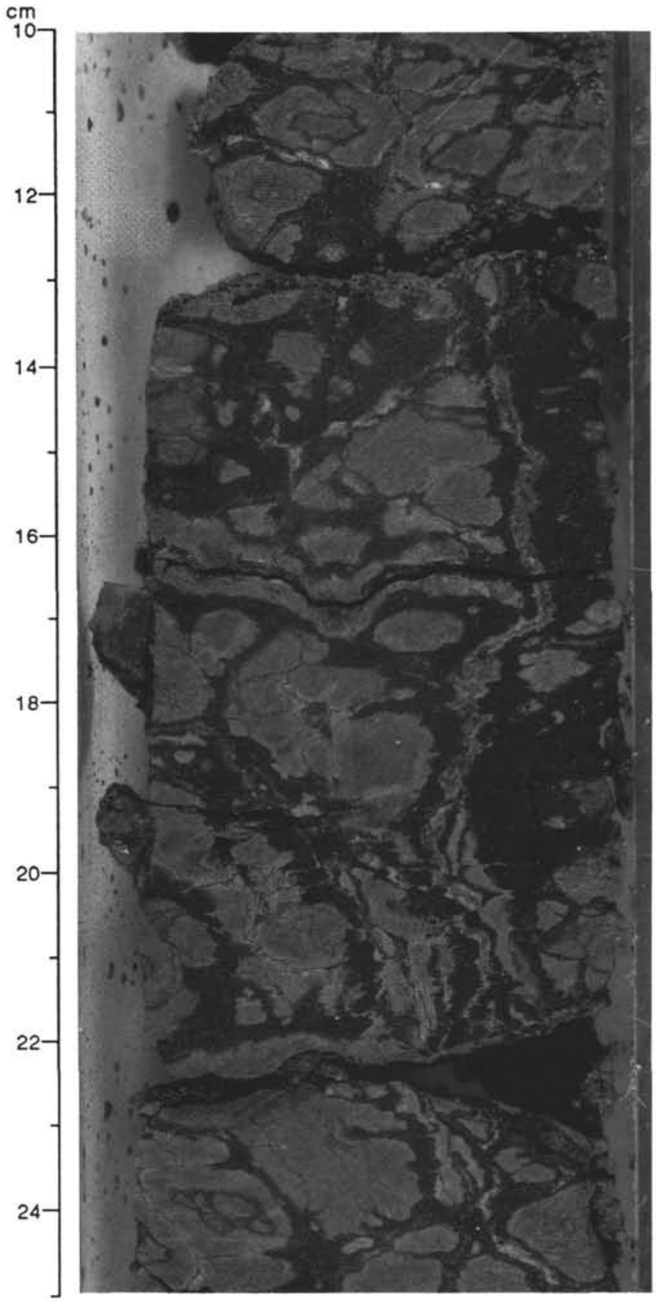

Figure 25. Close-up core photograph of claystone from Unit IV with "marbled" appearance caused by anastomosing veins of clay surrounding more indurated claystone clasts (Interval 144-873A-13R-1, 10–25 cm).

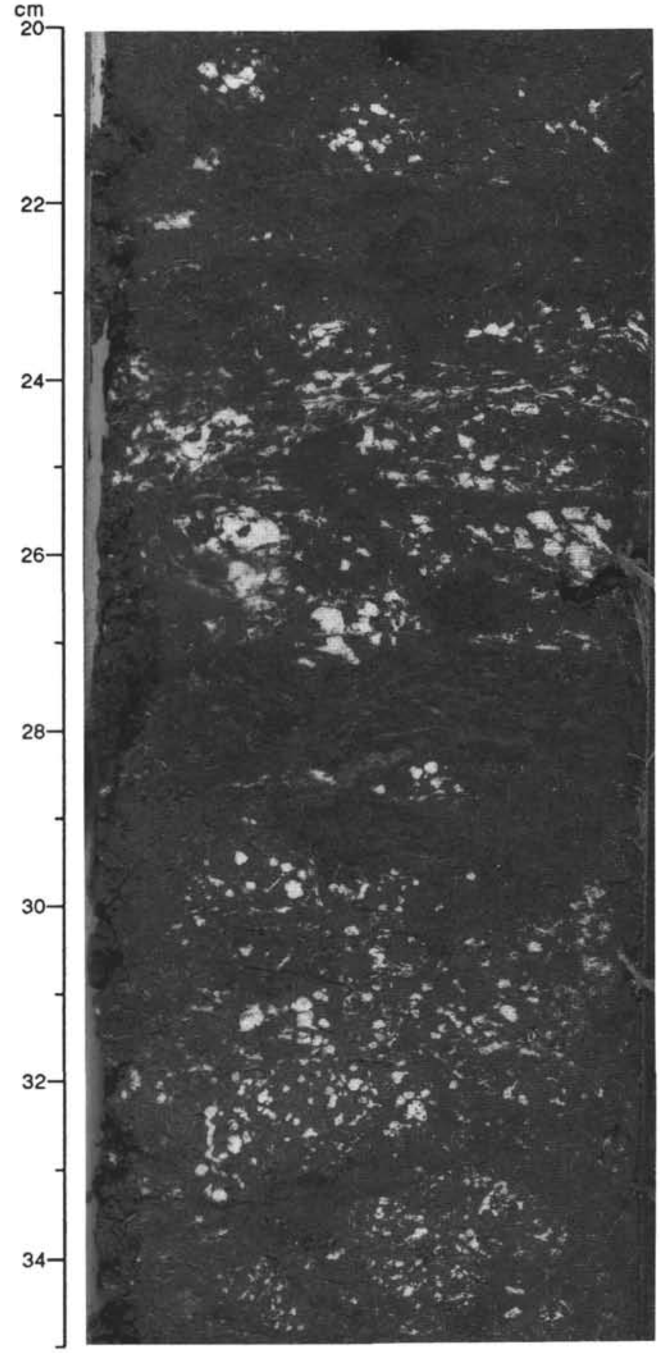

Figure 26. Close-up core photograph of claystone from Unit IV with zeolite patches that may be remnant vesicles in altered basalt (Interval 144-873A-13R-3, 20–35 cm).

nannofossil assemblage. Several hours of observation yielded 33 specimens. Most of these specimens are Upper Cretaceous "background" taxa such as *Watznaueria barnesae, Glaukolithus diplogrammus, Prediscosphaera cretacea* (s.s.), and *Placozygus sigmoides.* The presence of *Arkhangelskiella specillata* and *Orastrum campanensis* indicates a Campanian age.

Planktonic Foraminifers

Pelagic Cap

Planktonic foraminifers are the principal constituent of the winnowed pelagic sediments on Wodejebato Guyot, as was previously found to be the case for the pelagic caps of Limalok and Lo-En guyots. Fragmentation, iron staining, and dissolution are common in the sequence. One sample was analyzed from each section through Hole 873B (Fig. 30). Pervasive mixing of faunas, caused both by reworking and downhole contamination, has rendered the zonation of some intervals problematic.

Sample 144-873B-1H-1, 36–38 cm, contains infrequent *Truncorotalia truncatulinoides* and *Globorotalia fimbriata* with common *Pulleniatina obliquiloculata, Globorotalia tumida tumida,* and *Sphaeroidinella dehiscens* among others; it is assigned to the upper part of

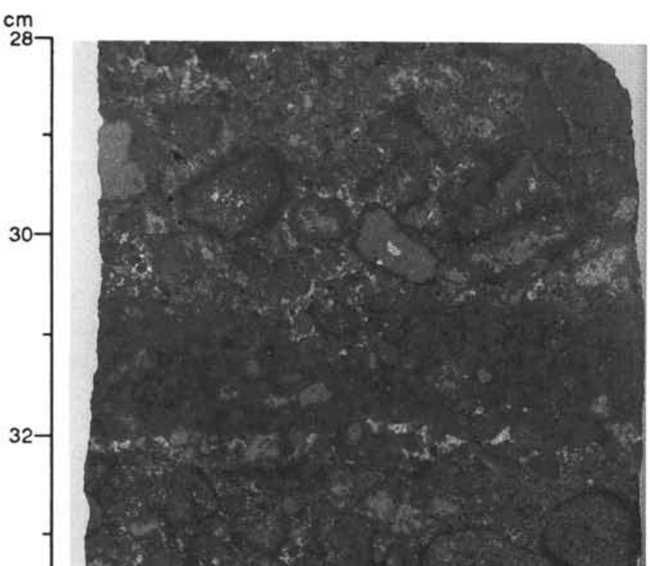

Figure 27. Close-up photograph of bedded volcanic breccia from Unit VI (Interval 144-873A-21R-1, 28–40 cm).

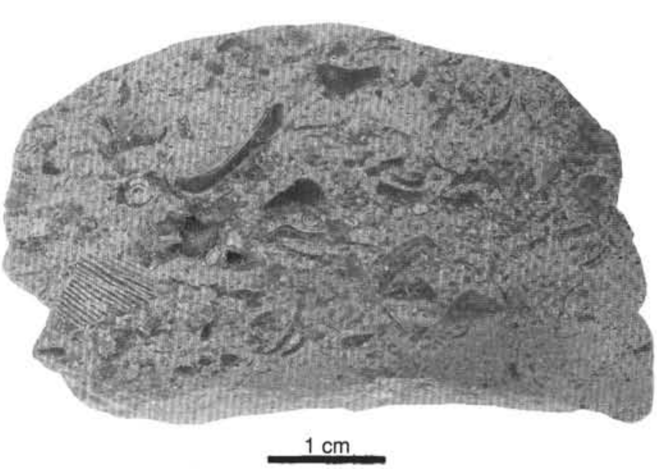

Figure 28. Close-up photograph of skeletal rudstone from Subunit IIIA with radiolitid fragments, calcite cement-filled molds of other mollusks, and vugs lined with bladed calcite cement (Interval 144-873A-6R-1, 88–92 cm).

Zone N22 (Pleistocene to Holocene). *Truncorotalia truncatulinoides* co-occurs in Samples 144-873B-1H-2, 36–38 cm, and -1H-3, 36–38 cm, with a similar fauna, although *G. fimbriata* is absent. These samples are still within Zone N22 (Pleistocene).

Sample 144-873B-1H-4, 36–38 cm, lacks *T. truncatulinoides,* but it does contain rare *T. tosaensis* with common *Globigerinoides fistulosus.* It is assigned to Zone N21 (late Pliocene). In Samples 144-873B-1H-5, 36–38 cm, and -1H-CC, *Truncorotalia tosaensis* was not found. However, in Sample 144-873B-2H-1, 36–38 cm, rare specimens of *T. tosaensis* showing features transitional to *Globorotalia crassaformis* are present, indicating that this sample and the two samples above probably belong in Zone N21. *Pulleniatina praecursor* and rare *P. primalis* (i.e., the more primitive representatives of the *Pulleniatina* lineage) are found in Sample 144-873B-2H-2, 36–38 cm, and all lower sections of Core 144-873B-2H. The occurrence of these species, in the absence of *T. tosaensis,* places this interval within the combined Zone N19/20 (Pliocene).

In all samples examined from Core 144-873B-3H, with the exception of the core catcher, *Dentoglobigerina altispira* is a common constituent and occurs with *Globorotalia tumida flexuosa, Sphaeroidinellopsis seminulina,* and rare *Sphaeroidinella dehiscens.* These indicate the lower part of Zone N19/20. The core-catcher sample, Sample 144-873B-3H-CC, lacks *Sphaeroidinella,* but it does contain common *Sphaeroidinellopsis seminulina* and a few *Globoquadrina dehiscens.* This sample, therefore, is tentatively assigned to Zone N18 (upper Miocene). However, this assignment must be regarded with caution because the Pliocene through Holocene indicator *Sphaeroidinella dehiscens* is always rare and subordinate to *Sphaeroidinellopsis* when it does occur through the lower Pliocene of Core 144-873B-3H. Furthermore, the infrequently occurring specimens of *Globoquadrina dehiscens* could be reworked individuals.

Pervasive downhole contamination of Pleistocene and probably also Pliocene forms was encountered in Sample 144-873B-4H-1, 36–38 cm, making placement of the Miocene/Pliocene boundary impossible at this stage of investigation. Common downhole contaminants were also encountered in Samples 144-873B-4H-2, 36–38 cm, and -4H-3, 36–38 cm, in addition to many reworked forms from the lower middle Miocene (*Globigerinoides bisphericus, Praeorbulina* spp.). Sample 144-873B-4H-4, 36–38 cm, also contains a mixture of species, some of which are long ranging and difficult to place, others of which are characteristic of various intervals from the Pliocene-Pleistocene through the lower middle Miocene. These forms include *Globorotalia tumida, Sphaeroidinella dehiscens* (both probably contaminants), *Sphaeroidinellopsis seminulina, Globorotalia fohsi lobata, G. peripheroronda, Praeorbulina sicana,* and *Globigerinoides bisphericus.* A similar mixed fauna was found in Samples 144-873B-4H-5, 36–38 cm, -4H-CC, and throughout Core 144-873B-5H. Downhole contaminants apart, this assemblage is taken to represent a pervasive mixing of faunas from at least Zone N8 to Zones N12–N13 age.

Sample 144-873B-6H-1, 36–38 cm, is apparently free of downhole contaminants and reworked forms. *Globigerinoides bisphericus* and *Praeorbulina sicana* occur in the absence of *Orbulina,* indicating the higher part of Zone N8 (early to middle Miocene). A similar assemblage, also indicative of Zone N8, was found in Sample 144-873B-6H-3, 36–38 cm, associated with rare *Globigerinatella insueta. Praeorbulina* is absent from Sample 144-873B-6H-CC, but *Globigerinoides bisphericus* is common in the sample; thus, the assemblage is

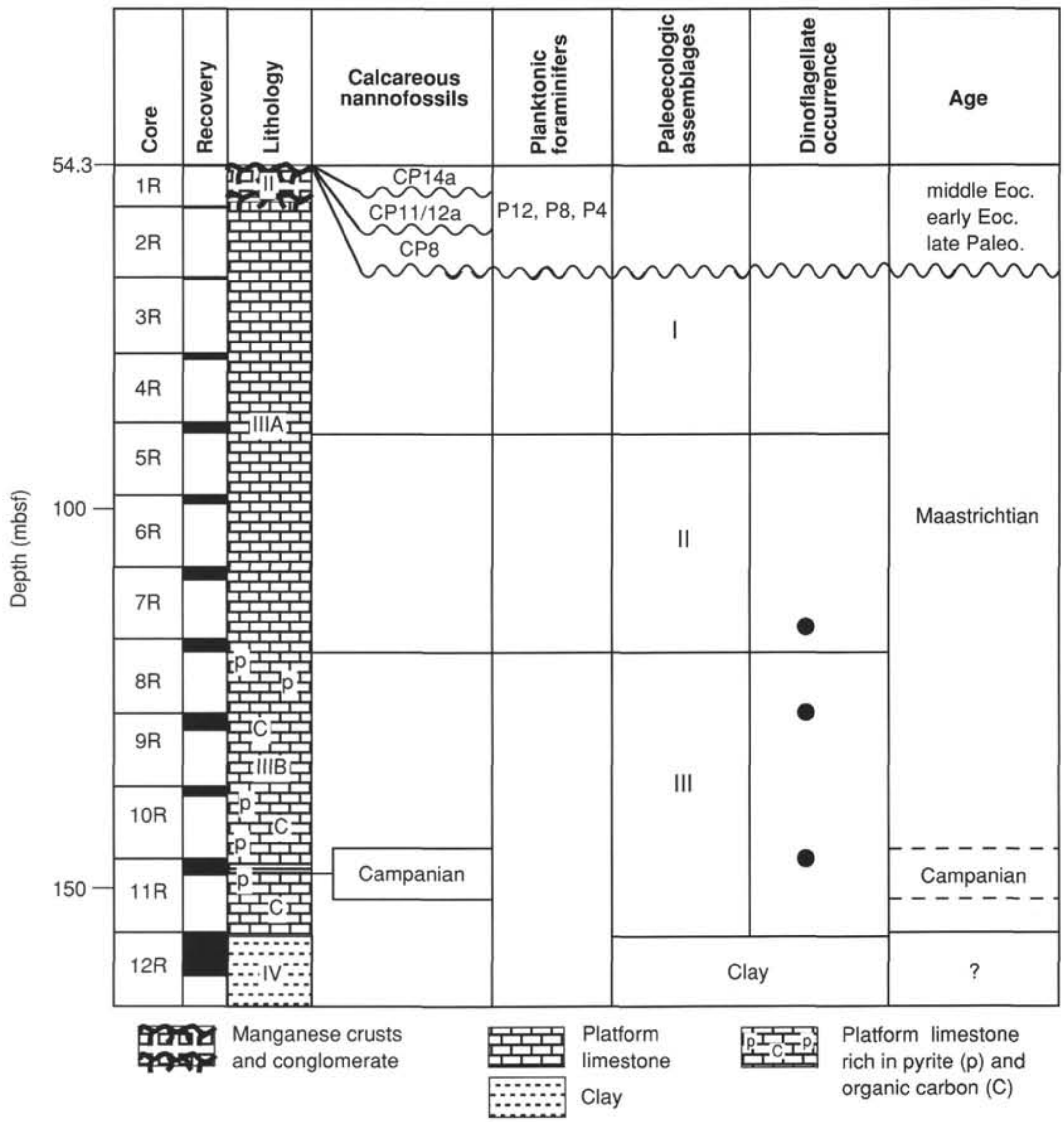

Figure 29. Biostratigraphy of Hole 873A, Wodejebato Guyot.

assigned to the lower part of Zone N8. In Sample 144-873B-7H-CC, too little calcareous material was recovered to find any foraminifers.

Manganese-oxide-coated, Phosphatized Limestone Conglomerate

The boundary between the pelagic cap and the platform limestone is marked by a manganese crust covering a phosphatized limestone conglomerate containing reworked pebbles from lithologies similar to the underlying platform carbonates. The hardground was recovered in Samples 144-873A-1R-1, 0–26 cm, 144-873B-7N-1, 0–1 cm, and 144-873B-8N-1, 4–8 cm. Thin-section samples and slabs were used to determine planktonic foraminifers from the manganese crusts and the underlying conglomerate.

The planktonic foraminifers of the outer portion of the crust belong to the upper part of Zone P12 of late middle Eocene age. This zone was identified based on the presence of *Turborotalia cerroazulensis* s.s., *T. pomeroli, Morozovella lehneri, M. crassata, Truncorotaloides topilensis, T. rohri, Globigerinatheka index, G. senni, Acarinina rohri,* and various subbotinids and the absence of large globigerinathekids. In the same sample (Sample 144-873A-1R-1, 0–7 cm), but below the manganese crust, is the conglomerate. In this sample, a pebble of Upper Cretaceous platform limestone with distinct patches of strongly phosphatized upper Paleocene (Zone P4) sediment is apparently infilled or cemented by sediment of early Eocene age (Zone P8). Therefore, the reworking probably postdates the late Paleocene.

The upper Paleocene (Zone P4) planktonic foraminifer assemblage includes *Morozovella velascoensis, M. conicotruncata, M. occlusa, M. pusilla, M. albeari, M.* sp. cf. *M. acuta, Acarinina nitida, Chiloguembelina* sp., *Planorotalites compressus*, and possibly *P. pseudomenardii.* The cemented lower Eocene sediment contains an assemblage characteristic for Zone P8, based on the occurrence of *Morozovella aragonensis, M. crassata, M. gracilis, Acarinina pseudotopilensis, A. intermedia, A. esnaensis, "Globigerinatheka" senni*, and *Pseudohastigerina danvillensis* in the absence of globigerinathekids, hantkeninids, and turborotaliids. Occasionally, some middle Eocene forms are admixed at the edges of the lower Eocene infilled portions. The same association of platform debris with pelagic sediments of all three ages was recovered as deep as Sample 144-873A-1R-1, 16–20 cm. The next sample below, Sample 144-873A-1R-1, 20–25 cm, which is composed only of manganese crust impregnating pelagic sediments, is attributed to Zone P12. It is not clear if the position of these two latter samples reflect the real thickness of the hardground or is an artifact caused by

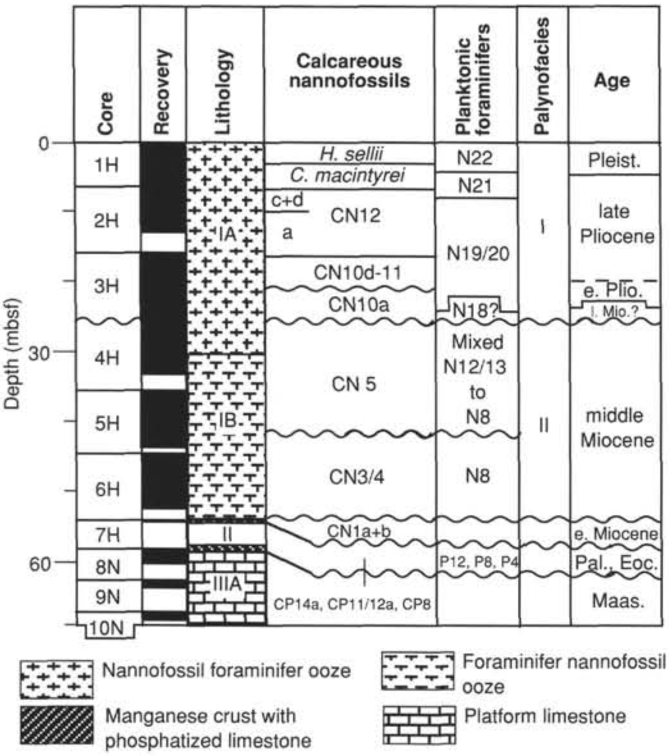

Figure 30. Biostratigraphy of Hole 873B, Wodejebato Guyot.

drilling. A similar lithology was also recovered from the top of Core 144-873A-2R, but this record is interpreted to represent downhole contamination from the caving-in of the borehole.

Carbonate Platform Sequence

Rare planktonic foraminifers occur in two samples further down in the limestone section. Sample 144-873A-9R-1, 78–81 cm, yielded *Archaeoglobigerina cretacea* and *A. blowi,* whereas *Globigerinelloides messinae* was found in Sample 144-873-10R-1, 46–50 cm. These species indicate a generalized Campanian-Maastrichtian age.

Benthic Foraminifers and Other Shallow-water Fossils

The 98-m-thick sequence of platform carbonates (Lithologic Unit II) recovered in Holes 873A (Cores 144-873A-2R to the top of -12R) and 873B (Cores 144-873B-8N to -10N) was studied using sieved core-catcher samples, 78 thin-section samples, and isolated specimens recovered from cuttings obtained when the cores were split. This analysis yielded common larger foraminifers, frequently associated with common mollusks and molluscan fragments, rhodoliths and corallinaceae, echinoid fragments, less frequent corals, and common to abundant rudists in discrete intervals. The distribution and relative abundance of these fossil groups as determined in the thin-section samples is given in Figure 31.

Several of the organism groups encountered are characteristic of the Upper Cretaceous. These include mollusks (e.g., rudists), benthic foraminifers such as *Asterorbis,* lepidorbitoids, *Sulcoperculina, Nummuloculina, Dicyclina* sp. cf. *D. schlumbergeri, Vidalina* sp. cf. *V. hispanica, Idalina antiqua,* the marine green algae (*Dasycladaceae*), *Terquemella* and *Cymopolia*?. The main group providing biostratigraphic information were the larger foraminifers. The study of the rudists was deferred for shore-based research.

Shallow-water organisms, including the larger foraminifers, are very facies-dependent. Therefore, no routine biostratigraphic scheme could be applied to the recovered succession. However, the age of the assemblages could be constrained to be Campanian-Maastrichtian in comparison with other sequences in the Pacific area, where the same larger foraminifer species were collected in layers well dated by planktonic foraminifers (Premoli Silva and Brusa, 1981).

The most common larger foraminifers that occur throughout the studied sequence are representatives of the genera *Asterorbis* and *Sulcoperculina,* including *Asterorbis havanensis, Sulcoperculina globosa, S. dickersoni,* and *S. vermunti.* Less common species are representatives of the genus *Lepidorbitoides.* A similar assemblage is recorded from DSDP Site 462 in the Nauru Basin from within the *Gansserina gansseri* Zone (middle Maastrichtian). This age is corroborated by the occurrence of *Omphalocyclus macroporus,* a species known to be confined to the middle and late Maastrichtian, in Sample 144-873A-9R-2, 122–125 cm, and Samples 144-873B-8N-1, 56–57 cm, to -10N-1, 62–65 cm. A slightly different assemblage is recorded in Samples 144-873A-11R-2, 105–107 cm, to -11R-2, 135–139 cm, where a single, questionable specimen of *O. macroporus* is associated with poorly identified *Vaughanina* and *Pseudorbitoides.* At DSDP Site 462, the last two taxa are recorded within the *Globotruncanita calcarata* Zone of latest Campanian age. This dating would be consistent with the Campanian age inferred for the lower part of the limestone sequence by calcareous nannofossils, but it is inconsistent with the presence of *Omphalocyclus.* Further study is needed to clarify this discrepancy.

It is worth noting that the larger foraminifer assemblage recorded at Site 873 exhibits affinities with faunas from both the Caribbean and the Tethyan bioprovinces.

Paleoenvironment of Carbonate Platform Sediments

Three distinct fossil assemblages (numbered I–III) can be differentiated within the platform carbonate sequence (Lithologic Unit III) on the basis of diversity, dominant groups, and secondary taxa. Minor variations in distribution of some taxa within the assemblages were also detected. The distributions of the most important taxonomic groups that characterize these informal units are illustrated in Figures 31 and 32.

Paleoecologic Assemblage I (Intervals 144-873A-2R-1, 0–5 cm, to -5R-1, 13–18 cm; Intervals 144-873B-8N-1, 4–8 cm, to -10N-1, 106–108 cm) is characterized by abundant corallinacean algae, rudists, and the larger foraminifers *Sulcoperculina* and *Asterorbis.* Less frequent components are echinoderms and miliolids (Figs. 32–33). Other benthic foraminifers such as *Idalina antiqua, Vidalina* sp. cf. *V. hispanica, Pseudocyclammina,* and *Marssonella* are rare. The distribution of the various taxa, however, is uneven from layer to layer with miliolids, *I. antiqua,* and echinoderms more common when red algae, *Asterorbis,* and *Sulcoperculina* decrease in abundance.

The upper part of the carbonate platform was recovered only in Samples 144-873B-8N-1, 71–73 cm, through -9N-1, 130–135 cm; there the assemblage is characterized by very abundant *Omphalocyclus macroporus* associated with common echinoderms and few ostracodes, in addition to the fossil groups already mentioned.

This subassemblage indicates that during this interval the central part of the platform was under normal marine conditions, occasionally passing to shallower, possibly slightly more restricted environments, as suggested by a decrease in total diversity and the increasing abundance of miliolids.

Paleoecologic Assemblage II (Intervals 144-873A-5R-1, 41–46 cm, to -8R-2, 0–3 cm) differs from Assemblage I by the relatively persistent occurrence of common miliolids, gastropods, ostracodes, and discorbids associated with few echinoderm fragments. Corallinacean algae, rudists, *Sulcoperculina,* and *Asterorbis,* together with the fruiting bodies of the dasycladacean *Terquemella,* display a rhythmic distribution alternating from common to absent. The assemblage

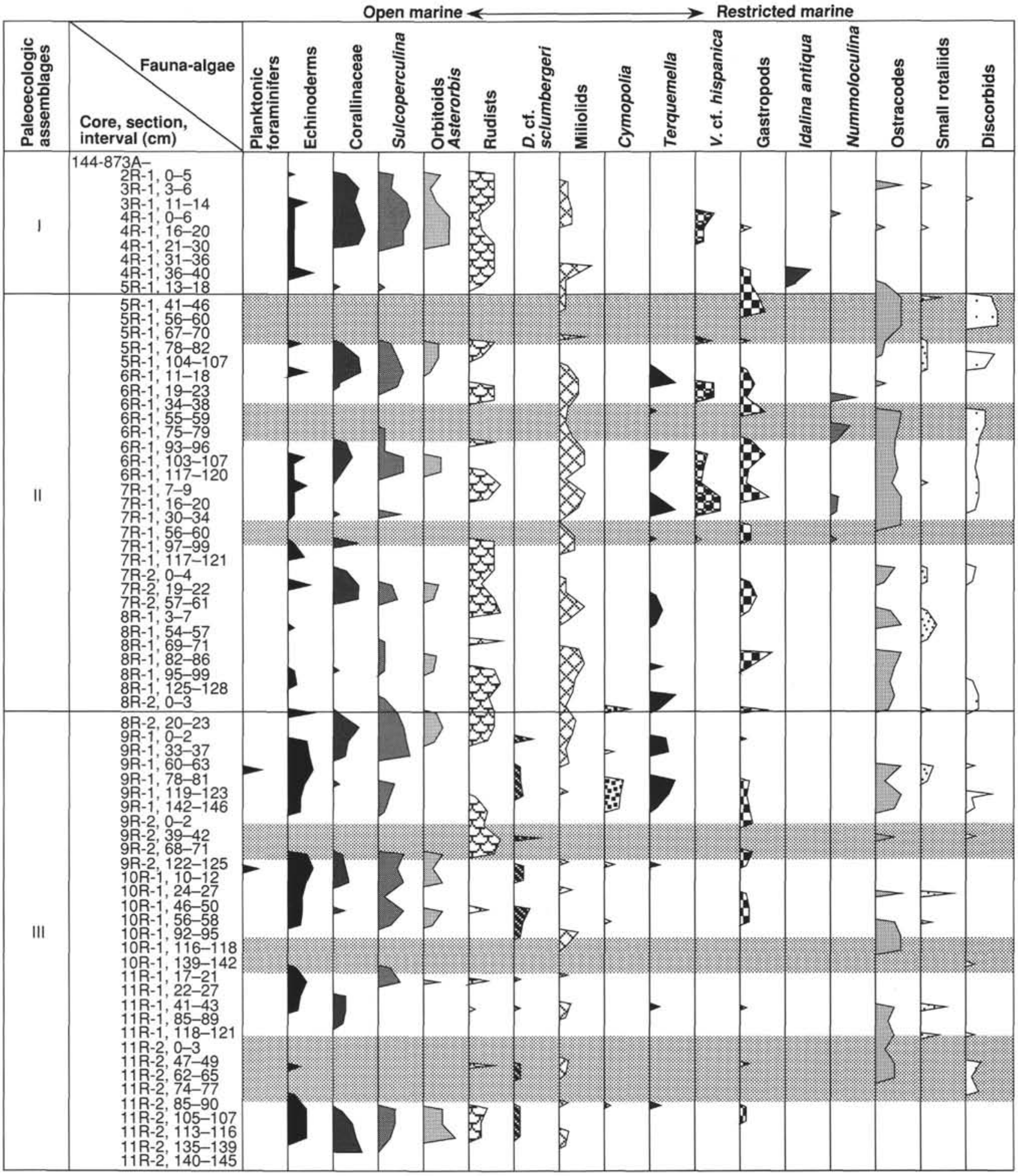

Figure 31. Distribution and relative abundance of paleoecologically significant organism groups in Lithologic Unit III, Hole 873A. Loosely hatched area = more restricted environmental conditions.

becomes less diversified in the lower portion of this interval, with larger calcareous foraminifers present in few layers.

Overall, this assemblage can be interpreted as characteristic of a lagoonal environment with strong marine influences but not open-marine conditions. These conditions alternate with episodes of a more restricted, possibly very shallow environment (intertidal to supratidal?), as determined by the depauperate assemblage. Horizons of emergence are suggested by the presence of dissolved shells, early infillings, and microcavities (see also "Lithostratigraphy" section, this chapter) in some layers (e.g., in Sample 144-873A-5R-1, 41–46 cm).

Paleoecologic Assemblage III (Intervals 144-873A-8R-2, 20–23 cm, to -11R-2, 140–145 cm) is defined by the occurrence of *Dicyclina* sp. cf. *D. schlumbergeri* and the dasycladacean alga *Cymopolia*? in the absence of *Vidalina* sp. cf. *V. hispanica* and *Nummoloculina*. A

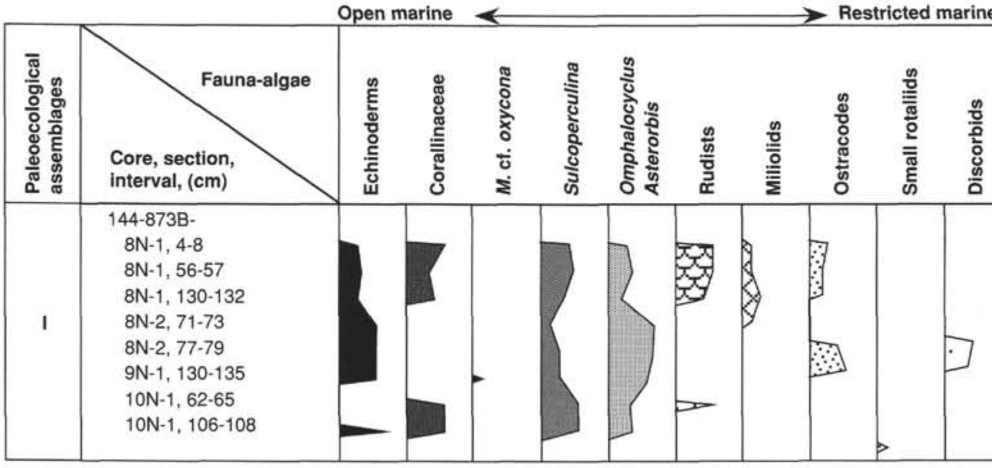

Figure 32. Distribution and relative abundance of significant organism groups from Lithologic Subunit IIIA, Hole 873B, arranged according to their paleoecologic affinities.

few specimens of *Pseudocyclammina* (e.g., Samples 144-873A-9R-1, 33–37 cm, and 9R-1, 60–63 cm) and *Montsechiana* sp. cf. *M. montsechiensis* (Samples 144-873A-9R-1, 33–37 cm, -10R-1, 24–25 cm, and -11R-1, 22–27 cm) occur within this interval. The most consistent components are echinoderms, corallinacean algae, rudist fragments, ostracodes, gastropods, miliolids, and *Sulcoperculina;* they all decrease in abundance in the lower part of this interval, however. *Terquemella* occurs in the upper samples. Discorbids and small rotaliids are few and scattered throughout. Planktonic foraminifers occur at two levels (Samples 144-873A-9R-1, 78–81 cm, and -10R-1, 10–12 cm; see above). Small, rounded, pyritized extraclasts occur frequently.

Three discrete intervals, characterized by a very low diversity, divide this assemblage interval into roughly four parts (see Fig. 32). The uppermost part yields an assemblage characterized by the maximum diversity in fauna and frequent bioturbation (Fig. 32). In general, faunas and floras dominated by corallinacean fragments, *Sulcoperculina, Orbitoididae,* and bivalve and echinoderm fragments alternate with ones dominated by Discorbidae, small rotaliids, and ostracodes. Diversity gradually decreases downward except in the lowermost part of the interval, in which higher diversity resumes along with coarser skeletal fragments, many of which are probably reworked.

The succession of fossil faunas and floras at the base of the carbonate sequence can be interpreted as characteristic of a gradually deepening environment under normal marine conditions. This is demonstrated by a peak in diversity and by the presence of planktonic foraminifers in the upper part of the interval, probably indicating the point of maximum water depth. This trend, however, was interrupted by periods characterized by shallower environments (intertidal to supratidal?), as demonstrated by interbedded horizons with poorly diversified flora and faunas.

Palynomorphs

Pelagic Cap

No dinoflagellates, pollen, or embryophyte spores were seen in the HCl-insoluble fraction (unsieved and sieved >20 μm) of the six core-catcher samples through the pelagic cap (Samples 144-873B-1H-CC to -6H-CC) plus one additional sample from the top of Section 144-873B-1H-2.

Palynofacies

Based on other organic remains such as (1) loosely granular amorphogen clasts with numerous inclusions of fine, colorless mineral particles (interpreted to be fecal pellets or fragments of them); (2) the organic infilling of foraminifer chambers: and (3) a diverse group of mainly dark-brown- to amber-colored fragments of for-aminifer linings, two distinct palynofacies units were recognized (Fig. 30).

Palynofacies Unit I (Samples 144-873B-1H-CC through -3H-CC) is defined by the dominance of well-preserved fecal pellets together with rarely occurring foraminifer linings and fragments. Foraminifer infillings also occur rarely. The organic component is well preserved. Unsieved residues from Palynofacies Unit I contain common silt-sized quartz grains and abundant small (mostly <5 μm) colorless mineral grains.

Palynofacies Unit II is recognized in Samples 144-873B-4H-CC through -6H-CC (Fig. 30). It is defined by common to dominant foraminifer linings and fragments and moderate to rare occurrences of fecal pellets. Foraminifer infillings are rare to common. The organic component is moderately preserved in Samples 144-873B-4H-CC and -5H-CC, but poorly preserved in Sample 144-873B-6H-CC. Unsieved residues from Palynofacies Unit II contain only rare mineral grains and silt.

The boundary between Palynofacies Units I and II coincides with a major disconformity in Hole 873B, representing most or all of the upper Miocene. Differences between Palynofacies Units I and II are interpreted to be largely taphonomic. Notably, sediments of Palynofacies Unit II (foraminifer ooze) have been more greatly winnowed than those of Palynofacies Unit I (nannofossil foraminifer ooze). It is thus feasible that the high relative abundance of foraminifer linings characterizing Palynofacies Unit II results from concentration through disintegration followed by winnowing of the more fragile fecal pellets.

Silt-sized quartz is common throughout Palynofacies Unit I. It is least common at the base of Palynofacies Unit I in Sample 144-873B-3H-CC and may relate to a similar horizon in the pelagic cap of Lo-En Guyot (Site 872). The horizon occurs within the lower Miocene at both sites and is hypothesized to reflect a sustained change in atmospheric/oceanic conditions that brought wind-blown silt to this part of the western Pacific and caused a reduction in velocity (and thus winnowing potential) of intermediate-depth waters.

Platform Carbonates (Hole 873A)

Eight samples from the platform carbonate sequence of Hole 873A were processed for palynology. One sample (Sample 144-873A-6R-1, 62–67 cm) is from a pale fine-grained limestone; the others are from the underlying medium to dark gray limestone.

All samples have a strong terrigenous representation. This is most pronounced in the lower part of the interval studied (Sample 144-873A-11R-2, 1–3 cm), in which woody and cuticular tissues predominate.

Dinoflagellates occur in Samples 144-873A-11R-2, 1–3 cm, through -8R-1, 128–137 cm, but their relative abundance is greatest in Core 144-873A-9R, suggesting increased marine influence in this part of the sequence. However, dinoflagellates are never abundant, and their low overall diversity indicates restricted marine conditions throughout their occurrence. Stratigraphic index species were not encountered, but the assemblage in toto suggests a Maastrichtian age. The dark gray color of the samples examined is largely caused by pyrite. One sample (Sample 144-873A-9R-2, 29–34 cm) has a moderate amount of organic matter and almost no pyrite; it is grayish brown in color.

Sample 144-873A-6R-1, 62–67 cm, is white and fine grained. The organic residue was found to be extremely lean, comprising just some membranous cuticle and wood fragments in the >20-μm fraction, although some small algal? vesicles were seen in the unsieved fraction. No pyrite was seen. Sample 144-873A-8R-1, 128–137 cm, is medium gray and fine grained. The organic residue is lean and many fragments are corroded. A few dinoflagellates were recorded, including *Operculodinium* sp. cf. *O. israelianum*. A single, smooth, trilete fern spore was also seen.

Sample 144-873A-9R-1, 79–83 cm, is dark gray and fine grained. The residue is moderately organic rich and very pyritic. Woody and cuticular tissues and microforaminifer linings are all abundant. Flocs of algal amorphogen with imbedded pyrite are common. Dinoflagellates are fairly common and include the following taxa: *Pyxidinopsis*? sp., *P. challengerensis*?, *Cordosphaeridium multispinosum*, *Operculodinium* sp. cf. *O. israelianum*, and *Spiniferites* sp. Fungal spores were also seen.

Sample 144-873A-9R-2, 29–34 cm, is medium gray-brown and fine grained. The residue is moderately organic rich and almost free of pyrite. Woody and cuticular tissues are common, together with thin-walled hyaline spherical palynomorphs that are possibly algal spores. Dinoflagellates are common and well preserved, with *Operculodinium* sp. cf. *O. israelianum* dominating the assemblage, and *C. multispinosum* occurring occasionally. Ferns are represented by occasional smooth and sculptured trilete spores and a single foveolate monolete spore.

Sample 144-873A-9R-2, 93–99 cm, is dark gray and fine grained. The residue is moderately organic rich and has abundant pyrite. Degraded woody and cuticular material is abundant. Flocs of pyrite-impregnated amorphogen are common. Foraminifer linings and translucent fungal hyphae are fairly common. Dinoflagellates are also fairly common and are represented mainly by *C. multispinosum*, together with occasional specimens of *Cordosphaeridium inoides*, *Spiniferites* sp., and *Dinogymnium* sp.

Sample 144-873A-11R-1, 9–13 cm, is dark gray, laminated, and fine grained. The residue is lean and consists mainly of pyrite. Organic remains are sparse but include some woody fragments, some pyrite-impregnated algal amorphogen, and thin, baglike palynomorphs that may be of algal affinity.

Sample 144-873A-11R-2, 1–3 cm, is dark gray, wavy-laminated, and fine grained. The organic residue is exceptionally rich with woody tissues predominating. Cuticle is common, foraminifer linings occur occasionally, and dinoflagellates are documented by a single specimen assignable to *Spiniferites*. Pyrite is abundant.

Sample 144-873A-11R-2, 80–84 cm, is dark gray and fine grained. The residue is lean and contains pyrite. Organic remains are mainly woody and cuticular; they are fairly corroded. There are occasional flocs of algal amorphogen, these being imbedded with fine pyrite, and rare torn dinoflagellates assignable to *Operculodinium*? and to *Cordosphaeridium*?.

Siliceous Microfossils and Early Silica Diagenesis

Pelagic Cap

The HCl-insoluble residue was examined for abundance of siliceous microfossils and authigenic silicates, from all core-catcher samples through the pelagic section of Hole 873B (Fig. 33). The occurrence of siliceous microfossils in the Neogene pelagic sediments is very similar to that found on Limalok and Lo-En guyots. Rare diatoms, radiolarians, archaeomonadaceans, and sponge spicules occur through Core 144-873B-1H and within Sample 144-873B-2H-1, 0–2 cm. The most common diatom species are *Thalassiosira leptoporus*, *Azpeitia nodulifer*, and *Ethmodiscus rex* fragments. These species are characteristic open-ocean forms; unfortunately, they have a long stratigraphic range and therefore are not useful for determining Pliocene to Pleistocene diatom zones. Isolated fragments of the more dissolution-resistant radiolarians persist to the base of Core 144-873B-2H. Below this level, silica dissolution is very intense. Not only does the abundance of zeolite crystals at the base of this core increase by more than 1 order of magnitude (Fig. 31), but also their size becomes much larger at this interval (Samples 144-873B-2H-CC and -3H-CC) than above.

A small peak of poorly preserved fragments of radiolarians occurs in the middle Miocene section (Sample 144-873B-4H-CC), as it did at Sites 871 and 872. The lower Miocene, which contained slightly more radiolarians in the previous sites, is represented by small quantities of chalk at Site 873.

Platform Carbonates

Three core-catcher samples from the Maastrichtian platform limestone in Hole 873B (Samples 144-873B-8N-CC through -10N-CC) were examined. All three samples contain rare zeolites, and one sample (Sample 144-873B-10N-CC) contains fragments of two diatom valves.

Clays

In Sample 144-873A-11R-2, 21 cm, which is a clay intercalated with limestones, the only siliceous microfossils found are a few monaxon sponge spicules.

Single siliceous sponge spicules as well as a single radiolarian fragment were recovered from the clays below the limestone sequence (Samples 144-873A-12R-CC and -13R-CC). No siliceous microfossils were found in Sample 144-873A-14R-CC. Further study is necessary to clarify if these finds of siliceous microfossils, in the upper half of the clays, are the result of downhole contamination.

Summary

The Campanian submergence of Wodejebato Guyot led to the establishment of a Campanian-Maastrichtian carbonate platform atop the weathered basaltic edifice. The generally low recovery of the carbonate platform sedimentary rocks (11.7% for Hole 873A) limits the interpretation of the platform sequence. However, some general trends are evident from the recovered material. Progressive flooding of the former island is evident in the lower part of the sequence, as represented by the interval containing Paleoecologic Assemblage III. Common plant remains and recurrent phases of restricted conditions (Paleoecologic Assemblage III interval) gave way to more open-marine conditions with common macro-algae and occasional invasions by planktonic foraminifers (upper Paleoecologic Assemblage III interval). The succeeding interval of Paleoecologic Assemblage II documents decreasing water paleodepth from the base to the top of the unit. This is indicated by the change from diverse assemblages (including rudists, coralline algae, and larger foraminifers) to increasingly depauperate assemblages. Evidence for restricted environments and emergence surfaces increases upsection in this interval. The interval of Paleoecologic Assemblage I documents a return to more open-marine conditions, with the rudist facies again dominating.

A manganese-encrusted, phosphatized limestone conglomerate is the first sedimentary record following the platform drowning. Pelagic carbonate was deposited atop the guyot during the late Paleocene. This material was subsequently broken, mixed with clasts of carbon-

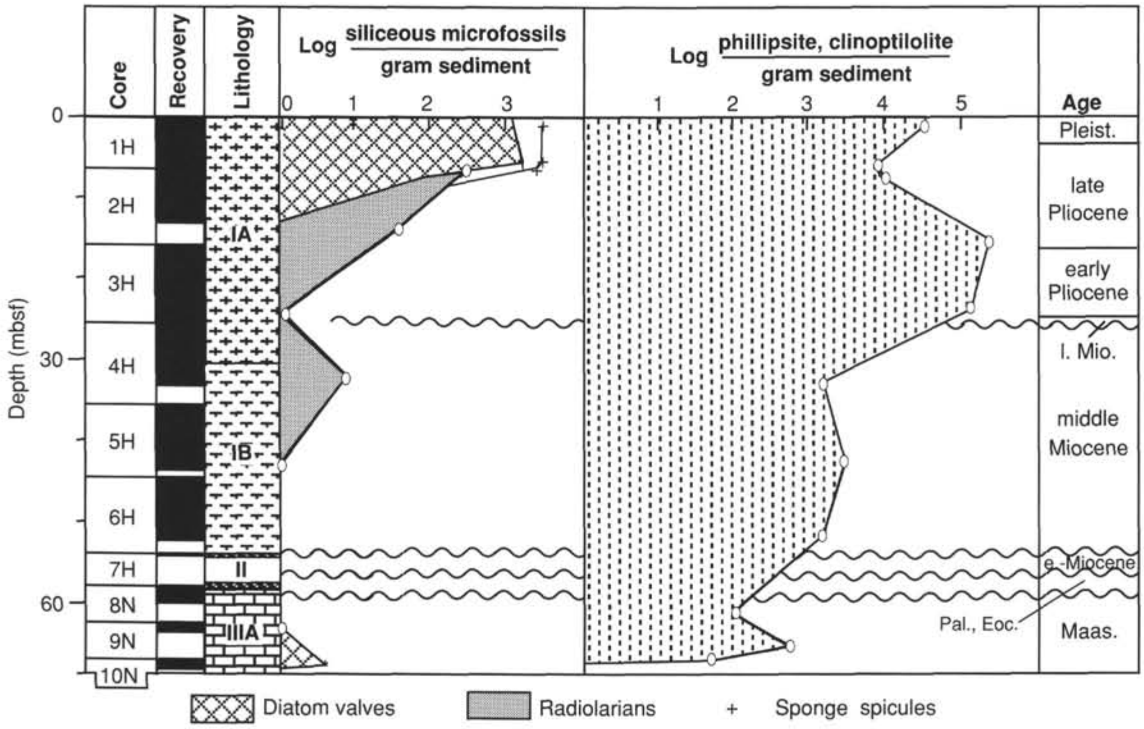

Figure 33. Siliceous microfossil and zeolite abundances in Hole 873B.

ate platform material, and phosphatized. These clasts were finally deposited in a matrix of pelagic ooze during the early Eocene. This conglomerate was encrusted by manganese oxides with intercalated nannofossil ooze during the late middle Eocene.

Deposition of calcareous pelagic ooze was sporadic throughout the Neogene, with accumulation and preservation occurring during the earliest Miocene, middle Miocene, and latest Miocene to early Pleistocene. Several additional hiatuses in sediment accumulation and preservation occurred during the latter two intervals. Relatively intense current activity, resulting in winnowed foraminifer oozes, characterized the early and middle Miocene. Following a major hiatus in the late Miocene, deposition resumed in the latest Miocene. Current activity was less intense in the Pliocene and Pleistocene, as evidenced by decreased winnowing of the nannofossil foraminifer oozes.

PALEOMAGNETISM

Initial magnetic susceptibility was measured at 5-cm intervals for most sections from the pelagic sediments in Hole 873B (Cores 144-873B-1H through -6H). Susceptibility in these cores is low (Fig. 34A); susceptibility peaks near core tops are probably associated with rust contamination. The downhole decrease in susceptibility near 10 mbsf is similar to that observed at Sites 871 and 872 (see "Physical Properties" section, this chapter, for a further discussion). The susceptibility of limestone cores was not routinely measured because of the low recovery.

Susceptibility in the clay interval (Cores 144-873A-12R and -13R; 155.9–175.1 mbsf) varies by more than 2 orders of magnitude (Fig. 34B). The highest values in this interval (ca. 6.0×10^{-3} cgs) are comparable with those measured in basaltic cores from this site (up to 5×10^{-3}cgs) and at previous sites (see "Paleomagnetism" section, "Site 871" and "Site 872" chapters, this volume). The intrinsic volume susceptibility of hematite is low (ca. $3–30 \times 10^{-3}$ cgs), roughly a factor of 100 lower than the value for magnetite (O'Reilly, 1984). Although X-ray diffraction (XRD) results suggest abundant hematite, the highest susceptibility peaks probably are not caused by the presence of hematite as this would require very high proportions of hematite. Thus, the susceptibility highs may reflect relatively less altered basaltic material with relict spinel phases also contributing to the measured susceptibility. Susceptibility values in the volcaniclastic material at the base of Hole 873A range from 1×10^{-4} to 5×10^{-4}cgs, about 1 order of magnitude less than that of the basalts. The volcaniclastic sediments are also characterized by a correspondingly low natural remanent magnetization.

Remanence measurements with the pass-through cryogenic magnetometer were made on the archive halves of pelagic cores from Hole 873B and on selected pieces of more indurated carbonate material from Hole 873A. The pelagic sediment from Hole 873B was treated in the same manner as the pelagic sediment from Hole 872C, with the sections stored vertically and the excess water drained. The resulting magnetic data (Fig. 35) have exclusively positive inclinations; therefore, no magnetostratigraphic interpretation was possible. The low magnetization of the Upper Cretaceous carbonates (Cores 144-873A-2R to -11R) precluded measurement of discrete (10 cm^3) samples. Instead, larger pieces of limestone from the archive half were demagnetized and measured in whole-core mode. Inclinations inferred from the pass-through measurements are generally between −30° and +30°, compatible with an original magnetization acquired at relatively low latitudes (see discussion below). Although results from these samples suggest that a reversal stratigraphy may be obtained from shore-based measurements, we have not attempted any magnetostratigraphic interpretation here.

Three discrete samples of basalt and two discrete samples from the volcaniclastic unit at the base of Hole 873A were measured with the pass-through cryogenic magnetometer (Table 4 and Figs. 36–37). These samples were demagnetized with the 2G coils (to a peak field of 20 mT) because the Schonstedt demagnetizer was temporarily out of order. All five samples have positive (downward) inclinations (+17° to +27°). The polarity is ambiguous as the inclinations are similar to the present field (13°) and geocentric axial dipole (24°) inclinations at the site. However, the presence of a small secondary component of magnetization nearly antipodal to the characteristic remanent magnetization (Figs. 36C and 37C) suggests that this positive inclination represents a reversed magnetization acquired at a low

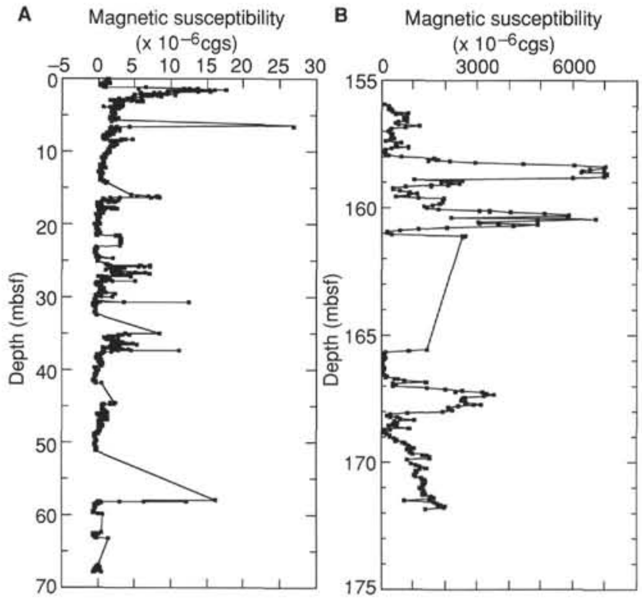

Figure 34. Magnetic susceptibility variations within the pelagic sediments from Hole 873B (**A**) and in the clay interval (Cores 144-873A-12R and -13R) from Hole 873A (**B**).

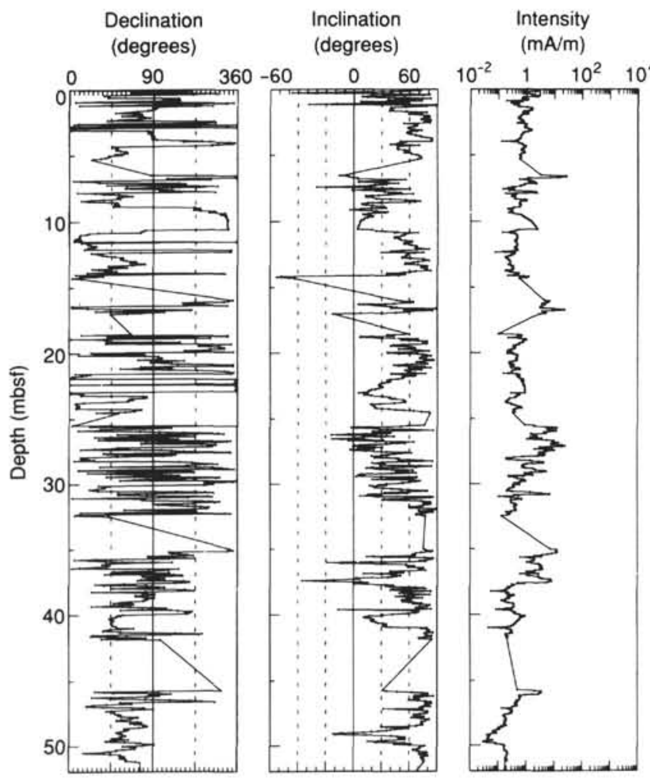

Figure 35. Declination, inclination, and intensity variations for Cores 144-873B-1H to -6H.

latitude (ca. 9°–14°S) in the Southern Hemisphere. Whole-core measurements from the clay interval (Cores 144-873A-12R to -13R) and from volcaniclastics at the base of Hole 873A yield similar positive inclinations (+20° to +30°; Fig. 38). This positive inclination may suggest that the reversed polarity magnetization extends at least as high as 155 mbsf.

SEDIMENTATION RATES

Sedimentation rates were calculated for the pelagic sediments recovered at Hole 873B using the age assignments for calcareous nannofossil and planktonic foraminifer datums taken from Berggren et al. (1985) (Table 5). Sediment accumulation is plotted graphically in Figure 39. Paleomagnetic data are not available because of core disturbance (see "Paleomagnetism" section, this chapter).

Benthic organisms (rudists and larger foraminifers) from the platform carbonates provide a Campanian to Maastrichtian age (for details see "Biostratigraphy" section, this chapter), but the age constraints are too imprecise to estimate accumulation rates.

Pelagic Cap

Following a long hiatus that extended from the middle Eocene (nannofossil Subzone CP14a and foraminifer Zone P12) through the Oligocene, pelagic sedimentation resumed in the earliest Miocene (nannofossil Subzone CN1a+b). Most of the lower Miocene is missing and a hiatus of 5 m.y. is estimated.

Foraminifer ooze began to accumulate in the early middle Miocene (nannofossil Zone CN4 and foraminifer Zone N8) at a rate of approximately 8 m/m.y. Within the middle Miocene, a short hiatus (approximately 1 m.y.) is inferred in the lowermost part of Core 144-873B-5H, at the boundary between nannofossil Zones CN4 and CN5.

The upper middle Miocene and a significant part of the upper Miocene interval are not recorded and the hiatus represents approximately 6 m.y. of missing time. During the early Pliocene, sediment accumulated at an accelerated rate of 20 m/m.y., but a short hiatus is noted across the lower/upper Pliocene boundary. For the remaining part of the sequence (upper Pliocene through Pleistocene), sediment accumulation rates are on the order of 15–20 m/m.y.

Sediment accumulation rates on Wodejebato Guyot are comparable with those observed on Lo-En and Limalok guyots only for the Pliocene to Pleistocene interval (see "Sedimentation Rates" section, "Site 871" and "Site 872" chapters, this volume). In the Miocene, hiatuses of various durations were recorded in different intervals on the three guyots.

INORGANIC GEOCHEMISTRY

Interstitial Waters

Interstitial waters were taken from seven core samples in Holes 873A and 873B; these were analyzed according to the methods outlined in the "Explanatory Notes" chapter (this volume). These methods were slightly modified to determine if there was a discrepancy between the first 30 ml of interstitial water squeezed out of the sediment and the subsequent interstitial water (labeled "second squeeze"). It was determined that the "second squeeze" chemical data are less contaminated with seawater than the data from the first squeeze. Data are presented from the second squeeze, where available.

Six of the seven samples came from calcareous oozes in the upper 54 m of sediment from the pelagic cap in Hole 873B. Limestones were cored from 54 to 149 mbsf; therefore, no interstitial water samples were extracted from this interval. A single interstitial water sample was extracted from soft sediment (primarily clay) recovered at 170 mbsf in Hole 873A. Shipboard interstitial water data from Site 873 are presented in Table 6.

Salinity and Chlorinity

Pore-water salinity values of samples from Holes 873A and 873B are indicative of normal seawater (consistently 35 ppt). Chlorine content is largely that of normal seawater (546–554 mM Cl^-).

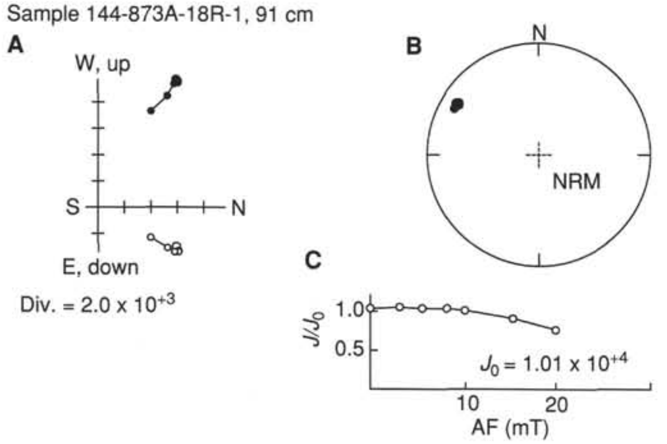

Figure 36. Alternating-field (AF) demagnetization results for basalt Sample 144-873A-18R-1, 91 cm. Demagnetization fields are 0, 2, 5, 7, 10, 15, and 20 mT. **A.** Orthogonal vector plot of the progressive AF demagnetization. Closed circles represent horizontal components of the magnetization, and open circles represent vertical components. **B.** Stereonet plot of vector end-points after progressive demagnetization. **C.** Variation of intensity after progressive AF demagnetization.

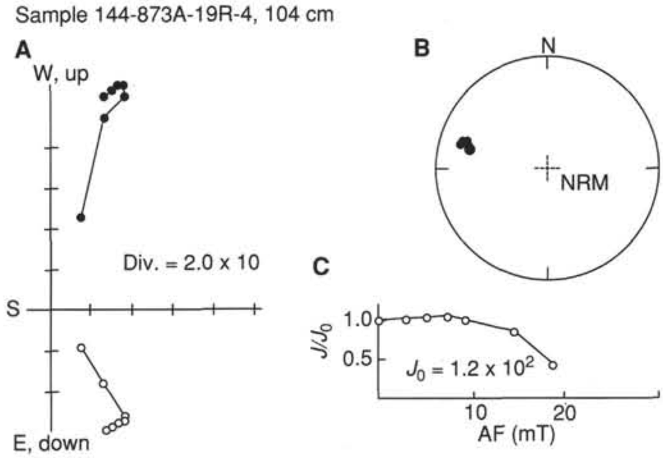

Figure 37. Alternating-field (AF) demagnetization results for basalt Sample 144-873A-19R-4, 104 cm. Demagnetization fields are 0, 2, 5, 7, 10, 15, and 20 mT. Other plot conventions are identical to Figure 36.

Alkalinity, pH, Calcium, Magnesium, Sodium, Strontium, Potassium, Rubidium, and Lithium

Concentrations of sodium, potassium, rubidium, and lithium in samples from the sediment of Hole 873B remain constant with increasing sub-bottom depth, similar to the seawater concentration of each element (Fig. 40). Mean values of pH (7.80 ± 0.20) and alkalinity (2.66 ± 0.05 mM/g) measured on these same sediment samples show no depth trend. Alkalinity from Sample 144-873A-13R-3 is 1.21 mM/g, significantly different from the shallower samples. Alkalinity depletion is indicative of calcium carbonate precipitation at this depth. Magnesium/calcium ratios steadily decline throughout the pelagic sediment sequence (Fig. 40).

Minor element compositions in Sample 144-873A-13R-3, 140–150 cm, are consistent with chemical exchange between the interstitial water and the clay. Alteration is evident with respect to calcium, magnesium, potassium, strontium, rubidium, sodium, lithium, and fluoride. Concentrations of calcium and strontium increased whereas magnesium, potassium, fluoride, lithium, sodium, and rubidium decreased in these interstitial waters relative to overlying water samples (Table 6 and Fig. 40).

Silica

Silica concentrations of the interstitial water samples from Hole 873B range from 123 to 132 µM. These values are consistent with silica concentrations of Pacific seawater at 1400 m depth. The silica content of interstitial water from Sample 144-873A-13R-3, 140–150 cm, is unchanged relative to seawater.

Sulfate and Ammonium

Sulfate contents of the interstitial waters from the pelagic cap sediments are equal to seawater values, approximately 29 mM. A slightly lower sulfate concentration (26 mM) in Sample 144-873A-13R-3, 140–150 cm, is indicative of some local sulfate reduction. Ammonium contents vary between 29 and 46 µM in interstitial waters from the pelagic cap sediment samples but increase to 130 µM in the interstitial water from Sample 144-873A-13R-3, 140–150 cm. The increased ammonium content provides additional evidence of locally reducing conditions near this sample.

Fluoride

Fluoride concentrations within seawater are typically 68–70 µM (e.g., Brewer, 1971), whereas the fluoride concentrations of the interstitial waters from the pelagic cap sediments are consistently near 88 µM (Hole 873B). The fluoride content of interstitial water from the clay (Hole 873A) is reduced to 57 µM.

Conclusions

Interstitial water chemistry from Site 873 is remarkable for a number of reasons. First, the fact that significant chemical gradients are preserved in the interstitial waters from these sandy pelagic sediments is unusual when compared with the relatively constant chemical gradients measured from Sites 871 and 872. Second, Mg/Ca ratios from the interstitial waters of the pelagic cap decrease with depth. The simplest explanation for this would be that these waters are in chemical communication with the interstitial water from the sediments beneath the limestone, where the magnesium-calcium exchange is presumably taking place. If this is true, then there must be an unmeasured Mg/Ca gradient within interstitial water through the limestone sequence.

ORGANIC GEOCHEMISTRY

At Site 873, in addition to safety monitoring for hydrocarbon gases, 37 samples were analyzed to determine the content of inorganic carbon (IC), total organic carbon (TOC), nitrogen (N), and total sulfur (TS). Moreover, 5 samples were analyzed for organic matter type by the Rock-Eval instrument. The procedures used for the analytical program are described in the "Organic Geochemistry" section, "Explanatory Notes" chapter (this volume).

Volatile Hydrocarbons

The shipboard safety and pollution monitoring program requires measurements of light hydrocarbon gases (C_1 to C_3) in cores immediately after retrieval onto the core deck. At Site 873, four headspace gas samples were obtained from the pelagic carbonate ooze in Hole 873B. Cores from Hole 873A consisted mainly of indurated limestone with little recovery, so sampling for headspace gas was impossible. The results of the headspace gas analyses are given in Table 7. Very low concentrations of light hydrocarbon gases were detected. Methane concentrations varied between 2 and 3 ppm. These numbers are

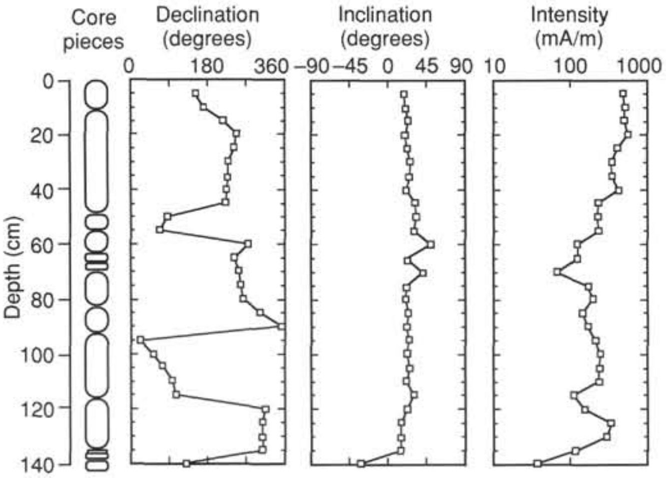

Figure 38. Representative declination, inclination, and intensity variations for Section 144-873A-21R-2 within the volcaniclastic section. Note that the longer continuous pieces (column at left) are characterized by consistent declinations and an inclination of 20°–30°.

only slightly higher than the general background of methane in the laboratory and on the core deck, which was found to be 2.2 and 1.8 ppm, respectively. Traces of ethane and propane were found in two of the samples. The very low light gas concentration in the pelagic cap can be attributed to low concentrations of organic carbon in these sediments (TOC below 0.3%; see paragraph on organic carbon).

Carbonate Carbon

Inorganic carbon (IC) content was measured in 37 samples from Holes 873A and 873B with the Coulometrics carbon dioxide coulometer. In the indurated limestone intervals of Holes 873A and 873B, 30 microsamples (approximately 100 mg each) were collected by means of a hand drill using a standard 5-mm drill bit. Sampling was performed in a way to obtain representative samples with regard to both lithofacies and depth. One sample was analyzed from the red clay underlying the limestone in Hole 873A. In addition to this, one sample from each core of the pelagic cap in Hole 873B was analyzed for IC. These samples were obtained from the material squeezed for pore-water analysis (as described in the "Inorganic Geochemistry" section, "Explanatory Notes" chapter, this volume). By this approach, samples should be virtually free of pore water before drying and no pore-water precipitates are expected.

The IC and calcium carbonate values for Holes 873A and 873B are given in Tables 8–9, and calcium carbonate data are shown in Figure 41. Carbonate content was very high in all samples from the pelagic cap in Cores 144-873B-1H through -6H (Lithologic Subunits IA and IB), ranging from 96% to 98% (average $CaCO_3$ = 97.1%). No significant changes were seen with depth. Similar high carbonate values were found in the light pale platform limestone sampled from Cores 144-873A-5R through -7R, and Cores 144-873B-8N through -10N (Lithologic Subunit IIIA, average $CaCO_3$ = 97.9%). The shallow-water limestone in Cores 144-873A-8R through -11R (Lithologic Subunit IIIB), characterized by gray skeletal wackestones and packstones and visible pyrite, contained slightly lower, but variable amounts of carbonate (average $CaCO_3$ = 94.3%). The lowest values of carbonate in this unit were found in the gray, partly laminated packstones and grainstones from Section 144-873A-11R-1, 98 cm, through Section 144-873A-11R-2, 17 cm, and in the dark, clayey chalk of Interval 144-873A-11R-2, 17–22 cm. These low carbonate values cannot be completely attributed to increased amounts of organic matter and pyrite in the rock, and a higher terrigenous input must also be considered. The red clay below the limestone in Core 144-873A-12R-1 (Lithologic Unit IV) is virtually carbonate free.

Organic Carbon and Total Sulfur

The content of total carbon (TC) and total sulfur (TS) was determined using the Carlo Erba Model NA1500 elemental analyzer. Total organic carbon (TOC) values were calculated from the difference between TC and IC. Detection limits for TOC and TS are 0.2% and 0.02%, respectively. The results of the TOC and TS determinations are given in Tables 8–9 and Figure 41.

In the pelagic cap (Lithologic Unit I), TOC was below 0.3% in all samples investigated. No sulfur was detected. Similar low values were found in the upper part of the platform limestone (Lithologic Subunit IIIA). The lower part of the platform limestone, characterized by gray colors and visible pyrite (Lithologic Subunit IIIB), was slightly enriched in TOC (average = 0.43%) and TS (average = 1.16%). Very high sulfur values were found in Sample 144-873A-8R-1, 108–110 cm, which is a pyrite-bearing algal wackestone. The measured sulfur content varied from 25% to 35%, which corresponds to approximately 50%–65% pyrite. The sample probably represents a strongly sulfate-reducing microenvironment. Values of TOC up to 2.5% were measured in the partly laminated packstones and grainstones from Sections 144-873A-11R-1, 98 cm, through -11R-2, 17 cm, and the dark clayey chalk of Interval 144-873A-11R-2, 17–22 cm. Macroscopic plant remains were observed on bedding surfaces of the laminated packstones (see "Biostratigraphy" section, this chapter), suggesting that the organic matter was dominantly of terrestrial origin. Sulfur and TS/TOC values were below 1% and 1.5%, respectively, in all samples.

The underlying clay (Lithologic Unit IV) contained no detectable organic matter and very little sulfur (0.08%).

Organic Matter Type and Thermal Maturation Level

Shipboard geochemical characterization of organic matter is performed by Rock-Eval (RE) and pyrolysis gas chromatographic (Py-GC) analysis. Only samples containing more than 1% organic matter are considered suitable for these types of analyses. During the time spent at Site 873, the Rock-Eval system was operating except for the T_{max} facility, and four samples from organic-rich Sections 144-873A-11R-1, 98 cm, through -11R-2, 22 cm (Lithologic Subunit IIIB) were analyzed for organic matter composition. The results are reported in Table 10 and Figure 42. As T_{max} data were not available, thermal maturation was evaluated from the production index (PI). This approach only provides approximate results. The samples were also analyzed by the Geofina Py-GC. No pyrolyzable organic matter was detected by this method.

Sample 144-873A-11R-1, 98–115 cm (Lithologic Subunit IIIB), is a laminated carbonaceous packstone that is partly bioturbated. TOC is high (2.4%), TS is moderate (0.5%), TS/TOC is low (0.21), S_1 is moderate, the hydrogen (HI) and oxygen (OI) indices are low (Fig. 42), and PI is low.

Sample 144-873A-11R-1, 130–136 cm (Lithologic Subunit IIIB), is a laminated skeletal grainstone. TOC is moderate (1.26%), TS is low (0.6%), TS/TOC is low (0.48), S_1 is moderate, HI is low, OI is moderate, and PI is moderate.

Sample 144-873A-11R-2, 0–17 cm (Lithologic Subunit IIIB), is a laminated packstone with plant fragments. TOC is high (2.79%), TS is low (0.4%), TS/TOC is low (0.16), S_1 is low, HI is low, OI is low, and PI is low.

Sample 144-873A-11R-2, 17–22 cm (Lithologic Subunit IIIB), is a dark, clayey chalk with visible pyrite. TOC is high (3.10%), TS is low (0.28%), TS/TOC is low (0.09), S_1 is below detection limit, HI is low, OI is low, and PI is below detection limit.

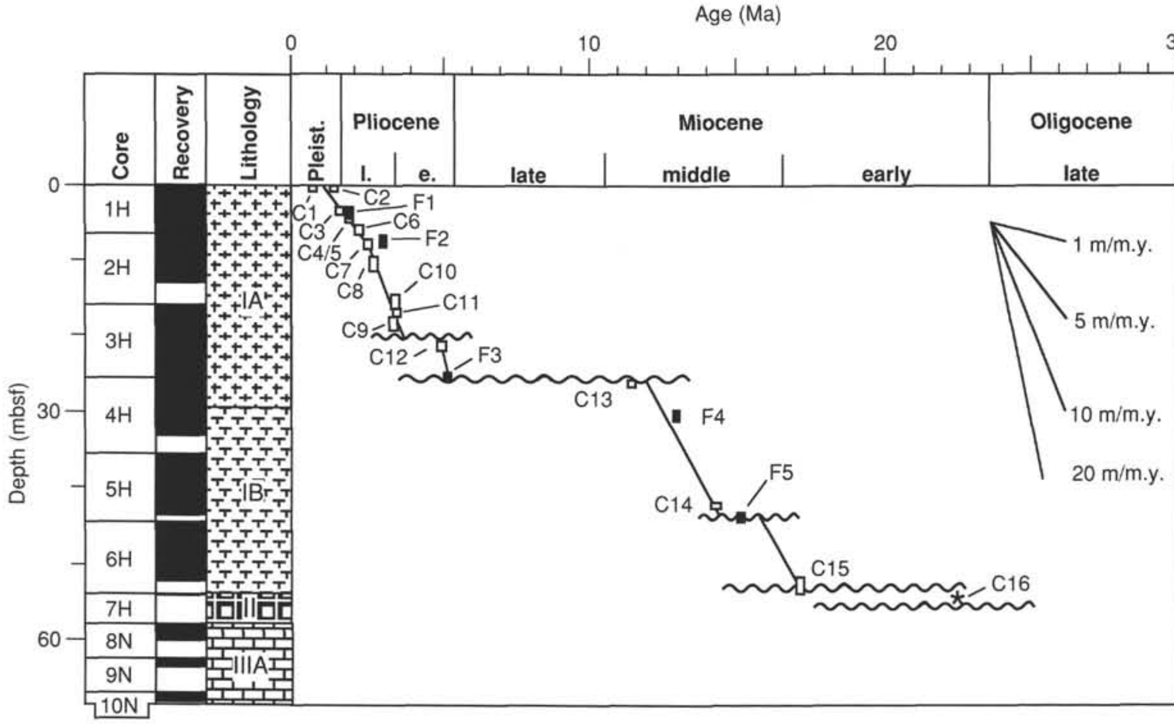

Figure 39. Sediment accumulation rates for the pelagic cap in Hole 873B. Bars represent the upper and lower limits of a biohorizon as constrained by sampling. Foraminifer biohorizons are indicated by filled bars, and calcareous nannofossils by open bars. Codes for biohorizons are keyed to Table 5.

Sample 144-873A-12R-1, 28–30 cm (Lithologic Unit IV), is a red clay that probably resulted from the subaerial weathering of basalt. TOC is very low (0.08%), and TS is very low (0.08%). The amount of organic matter was too low to yield reliable RE data.

Individual RE results should be interpreted with caution. However, in the present case, four samples representing at least three different lithofacies yielded corresponding results with regard to organic type and thermal maturation. The RE data indicate thermally immature to marginally mature organic matter of a composition corresponding to a type III ("woody" or vitrinitic) kerogen of terrestrial origin (Fig. 42). The observed thermal maturity level is normal for partly decomposed organic matter that has not been exposed to thermal modification. The low TS/TOC ratio suggests only limited influence from sulfate reduction (Fig. 43). The organic matter interpretation is in accordance with visual observations made from the same sections (see "Biostratigraphy" section, this chapter).

Organic Facies and Depositional Environment

Three major depositional environments are represented in Holes 873A and 873B: (1) pelagic (calcareous ooze, Lithologic Unit I); (2) shallow-water marine (platform limestone, Lithologic Unit III); and (3) terrestrial (red clay and weathered basalt, Lithologic Units IV and V).

In the first environment, preservation of organic matter was extremely poor. Values of TOC below 0.3% and of TS below the detection limit indicate deposition under oxic conditions with very low preservation potential for organic matter. Most of the organic matter was probably of marine origin, as indicated by the TOC/N ratios.

In the second environment, two organic facies can be distinguished. In the upper part of the platform limestone (Lithologic Subunit IIIA), TOC and TS values are very low. The frequent occurrence of algal structures in the limestone points to a depositional environment of relatively high organic productivity. The low TOC data, therefore, reflect very poor preservation of organic matter, probably under strongly oxic depositional conditions.

The lower part of the platform limestone is characterized by raised TOC and TS values. The gray colors seen in this unit are caused by finely disseminated pyrite. The high TS content and the pyritized algal structures point to sulfate-reducing conditions at the sediment/water interface or within the uppermost centimeter of the sediments, at least in sheltered microenvironments. However, as most of the organic matter found in this unit is of terrestrial (woody) origin, preservation potential for marine organic matter was poor. The co-occurrence of pyrite and woody material is typical for a near-coast, low-energy environment characterized by mildly reducing conditions, where most of the autochthonous, marine organic matter was decomposed by biological activity.

The very low content of organic matter and sulfur in the red clay below the shallow-water limestone (Lithologic Unit IV) probably reflects subaerial weathering under strongly oxidizing conditions.

Conclusions

The following conclusions can be made regarding the organic geochemistry at Site 873:

1. No volatile hydrocarbons were encountered at this site.
2. The pelagic cap sediments (Lithologic Unit I) have a calcium carbonate content of almost 100%. Only very low concentrations of organic matter have been encountered. The unit was deposited under oxic conditions.
3. The upper part of the platform limestone (Lithologic Subunit IIIA) consists of almost pure calcium carbonate with no detectable organic matter. The unit was exposed to oxic conditions during or subsequent to deposition.
4. The lower part of the platform limestone (Lithologic Subunit IIIB) contains minor amounts of pyrite and organic matter, predominantly of woody composition. The woody component indicates nearby

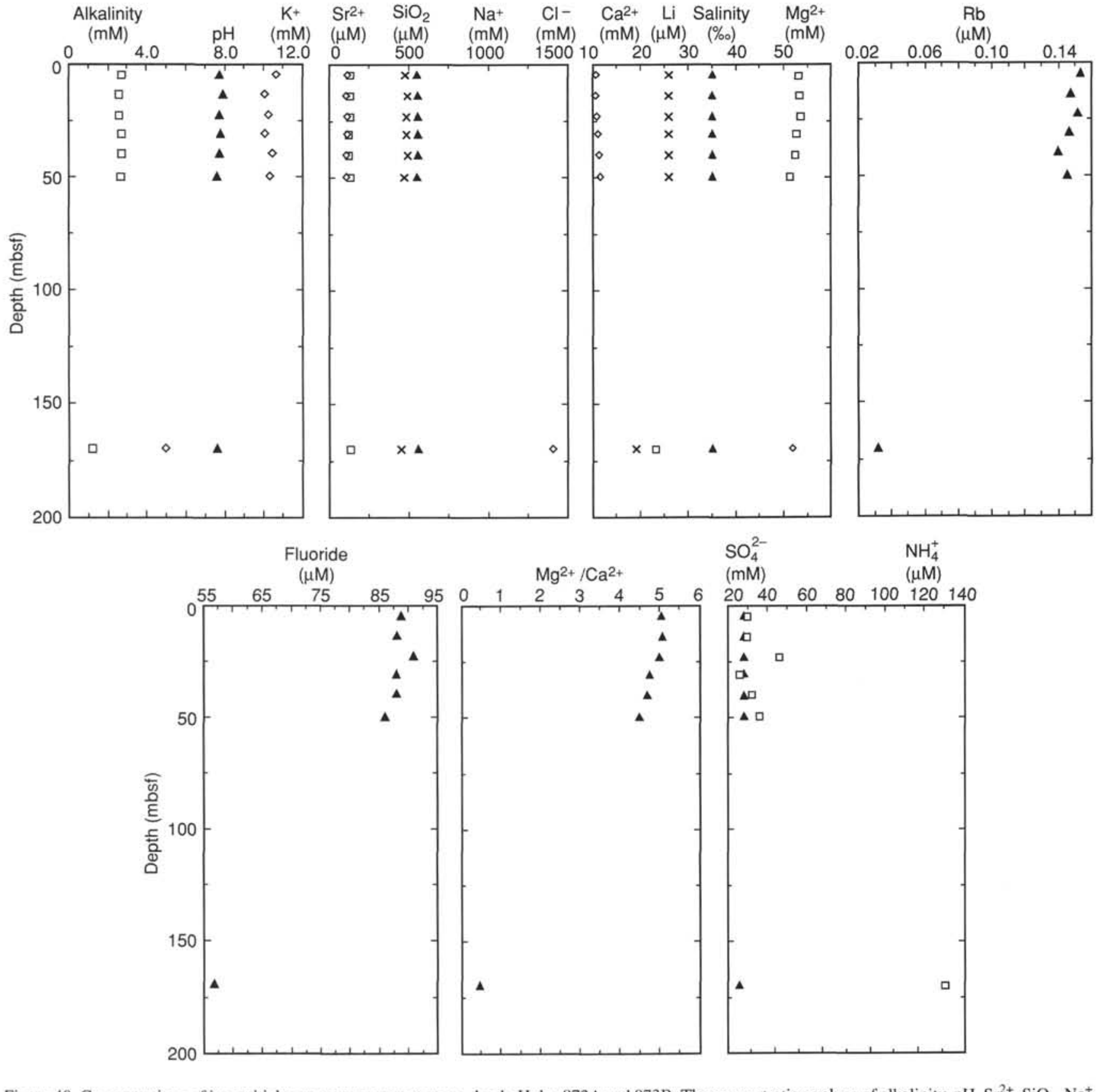

Figure 40. Concentrations of interstitial pore-water parameters vs. depth, Holes 873A and 873B. The concentration values of alkalinity, pH, Sr^{2+}, SiO_2, Na^+, Cl^-, Li, salinity, and Rb remain relatively constant values throughout the 54-m-thick pelagic cap. In Hole 873B, Ca^{2+} concentrations increase, whereas Mg^{2+} values decrease downhole. Concentrations of alkalinity, Ca^{2+}, Mg^{2+}, K^+, and Sr^{2+} in the interstitial water of Hole 873A may have been altered by chemical reactions between the interstitial water and the clay. Fluoride concentrations are elevated by 18 to 21 µM over seawater values in Hole 873B, whereas fluoride contents from Hole 873A decline to 57 µM. Concentrations of SO_4^{2-} decrease in Hole 873A, whereas NH_4^+ increases presumably as a result of reducing conditions. Interstitial water interactions in clay samples are inferred by the decline of the molar ratio of Mg^{2+} and Ca^{2+}. Rubidium concentrations decline from 0.149 to 154 µM in the top half of Hole 873B to 0.141-0.147 µM in the deeper three samples. In Sample 144-873A-13R-3, rubidium concentrations are reduced to 0.033 µM in the interstitial water samples.

vegetated land. The sediments underwent mild sulfate reduction after deposition, at least in sheltered microenvironments. A near-coast, low-energy environment probably prevailed during most of the deposition of this subunit.

5. The red clay (Lithologic Unit IV) contains very little organic matter and sulfur. The unit was formed by subaerial weathering under oxic conditions.

6. Organic matter at this site is thermally immature to marginally mature with regard to hydrocarbon formation.

IGNEOUS PETROLOGY

Introduction

Hole 873A passed from limestone into a thick claystone unit (Lithologic Unit IV) at 155.9 mbsf. This unit represents a weathering profile developed on the underlying basaltic lava flows of Lithologic Unit V (175.1–204.3 mbsf). These flows do not, however, represent the main volcanic edifice, as they are underlain by a thick sequence

Table 4. Results of demagnitization of basalts from Hole 873A.

Core, section, interval (cm)	Lithology	Inclination (degrees)
144-873A-		
15R-1, 23–25	Basalt	+23.4
18R-1, 19–21	Basalt	+26.9
18R-1, 91–93	Basalt	+16.7
19R-4, 104–106	Volcaniclastic	+23.6
21R-1, 126–128	Volcaniclastic	+18.9

Table 5. Biohorizons used to compute sediment accumulation rates for the pelagic cap in Hole 873B.

Code	Datum	Age (Ma)	Top depth (mbsf)	Base depth (mbsf)
Calcareous nannofossils:				
C1	LAD *P. lacunosa*	0.47	0	0.05
C2	LAD *H. sellii*	1.37	0	0.05
C3	LAD *C. macintyrei*	1.45	3.07	4.02
C4	LAD *D. brouweri*	1.90	4.45	4.95
C5	LAD *D. triradiatus*	1.90	4.45	4.95
C6	LAD *D. asymmetricus*	2.20	5.38	6.59
C7	LAD *D. pentaradiatus*	2.40	7.12	8.57
C8	LAD *D. tamalis*	2.60	9.88	11.38
C9	FAD *P. lacunosa*	3.40	17.56	19.06
C10	LAD *S. abies + S. neoabies*	3.47	14.53	16.50
C11	LAD *R. pseudoumbilica*	3.50	16.50	17.57
C12	LAD *T. rugosus*	5.00	20.56	22.06
C13	LAD *C. floridanus*	11.60	25.48	25.55
C14	LAD *S. heteromorphus*	14.40	42.48	41.92
C15	FAD *S. heteromorphus*	17.10	51.82	54.01
C16	(CN1a+b assemblage)	23.20–23.70	54.01	58.0
Planktonic foraminifers:				
F1	FAD *T. truncatulinoides*	1.90	2.93	4.33
F2	FAD *T. tosaensis*	3.10	6.86	8.28
F3	FAD *S. dehiscens*	5.10	24.92	25.86
F4	FAD *G. fohsi lobata*	13.10	29.84	31.34
F5	*FAD *O. suturalis*	15.20	44.50	44.86

Notes: Ages given are from Berggren et al. (1985). "Top depth" denotes the lowest sample above a biohorizon, and "Base depth" the highest sample below the biohorizon.
*This datum is inferred to lie within the unconformity.

of volcanic debris-flow breccias (Lithologic Unit VI) below 204.3 mbsf. The hole ended within this unit at 232.3 mbsf.

Visual Descriptions

Recovery of basalt lavas was poor, averaging only 6.3%; the majority of the material recovered was in the form of small, partially rounded (by drilling) pieces. Nevertheless, the recovered material appears to represent eight texturally distinct flow units (Table 11). A ninth unit consists of two basalt pieces that were recovered within the underlying breccia (Interval 144-873A-19R-3, 95–102 cm), but which are larger and less altered than any breccia clast; they most likely represent a small dike related to the overlying flows.

Major Basaltic Units

All the basaltic lavas recovered are aphyric or sparsely phyric. Most are devoid of visible phenocrysts, but some pieces contain scattered dark green pseudomorphs after olivine or clinopyroxene. The only exceptions to this observation are several small layers within Unit 8, which are defined by phenocryst concentrations up to about 10%.

Based primarily on their visible textures, the basaltic lavas can be divided into four groups:

1. Aphyric, microcrystalline basalts of Unit 3 (Interval 144-873A-14R-CC, 0–39 cm), Unit 5 (Interval 144-873A-17R-1, 0–39 cm), Unit 8 (Interval 144-873A-18R-1, 32–37 cm), and Unit 9 (Interval 144-873A-19R-3, 95–102 cm) consist of medium to dark gray basalts, generally with only a few sparse phenocrysts. They include the least altered of the basalt fragments recovered in Hole 873A. In Intervals 144-873A-18R-1, 30–70 cm, and -18R-1, 90–100 cm, several layers are defined by phenocryst concentrations up to about 10%. The orientations of the layers are uncertain as the pieces are small and their orientation are unknown. Within Unit 8, Interval 144-873A-18R-1, 50–75 cm, contains irregular, interconnected calcite patches up to 2 cm in width that have replaced up to 50% of the matrix. Adjacent to the calcite, the basalt appears to have been locally brecciated with a light green matrix of unknown composition separating the clasts.

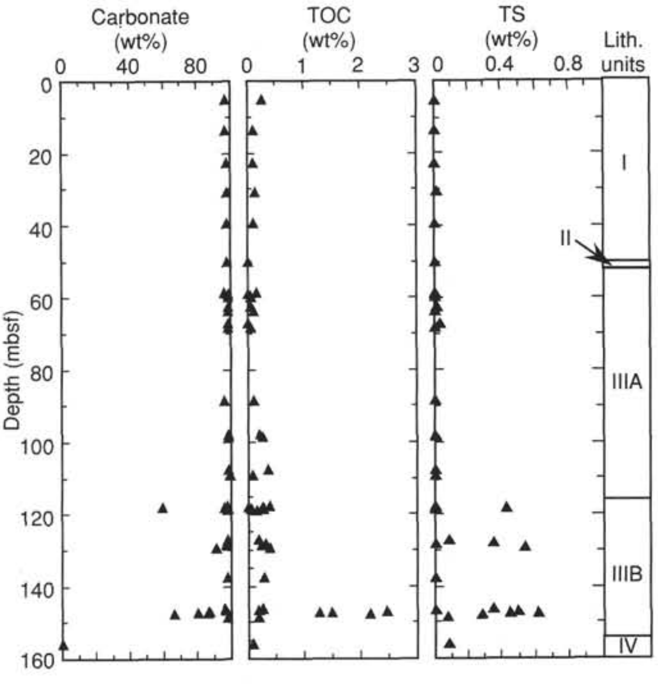

Figure 41. Carbonate (calculated as calcium carbonate), total organic carbon (TOC), and total sulfur (TS) contents of sediments in Holes 873A and 873B. Also shown are the major lithologic units, as given in the "Lithostratigraphy" section (this chapter).

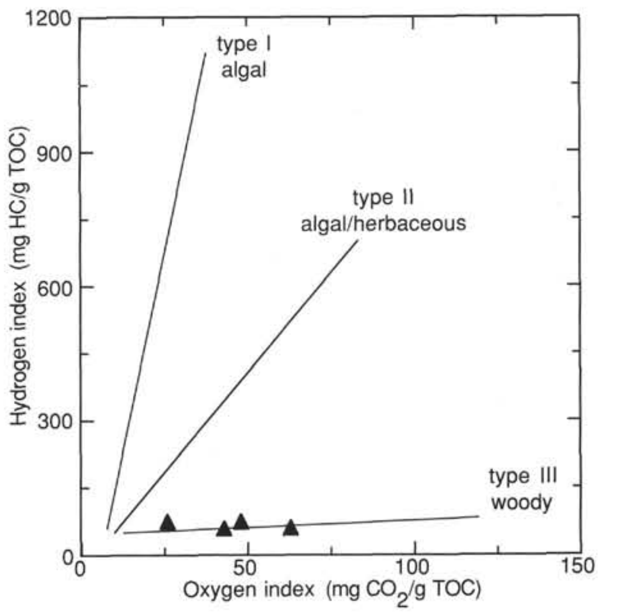

Figure 42. Modified van Krevelan diagram showing organic matter composition from Rock-Eval hydrogen and oxygen indices. Samples are from Sections 144-873A-11R-1, 98 cm, through 144-873A-11R-2, 22 cm.

Table 6. Surface seawater and interstitial water geochemical data, Site 873.

Core, section, interval (cm)	Depth (mbsf)	pH	Alkalinity (mM)	Salinity (g/kg)	Cl^- (mM)	Mg^{2+} (mM)	Ca^{2+} (mM)	SO_4^{2-} (mM)	NH_4^+ (μM)	SiO_2 (μM)	K^+ (mM)	Sr^{2+} (μM)	Na^+ (mM)	F (μM)	Rb (μM)	Li (μM)
Surface seawater	0	8.22	2.626	35.0	547	53.02	10.26	27	37	4	10.00	91	462	70	0.143	26
144-873B-																
First squeeze:																
1H-4, 145–150	5.31	7.73	2.696	35.0	546	53.11	10.65	29	29	132	9.82	102	478	84	0.152	26
2H-5, 143–150	13.71	7.91	2.600	35.0	554	53.03	10.49	29	28	130	9.92	100	489	81	0.148	26
3H-5, 145–150	23.01	7.70	2.587	35.0	553	50.35	10.53	29	57	128	10.11	96	483	82	0.154	26
4H-4, 140–155	30.88	7.76	2.701	35.0	553	53.44	10.96	29	29	125	10.46	95	484	81	0.147	26
5H-4, 143–148	39.56	7.68	2.720	35.0	552	53.16	10.92	29	31	123	10.01	93	490	83	0.151	26
6H-4, 143–150	49.82	7.57	2.672	35.0	551	51.54	11.02	29	50	130	9.72	97	470	82	0.143	26
Second squeeze:																
1H-4, 145–150	5.31					53.27	10.57	28	29		10.62	107		89	0.154	
2H-5, 143–150	13.71					53.57	10.51	28	29		10.07	105		88	0.149	
3H-5, 145–150	23.01					53.71	10.69	28	46		10.22	107		91	0.153	
4H-4, 140–155	30.88					52.96	11.12	28	26		10.02	106		88	0.147	
5H-4, 143–148	39.56					52.53	11.14	28	32		10.42	102		88	0.141	
6H-4, 143–150	49.82					51.41	11.47	28	36		10.32	103		86	0.146	
144-873A-																
13R-3, 140–150	169.90	7.60	1.209	35.0	554	23.26	51.91	26	130	130	4.93	1405	452	57	0.033	19

Notes: "First squeeze" refers to the first 30 ml of solution taken during the sample squeeze, and "Second squeeze" to the remaining interstitial water obtained.

Table 7. Results of headspace gas analyses, Hole 873B.

Core, section, interval (cm)	Methane (ppm)	Ethane (ppm)	Propane (ppm)	Lithology
144-873B-				
3H-6, 0–5	2.0	Tr	Tr	Nannofossil foraminifer ooze
4H-5, 0–5	2.3	None	None	Nannofossil foraminifer ooze
5H-5, 0–5	2.7	None	None	Foraminifer ooze
6H-5, 0–5	2.2	Tr	Tr	Foraminifer ooze
Laboratory background	2.2	None	None	
Core deck background	1.8	None	None	
Sea air background	1.8	None	None	

Notes: Tr = trace, and None = no gas detected.

2. Feldspathic basalts of Unit 1 (Intervals 144-873A-14R-CC, 0–4 cm, and -14R-CC, 9–32 cm) and Unit 4 (Interval 144-873A-15R-1, 2–54 cm) contain approximately 40% feldspar, forming a meshwork of laths up to 0.5 mm long. The feldspars are set in a dark-colored matrix, which is altered dark green in Unit 1. In both units the feldspar appears to have been largely replaced by whitish clays.

3. Aphanitic lavas of Unit 2 (Interval 144-873A-14R-CC, 4-9 cm) and Unit 6 (Interval 144-873A-17R-1, 39-50 cm) are altered to a dark purplish gray and contain sparse, elongate vesicles. They appear in thin section to be severely altered basalt.

4. Scoriaceous basalt of Unit 7 (Interval 144-873A-17R-1, 50–54 cm) consists of a single piece. This piece has a dense basaltic core surrounded by vesicular basalt in which the vesicles are arranged in concentric whorls (Fig. 44), strongly suggesting that this is a portion of a pyroclastic bomb.

Basalt Mineralogy

Four of the nine basaltic units were examined in thin section. The differences in texture among the recovered lavas outlined in the visual descriptions are not strongly reflected in their primary mineralogy. All are dominated by plagioclase, which occurs both as an interstitial phase and as abundant laths that show some degree of preferred orientation. Clinopyroxene is present as small equant prisms in the groundmass and sometimes as sparse microphenocrysts. In some cases, a weak pinkish coloration and strong dispersion suggest that this is titanaugite; in others, the clinopyroxene is pale green. Magnetite is abundant in all unaltered samples as well-formed, widely dispersed cubes. Olivine is not an identifiable groundmass phase and is only sparsely present as (completely altered) phenocrysts. At least 20% of the matrix has been altered to pale green clay. In some places, this clay is clearly replacing clinopyroxene, but in most cases the original mineralogy is not discernible.

Unit 4 (Interval 144-873A-15R-1, 23–26 cm) contains minor biotite, and plagioclase compositions are close to An35 (based on extinction angles). It is tentatively identified as a hawaiite. The mineralogy of the remaining units, especially the apparent early crystallization of magnetite, is consistent with their classification as olivine-poor alkali basalts.

The lower part of Unit 8 (Interval 144-873A-18R-1, 91–93 cm) is distinct in thin section from the upper part. It contains about 10% remarkably fresh, euhedral, or broken clinopyroxene microphenocrysts in an altered, highly vesicular groundmass that is now composed primarily of bright green and brown clay with some unaltered plagioclase laths. Small euhedral chrome spinels in green clay pseudomorphs after olivine also serve to distinguish this sample from the other lavas examined and suggest that this may be a separate flow that was not recognized in hand specimen.

Volcanic Breccias

Beneath the basalt lavas, a thick sequence of volcanic breccias, designated as Lithologic Unit VI, begins at 204.3 mbsf and continues to the bottom of the hole at 232.3 mbsf. The uppermost 3.8 m of the breccia (Sections 144-873A-19R-1 through -19R-3) are weathered to various shades of red and brown, but the deeper sections (Sections 144-873A-19R-1 through -20R-1) appear dark green to black in color and are unweathered. Three thin sections of the unweathered breccia (Intervals 144-873A-19R-4, 104–108 cm, -19R-4, 132–134 cm, and -21R-1, 40–43 cm) were examined.

The breccias consist primarily of subangular to subrounded clasts of glassy, highly vesicular basalt with sparse plagioclase microphenocrysts, commonly with swallowtail terminations. The glassy basalts have all been completely altered either to opaque tachylite or, more commonly, to bright green clay. None of the primary igneous material is preserved. Between the clasts is a matrix that now consists almost

Table 8. Results of geochemical analyses, Holes 873A and 873B.

Core, section, interval (cm)	Depth (mbsf)	IC (wt%)	$CaCO_3$ (wt%)	TC (wt%)	TOC (wt%)	N (wt%)	TS (wt%)	TS/TOC	Lithology
144-873A-									
5R-1, 27–33	88.57	11.52	96.0	11.63	0.11	0.03	0	0.01	Mudstone
6R-1, 13–17	98.13	11.77	98.0	11.96	0.19	0.03	0	0.02	Packstone
6R-1, 68–71	98.68	11.85	98.7	12.11	0.26	0.03	0	0	Wackestone
7R-1, 31–33	107.91	11.78	98.1	12.14	0.36	0.04	0	0	Wackestone
7R-2, 31–33	109.41	11.87	98.9	11.94	0.07	0.03	0	0.01	Grainstone
8R-1, 58–62	117.88	11.74	97.8	12.12	0.38	0.04	0	0	Wackestone
8R-1, 101–106	118.31	11.53	96.0	11.78	0.25	0.03	0.43	1.69	Pyritic packstone
8R-1, 108–110	118.38	7.12	59.3	6.74	0	0.08	25.26	0	Algal wackestone
8R-1, 126–127	118.56	11.83	98.5	11.90	0.07	0.02	0	0.02	Packstone
8R-2, 5–6	118.85	11.69	97.4	11.96	0.27	0.03	0	0.01	Mudstone
8R-2, 16–17	118.96	11.69	97.4	11.83	0.14	0.02	0	0	Mudstone
9R-1, 30–32	127.20	11.67	97.2	11.85	0.18	0.03	0.08	0.41	Grainstone
9R-1, 135–141	128.25	11.57	96.4	11.87	0.30	0.03	0.35	1.17	Wackestone
9R-2, 28–34	128.68	11.69	97.4	11.91	0.22	0.03	0	0	Mudstone
9R-2, 100–108	129.40	10.94	91.1	11.31	0.37	0.05	0.53	1.45	Packstone
10R-1, 107–118	137.67	11.73	97.7	12.01	0.28	0.02	0	0	Packstone
11R-1, 28–34	146.48	11.53	96.0	11.77	0.24	0.02	0.35	1.45	Grainstone
11R-1, 66–76	146.86	11.65	97.0	11.83	0.18	0.02	0	0	Grainstone
11R-1, 98–115	147.18	10.40	86.6	12.84	2.44	0.06	0.49	0.20	Carbonaceous packstone
11R-1, 130–136	147.50	10.30	85.8	11.56	1.26	0.05	0.61	0.49	Grainstone
11R-2, 0–17	147.66	9.61	80.1	11.08	1.47	0.05	0.45	0.31	Packstone
11R-2, 17–22	147.83	7.89	65.7	10.03	2.14	0.10	0.28	0.13	Limestone
11R-2, 91–104	148.57	11.71	97.5	11.89	0.18	0.02	0.07	0.41	Skeletal grainstone
12R-1, 28–30	156.18	0.03	0.2	0.11	0.08	0.01	0.08	1.00	Red clay
144-873B-									
1H-4, 145–150	5.42	11.61	96.71	11.87	0.26	0.01	0	0	Nannofossil foraminifer ooze
2H-5, 143–150	13.79	11.61	96.71	11.70	0.09	0.01	0	0	Nannofossil foraminifer ooze
3H-5, 145–150	23.01	11.73	97.71	11.82	0.09	0.01	0	0	Nannofossil foraminifer ooze
4H-4, 140–155	30.88	11.67	97.21	11.79	0.12	0.01	0.01	0.08	Foraminifer ooze
5H-4, 143–148	39.64	11.67	97.21	11.77	0.10	0.01	0	0	Foraminifer ooze
6H-4, 143–150	49.96	11.66	97.13	11.54	0	0.01	0		Foraminifer ooze
8N-1, 50–53	58.50	11.53	96.04	11.68	0.15	0.01	0	0	Algal rudstone
8N-1, 113–120	59.13	11.77	98.04	11.71	0	0	0		Skeletal grainstone
8N-2, 38–40	59.75	11.80	98.29	11.85	0.05	0.01	0	0	Skeletal grainstone
9N-1, 14–21	62.64	11.85	98.71	11.91	0.06	0.01	0.01	0.17	Skeletal grainstone
9N-1, 120–129	63.70	11.81	98.38	11.92	0.11	0.01	0	0	Skeletal grainstone
10N-1, 17–27	67.17	11.86	98.79	11.50	0	0.01	0.03		Skeletal packstone
10N-1, 131–137	68.31	11.78	98.13	11.83	0.05	0	0	0	Skeletal grainstone

Notes: IC = inorganic carbon, $CaCO_3$ = carbonate carbon calculated as calcium carbonate, TC = total carbon, TOC = total organic carbon, N = nitrogen, and TS = total sulfur. All numbers are in weight percent.

entirely of bright green clay, within which the outlines of the original clasts are well preserved. In its initial state, the matrix consisted entirely of highly angular glass shards and fine, broken fragments of glassy basalt. These materials were clearly not exposed to a weathering environment before deposition, and they can only have been transported by some form of mass flow. We interpret these deposits as hyaloclastite debris flows derived either from phreatomagmatic eruptions or from the fragmentation of active submarine lava flows. Some reworking of the upper parts of individual debris flows has led to the formation of narrow, laminated, or graded intervals (see "Lithostratigraphy" section, this chapter).

Summary and Conclusions

The igneous materials from Site 873 record three phases in the evolution of the volcanic edifice from which Wodejebato Guyot has evolved:

1. Submarine or near-shore phreatomagmatic eruption of vesicular basalts of unknown chemical affinity. These eruptions led to the rapid formation of hyaloclastite debris flows, almost certainly in a marine environment, with minor reworking between flows. Continued activity of this type could lead to extensive outbuilding of the volcanic edifice, and it presents a highly plausible explanation for the outward-dipping seismic reflectors that characterize the basement of this and other guyots, including both Lo-En and Limalok guyots.
2. Weathering in an oxidative environment for a sufficient period of time to oxidize at least the upper 5 m of hyaloclastic material.
3. Eruption and deposition of a series of at least eight differentiated (olivine poor) alkalic basalt and hawaiite flows in an unknown, probably subaerial environment. These lavas are texturally, and most likely chemically, distinct from those that produced the hyaloclastites. They represent the last volcanic episode at this site and likely represent the waning stages of volcanism on the edifice as a whole. They are literally "posterosional," but it is not known whether they represent a distinctly different eruptive phase from the eruptions that gave rise to the hyaloclastites.
4. A period of weathering of sufficient length to produce a clay-rich, in-situ weathering profile at least 20 m thick before the onset of marine conditions. This weathering is presumed to be subaerial because of its oxidative nature.

In summary, Site 873 records two volcanic events from a late stage in the development of the volcanic core of Wodejebato Guyot. Hyaloclastic breccias developed as a result of phreatomagmatic, near-shore, or submarine basaltic eruptions of unknown chemical or petrologic affinity, and subsequently developed a deep oxidative weathering profile. After an unknown period of time, a number of relatively thin, massive flows of differentiated, olivine-poor alkali basalt and hawaiite were emplaced by the last eruptions recorded at this site. After volcanism ceased, a second deep oxidative weathering profile developed and was preserved through an apparently rapid transition to low-energy marine conditions.

PHYSICAL PROPERTIES

Introduction

The objectives of the physical properties measurement program at Site 873 were (1) to measure the standard shipboard physical properties and (2) to identify geotechnical units for downhole and cross-hole correlations. The standard shipboard physical properties program included (1) nondestructive measurements of wet-bulk den-

Table 9. Averages of geochemical results from Holes 873A and 873B.

Lithologic units	$CaCO_3$ (wt%)	TOC (wt%)	N (wt%)	TS (wt%)	General lithology
IA and IB					
Average	97.1	0.11	0.01	0	Nannofossil foraminifer ooze
SD	0.4	0.08	0	0	to foraminifer ooze
N	6	6	6	6	
IIIA					
Average	97.9	0.20	0.03	0	Very pale to pale brown
SD	1.2	0.11	0.01	0	skeletal packstones and
N	5	5	5	5	grainstones
IIIB					
Average	94.3	0.43	0.03	1.16	Light gray skeletal
SD	7.7	0.66	0.02	5.03	wackestones, packstones,
N	24	25	25	25	and grainstones
IV					
Average	0.2	0.08	0.01	0.08	Red clay
SD					
N	1	1	1	1	

Note: SD = standard deviation, and *N* = number of samples.

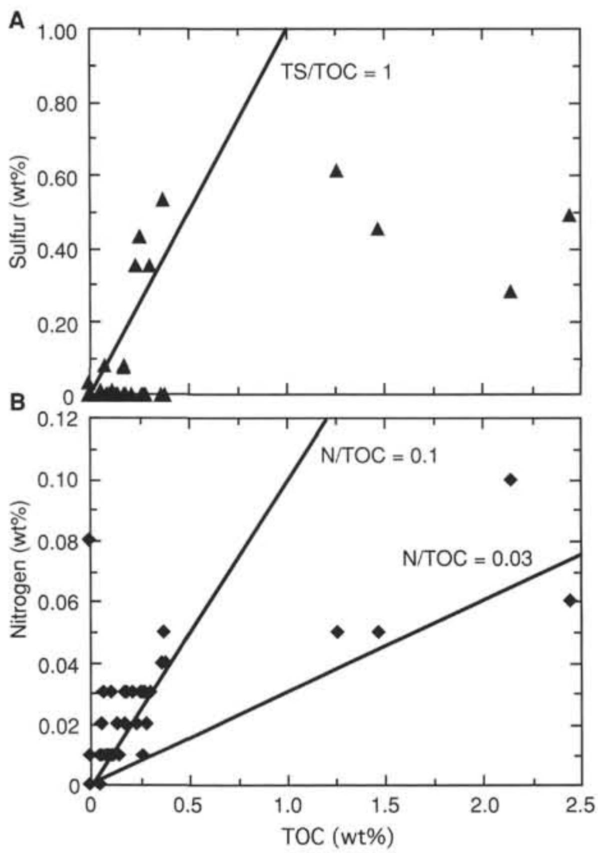

Figure 43. Plots of total sulfur vs. total organic carbon (TS/TOC) and nitrogen vs. total organic carbon (N/TOC), Holes 873A and 873B.

sity, acoustic compressional wave velocity, and magnetic susceptibility by means of sensors mounted on the multisensor track (MST); and (2) discrete measurements of index properties, compressional wave velocity, thermal conductivity, and vane shear strength, (see "Explanatory Notes" section, this volume). Shear strength was measured on the pelagic sediments using the Wykeham-Farrance vane shear device. Thermal conductivity measurements were made using the needle-probe method in unlithified sediments (von Herzen and Maxwell, 1959) and the split core (slab) method in basalts (Vacquier, 1985). Compressional wave velocities were measured using the digital sediment velocimeter (DSV) in the pelagic sediments, and using the

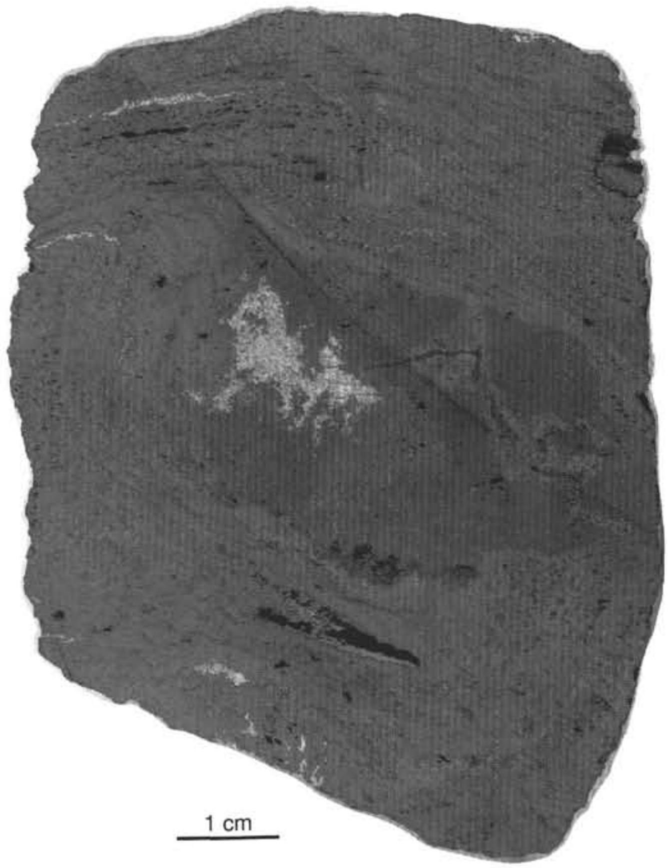

Figure 44. Portion of a pyroclastic bomb recovered in Interval 144-873A-17R-1, 47–54 cm. Note solid core surrounded by concentric whorls defined by vesicle trains.

Hamilton Frame (HF) on sample cubes and cylinders (mini-cores) of limestone and basalt.

Whole-round sections of pelagic sediment were passed through the sensors on the MST before splitting; shipboard and shore-based whole-round samples having been cut first from either end of the section. Magnetic susceptibility alone was measured on specific sections of limestone, basalt, and clay. Unlithified white and mottled gray nannofossil foraminifer ooze (Hole 873B, 0–28 mbsf) and light-brown foraminifer ooze (Hole 873B, 28–53 mbsf), forming the pelagic cap on the guyot were sampled only in Hole 873B. (In Hole 873A, the pelagic cap was not cored.) The upper limestone in both holes exhibited a thin burrowed surface encrusted with manganese oxide. The index properties measured on samples from Holes 873B and 873A are summarized in Figures 45–46 and Table 12.

The pelagic oozes from Hole 873B suffered disturbance from drilling, handling, and splitting operations. To reduce handling and preparation disturbance of pelagic sediments, special core handling procedures (see "Physical Properties" section, "Site 872" chapter, this volume) were continued at Hole 873B; these procedures were successful in reducing core disturbance.

Below the pelagic cap, recovery at Site 873 consists of white to pale brown, skeletal, shelly, Campanian to Maastrichtian packstone and grainstone (Hole 873A, 53–117 mbsf); gray-colored wackestone, packstone, and grainstone with pyrite (Hole 873A, 117–152 mbsf); saprolitic red clays derived from the weathering of basalts (Hole 873A, 152–174 mbsf); weathered basalt (Hole 873A, 174–203 mbsf); and volcaniclastic breccia (Hole 873A, 199–232 mbsf).

Compressional wave velocity measurements were made at 17 intervals in the pelagic sediments from Hole 873B using the digital

Table 10. Results of the Rock-Eval analyses of organic-rich samples from Hole 873A.

Core, section, interval (cm)	S1 (mg/g)	S2 (mg/g)	S3 (mg/g)	TOC (%)	OI (mg/g)	HI (mg/g)	PI	S2/S3	PC	Lithology
144-873A-										
11R-1, 98–115	0.50	1.82	1.32	3.06	43	59	0.22	1.38	0.19	Carbonaceous packstone
11R-1, 130–136	0.96	1.02	1.07	1.69	63	60	0.48	0.95	0.16	Skeletal grainstone
11R-2, 0–17	0.34	1.45	0.92	1.93	48	75	0.19	1.58	0.15	Packstone with plant fragments
11R-2, 17–22	0.00	2.29	0.82	3.10	26	74	0.00	2.79	0.19	Clayey chalk
12R-1, 28–30	0.00	1.94	0.14	0.23	ND	ND	ND	ND	ND	Red clay

Notes: S1 and S2 = mg hydrocarbon/gram of rock; S3 = mg carbon dioxide/gram of rock; TOC = total organic carbon from Table 9; OI = oxygen index (mg carbon dioxide/gram organic carbon); HI = hydrogen index (mg hydrocarbon/g organic carbon); PI = production index (free hydrocarbons relative to total hydrocarbons); and PC = pyrolyzable carbon. ND = no determination, TOC too low. Further explanation of the Rock-Eval parameters is given in the "Organic Geochemistry" section, "Explanatory Notes" chapter (this volume).

sediment velocimeter (DSV) apparatus; 35 limestone samples from Hole 873A (plus 2 samples of limestone from Hole 873B) were measured using the Hamilton Frame (HF) apparatus. Compressional wave velocity determinations, using the MST-mounted *P*-wave logger (PWL) were unsuccessful because of poor sediment/liner contact. The data are not reported here. Thermal conductivity was measured in 28 core sections of pelagic sediment (full-round) and 8 core sections of red clay from Hole 873A using the needle-probe technique. Thermal conductivity was measured on 5 limestone samples and 7 volcaniclastic breccia samples using the slab method. Few samples were made available for thermal conductivity tests on Hole 873A limestones. A small number of vane shear strength tests were conducted: 20 tests on the pelagic sediment in Hole 873B using the Wykeham-Farrance (WF) apparatus, and 4 tests on the red clays in Hole 873A using the Torvane (TV) apparatus.

Geotechnical Units

Pelagic Cap

The pelagic cap in Hole 873B (Table 12) may tentatively be divided into two geotechnical subunits: Subunits 1A (0–27 mbsf) and 1B (27–53 mbsf). These subunits are not as clearly defined as those at Sites 871 and 872, but they generally coincide with Lithologic Subunits IA and IB (see "Lithostratigraphy" section, this chapter) and they suggest possible correlations to the position of hiatuses and/or depositional changes.

Within Geotechnical Subunit 1A, two decreases in wet- and dry-bulk density are seen at 3.0 and 8.5 mbsf, respectively, in Figure 45. The first of these appears to coincide with the Pleistocene/late Pliocene boundary. In Figure 47, a distinct rise in wet-bulk density is seen from 19 to 25 mbsf. This zone of higher GRAPE density values is superposed on what appears to be a steady density decrease beginning at 4 mbsf. Near the base of Geotechnical Subunit 1A (at 25 mbsf), bulk density values abruptly decrease (Fig. 45).

The change in GRAPE density from 25 mbsf appears to coincide with a significant late Miocene hiatus, a change in sedimentation rate, and a lithologic change from a nannofossil foraminifer ooze above to a dominantly foraminifer ooze below. This lithologic change is best indicated by an increase of the water content (% dry wt) from 65% at 25 mbsf, to more than 170% at 35 mbsf (Fig. 45). It would appear that this is a result of two factors: (1) a lithologic difference between the nannofossil foraminifer ooze and the foraminifer ooze, the latter being filled with water and the former containing less water; and (2) the difference in particle size and hence packing density. In Geotechnical Subunit 1B, a small bulk density peak is seen at 39 mbsf (Fig. 45). This coincides with a decrease in water content and may relate to the zone of bioturbation at that point.

Subunits 1A and 1B have calcium carbonate (calcite) contents between 97% and 99% by weight after correction for salt content (see "Organic Geochemistry" section, this chapter).

Wet- and dry-bulk densities in Geotechnical Subunit 1A range from 1.4 to 1.7 g/cm^3 and from 0.6 to 1.0 g/cm^3, respectively, with means of 1.54 and 0.78 g/cm^3, respectively. Grain density in Subunit 1A ranges from 2.60 to 2.78 g/cm^3, with a mean of 2.70 g/cm^3. Water content (% dry wt) and porosity (dry) range from 65% to 142% and from 66% to 81%, respectively. The mean water content (% dry wt) and porosity for Subunit 1A are 100.7% and 74.0%, respectively.

For Geotechnical Subunit 1B, wet- and dry-bulk densities range from 1.35 to 1.49 g/cm^3 and from 0.49 to 0.70 g/cm^3, respectively, with means of 1.42 and 0.60 g/cm^3, respectively. The grain density for Subunit 1B ranges from 2.57 to 2.78 g/cm^3, with a mean of 2.68 g/cm^3. For Subunit 1B, water content and porosity values are higher than for Subunit 1A, mean water content (% dry wt) and porosity being 139.3% and 78.5%, respectively.

Magnetic susceptibility data in Hole 873B (0–33 mbsf) are shown in Figure 47. Three features may be discerned: (1) a strong peak at approximately 2 mbsf, (2) small peaks at the tops and bottoms of cores (probably caused by rust contamination), and (3) a section of elevated values between 21.5 and 23 mbsf. The magnetic susceptibility data are discussed in the "Paleomagnetism" section (this chapter).

Compressional wave velocity (DSV) vs. depth profiles for Geotechnical Unit 1 (1–27 mbsf) are illustrated in Figure 48 and listed in Table 13. Velocity ranges from 1399 to 1582 m/s, with a mean of 1515 m/s. A drop in velocity is seen between 26.2 and 28.8 mbsf. This correlates with the density drop at this depth (Fig. 45).

The thermal conductivity vs. depth profile for Unit 1 is shown in Figure 49. From 0 to 27 mbsf, the profile is quite variable; below this, a more uniform profile is seen. Overall, thermal conductivity ranges from 0.90 to 1.59 W/(m · K) (Table 14), with a mean of 1.22 W/(m · K). These values agree with those from Holes 871A and 872A ("Physical Properties" section, "Site 871" and "Site 872" chapters, this volume). Thermal conductivity in clean saturated sands is dependent on water content (Lovell, 1984). However, a clear correlation between thermal conductivity and water content for the pelagic sediments in Hole 873B is not seen.

Shear strength data (Table 15) obtained with the Wykeham-Farrance vane, plotted vs. depth, are given in Figure 50. The scatter is high, ranging from 0 to 8.0 kPa, with a mean of 2.4 kPa. For comments on shear strength data and test conditions for the pelagic cap material, see the "Physical Properties" sections of the "Site 871" and "Site 872" chapters (this volume).

Limestone

Geotechnical Unit 2 (54.3–151.5 mbsf) represents the whole of the limestone sequence in Hole 873A. The limestone is divided into two lithologic subunits (IIIA and IIIB), based largely on color differences caused by the slight pyrite/organic enrichment in Subunit IIIB. These lithologic differences cannot be distinguished amid the moderate scatter of the geotechnical data. Wet- and dry-bulk densities range from 2.42 to 2.98 g/cm^3 and from 2.29 to 2.87 g/cm^3, respectively, with means of 2.69 and 2.56 g/cm^3, respectively. Grain density ranges from 2.74 to 3.35 g/cm^3, with a mean of 2.82 g/cm^3.

Water content (% dry wt) and porosity (dry) for Unit 2 range from 1.8% to 11.5% and from 4.7% to 24.7%, respectively; mean values are 5.1% and 12.2%, respectively. Compressional wave velocity data for Geotechnical Unit 2 (Table 16) are shown in Figure 48 (values from orthogonal faces of the same cube specimen are joined by a line).

Table 11. Summary of igneous units, Hole 873A.

Unit	Interval number	Description
1	144-873A-14R-CC, 0–4 cm and 9–32 cm	Hawaiite, subophitic texture
2	144-873A-14R-CC, 4–9 cm	Purplish aphanitic basalt
3	144-873A-14R-CC, 32–37 cm	Friable, altered aphanitic basalt
4	144-873A-15R-1, 2–54 cm	Aphyric plagioclase basalt
5	144-873A-17R-1, 0–39 cm	Microcrystalline
6	144-873A-17R-1, 39–50 cm	Purplish aphanitic basalt
7	144-873A-17R-1, 50–54 cm	Scoriaceous basalt bomb
8	144-873A-18R-1, 0–133 cm	Aphyric, microcrystalline basalt; bands of altered clinopytoxene micro-phenocrysts
9	144-873A-19R-3, 95–102 cm and 9–32 cm	Aphyric basalt; possible dike in hyaloclastite breccia

Results generally exhibit wide scatter, ranging from 2909 to 4923 m/s, with a mean of 3907 m/s. Two additional HF tests were conducted on limestone samples from Hole 873B at 60 and 68 mbsf (Table 16). These yielded velocities of 2455 and 3760 m/s, respectively. Downhole velocity logs generally produce lower values than laboratory tests, but they also have a moderate scatter. A mean of approximately 2500 m/s was obtained for downhole limestone data. In agreement with the laboratory data, a distinction between Lithologic Subunits IIIA and IIIB is difficult to make based on the velocity profile.

Clays

Geotechnical Unit 3 (151.5–174 mbsf) consists of an apparently terrestrial, basalt weathering profile, covering the whole of Lithologic Unit IV. This saprolite consists largely of a ferruginous red clay containing partially weathered basalt clasts; it is highly variable. Core recovery in this unit was good. The wet- and dry-bulk density data for the unit show a clear decrease in the profile (Fig. 46), ranging from 1.85 to 2.26 g/cm^3 and from 0.6 to 1.03 g/cm^3, respectively, with means of 2.01 and 1.40 g/cm^3, respectively. Grain density for the clays ranges from 3.09 to 3.52 g/cm^3, with a mean of 3.27 g/cm^3. These relatively high values are consistent with those for similar saprolite from Hole 871 ("Physical Properties" section, "Site 871" chapter, this volume). Two particularly high values of grain density (3.48 and 3.52 g/cm^3), at 157.9 and 171.8 mbsf, are probably a result of locally high proportions of iron-rich minerals. Goethite has a specific gravity of 4.3 g/cm^3, and hematite may have a specific gravity as high as 5.26 g/cm^3 (Deer et al., 1966). It is possible that larger errors than normal exist in the method of grain density measurements using the Penta-Pycnometer where highly plastic saprolitic clays are concerned. Incomplete saturation would tend to result in erroneous high volume values and hence lower, rather than higher, densities.

Despite considerable borehole washout (>500 mm), a clear correlation is observed between the relative trends in laboratory bulk densities and the trends in downhole logging measurements of "wet-bulk density" for the clays in Hole 873A; however, the latter produce values between 1.3 and 1.9 g/cm^3 compared with 1.9 to 2.3 g/cm^3 for the laboratory data ("Downhole Measurements and Seismic Stratigraphy" section, this chapter).

A small number of Torvane tests gave undrained shear strength values ranging from 34 to 140 kPa (Table 15). High variability in strength may be expected in such saprolitic materials because of the heterogeneity of the soil structure and the unsuitability of conducting this test on these materials.

Basalt

Geotechnical Unit 4 (below 174 mbsf) consists of weathered basalt in the upper half and volcanic breccia in the lower half. Poor recovery in the upper part meant that few tests could be conducted. Data for the lower half show considerable variability. A decreasing trend in grain density values with depth may be discerned within the unit (Fig. 46). Compressional wave velocity and thermal conductivity also appear to decrease with depth (Figs. 48–49). Compressional wave velocity for the unit ranges from 2892 to 5090 m/s, with a mean of 3907 m/s. Thermal conductivity ranges from 0.69 to 0.99 W/(m · K), with a mean of 0.82 W/(m · K).

DOWNHOLE MEASUREMENTS AND SEISMIC STRATIGRAPHY

Log Types, Processing, Reliability, and Resolution

Logs were obtained from the volcanic edifice through carbonate platform succession in Hole 873A on Wodejebato Guyot with the geophysical (two passes), Formation MicroScanner (FMS) (two passes), and geochemical tool strings. These logs are valuable for interpreting the sedimentary succession and possible discontinuities in accumulation, because core recovery within this 178-m interval (Cores 144-873A-1R through -21R) averaged only 20%. In particular, the high-resolution FMS coverage of the borehole wall is excellent for the complete basalt through carbonate platform succession. The FMS tool also has a three-axis magnetometer for orientation, and this instrument was used to observe the magnetic characteristics of the basaltic edifice.

Although all logging runs were conducted to the base of the hole (232 mbsf), the different position of tools on the various strings implies that the lower boundary of logging data from each tool will vary. The gamma-ray spectroscopy, resistivity, and FMS measurements extend down to about 225 mbsf, whereas the sonic velocity measurements extend down to only 200 mbsf. The upper limit of the geophysics and FMS logging runs was the base of the drill string at 51 mbsf, located within the pelagic sediments overlying the carbonate platform on the guyot. The geochemistry string, which can measure through the drill pipe, was run continuously to above the sediment surface.

The natural gamma-ray tool (NGT) run on each string provided a set of distinct peaks within the carbonate platform facies and within clay-rich intervals in the volcanic succession (Fig. 51). The locations of these natural gamma-ray events were used for calibrating among the wireline depths among the various runs. The geochemistry logging run recorded leaks in natural gamma-rays approximately 0.5 m lower than those in the geophysics logging run, and approximately 1.5 m higher than those in the FMS run. To calibrate these relative depths to drill depths in the hole, we used the location of the base of the drill pipe, which was at 1397 m below rig floor (mbrf) or at 51 mbsf. The end of the drill pipe can be recognized by a pronounced sharp increase in iron abundance, measured by the geochemical tool string, with the midpoint of this increase, corresponding to the approximate center of the tool resolution, which also occurs at 1397 m in log wireline depth. This base of the drill pipe is more difficult to fix precisely in the other logs. Therefore, we used the wireline depths of the geochemical logging run to define meters below seafloor (mbsf). These "mbsf" should be identical to those of the corresponding core intervals. The resulting conversion from wireline logging depths (meters below rig floor) to mbsf (meters below seafloor) is (1) subtraction of 11.0 m (distance from rig floor to mean sea surface), (2) subtraction of 1335.0 m (depth from sea surface to seafloor according to drilling operations), and (3) correction for offsets between logging and drilling depths by adding 0.5 m to geophysics log measurements or subtracting 1.5 m from FMS measurements. The range in daily tide during the drilling and logging operations was less than 1 m in this region (Hydrographer of the Navy, 1991), so we did not compute differential tide corrections to the intercalibration of logging and drilling depths.

The caliper log of the borehole diameter can be interpreted in terms of the relative degree of consolidation and cementation of the limestone facies. The main "washout" intervals in Hole 873A occurred within the unconsolidated pelagic foraminifer oozes directly overlying the carbonate platform (above 54 mbsf), within a porous grainstone interval at about 70 to 75 mbsf, and within the clay overlying

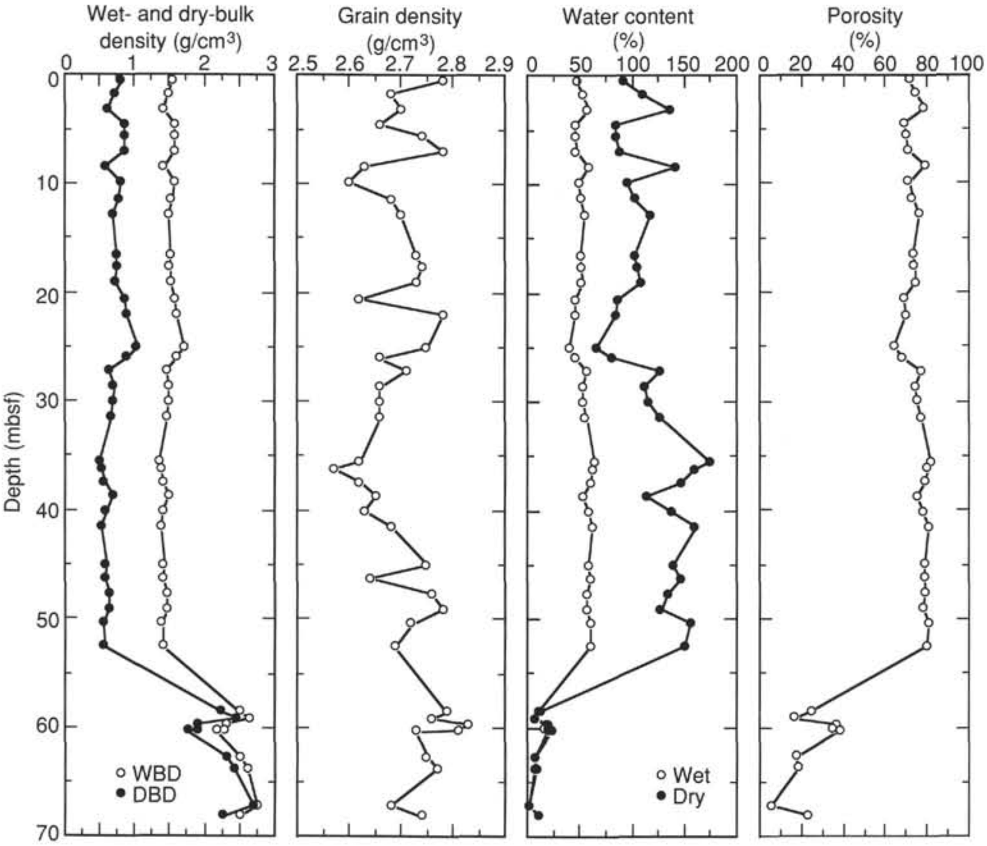

Figure 45. Measurements of index properties (wet- and dry-bulk density, grain density, water content, and porosity) vs. depth, Hole 873B.

basaltic basement at 150 to 170 mbsf (Fig. 51). Where the borehole diameter exceeds 38 cm (15 in.), the FMS pads are no longer in complete contact with the borehole walls, and one or more of the four traces may be incoherent (see "Explanatory Notes" chapter, this volume). The lithodensity tool has incomplete contact against the borehole wall when diameter exceeds 46 cm (18 in.), producing unreliably low values (Fig. 51). The irregular borehole diameter caused severe problems for the sonic velocity tool run in Hole 873A; therefore, despite systematic editing of the measurements, post-cruise total-waveform analysis will be necessary to produce reasonable velocity values.

Overview of Resistivity, Density, and Natural Gamma-ray Relationships

Resistivity, density, and sonic velocity are strongly correlated throughout the logged interval at Hole 873A, both in terms of changing average values among facies and as small-scale peaks within each facies (Fig. 52). A similar relationship was observed in Hole 871C, where these variations have been interpreted to reflect differences in carbonate depositional facies enhanced by differential porosity, cementation, and hole diameter (see discussion in "Downhole Measurements and Seismic Stratigraphy" section, "Site 871" chapter, this volume). Resistivity measurements were observed to depend on the depth of penetration of the different resistivity sondes, which is largely an artifact of the irregular hole diameter; therefore, we consider that the medium-penetration resistivity measurements provide the more reliable values and detail (see "Explanatory Notes" chapter, this volume). The FMS provides the highest resolution (about 5 mm) mapping of the resistivity variations of the borehole wall and indicates that many of these short-wavelength features have internal complexity, such as groupings of thin beds or irregular patterns of cementation. However, the FMS record is incomplete in the clay facies owing to enlarged borehole diameters.

Bulk densities measured within the thick clay layer overlying basalt are distorted by the widened borehole, but the weathered basalt unit displays a strong correlation between density and resistivity variations, which also correlated with geochemistry variations (Figs. 51, 53, and 54).

Some of the high-density, high-resistivity peaks within the carbonate platform also correlate with peaks in intensity of natural gamma rays, as would be expected from cementation differences (see "Explanatory Notes" chapter, this volume). However, these correlations were the exceptions, rather than the rule, in Hole 873A. Indeed, some of the strongest peaks in natural gamma rays, which mainly result from uranium enrichment, do not appear to have any corresponding features displayed in resistivity or density logs; for example, the major uranium concentration at 83–84 mbsf. We suspect that some of these uranium enrichments are associated with hiatuses or condensed sedimentary intervals, and other enrichment levels are associated with redox-front uranium precipitation (see discussion in "Downhole Measurements and Seismic Stratigraphy" section, "Site 871" chapter, this volume).

Sonic Traveltime Computations

An attempt was made to recover the seismic velocity profile from the sonic log by selecting the fastest of the four traveltimes from each sonic log measurement. After removing all traveltimes corresponding to velocities of greater than 4 km/s and less than 1.3 km/s, the remaining traveltimes were summed (integrated) to obtain two-way traveltime (TWT) as a function of depth in the hole (mbsf) (Fig. 55). This curve was calibrated to the well-established top of the limestone platform at 54 mbsf, where drill-pipe penetration slowed dramatically,

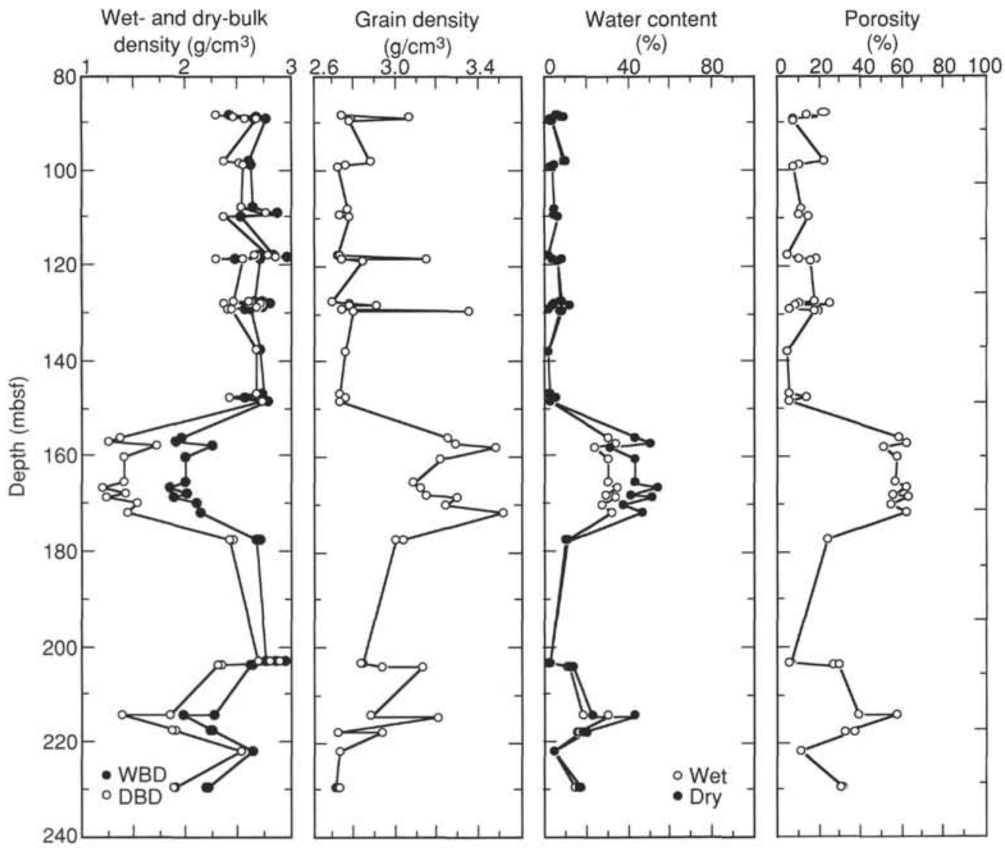

Figure 46. Measurements of index properties (wet- and dry-bulk density, grain density, water content, and porosity) vs. depth, Hole 873A.

corresponding to the 1.86 s TWT reflector from our 3.5-kHz record. This total two-way traveltime is similar to the time shown in Figure 56, which is a seismic record from a previous survey. We used the delay times to various horizons in this record (Fig. 56) to calculate interval velocities at Hole 873A, although the total two-way traveltimes from the sea surface measured in this profile are slightly greater than those measured during the Leg 144 seismic survey.

The traveltime vs. depth plot constructed from the sonic logs may be checked by comparing it to some event that can be confidently correlated in the seismic reflection profile (see seismic stratigraphy discussion below). Our most confident reflection is the top of basaltic basement at 0.11 s TWT below the top of the limestone platform reflection (see Fig. 56). This time corresponds to a depth of 158 mbsf in the plot of traveltime vs. depth, whereas the top of the solid basalts actually occurs at 175 mbsf in the cored section. Thus, the predicted depth of basalt in the plot of traveltime vs. depth appears to be too shallow relative to the actual depth in the cored section. However, inspection of the sonic log data suggests that the clay layer overlying basalt from 151 to 175 mbsf was accurately logged and has an average formation velocity of 1.5 km/s. Thus, a TWT of 0.03 s from the logs through the clay section can be subtracted from the 0.11 s TWT measured from the seismic record for the entire limestone-clay section (Fig. 56) to yield a TWT of 0.08 s for the limestone section. Combined with the total limestone thickness of 97 m measured from core recovery and other log data, this yields an average formation velocity of 2.4 km/s for the limestone section. This is slightly less than the average of 2.6 km/s measured in a similar limestone section at Hole 871C.

The basalt and volcaniclastic sequence was logged from 175 to 203 mbsf and found to have an average formation velocity of 2.9 km/s. This determination is uncertain because of the short section through a relatively high-velocity formation, and also because the sonic log records are noisy in this interval. It is likely that the true formation velocity has been underestimated. However, the impedance contrast implied by the measured velocity difference between the clay and basalt sections is sufficiently large to justify our original assumption that the "basement" reflection formed in Figure 56 is actually the basalt/clay boundary.

Downhole Magnetometer Observations

A three-axis fluxgate magnetometer was attached to the FMS tool. Data about the orientation and strength of the magnetic field within the borehole were collected at 15-cm (0.50-ft) intervals, whereas the FMS image data have a 2.5-mm sampling rate. The three-component magnetic data (FX is the horizontal "*x*" component, parallel to the FMS Pad 1 direction; FY is the horizontal "*y*" component, perpendicular to Pad 1 direction; and FZ is the vertical "*z*" component) enable one to compute horizontal intensity, total intensity, inclination, and relative declination (Fig. 57). The magnetic direction is used to orient the FMS traces with respect to magnetic north. Within rocks having a strong natural remanent magnetization (NRM) different in direction from the present-day magnetic field, the FMS orientations will be distorted, but we acquire valuable information about the NRM directions of those rocks.

Within the carbonate section, the magnetometer appears to be recording only the ambient present-day field (Fig. 57). These limestones have a very weak magnetization (see "Paleomagnetism" section, this chapter).

At about 175 mbsf, coinciding with the clay/basalt boundary, sharp decreases are seen in both the vertical and horizontal components of the downhole magnetic field (Fig. 57). These decreases are caused by the strong magnetization of the weathered basalt and underlying

Table 12. Index properties data, Holes 873A and 873B.

Core, section, interval (cm)	Depth (mbsf)	Wet-bulk density (g/cm³)	Dry-bulk density (g/cm³)	Grain density (g/cm³)	Porosity (%)	Water content (% dry wt)
144-873-A						
5R-1, 8–14	88.38	2.42	2.29	2.75	13.6	6.1
5R-1, 51–56	88.81	2.68	2.46	3.07	21.3	8.9
5R-1, 92–95	89.22	2.66	2.58	2.79	7.8	3.1
5R-1, 110–113	89.40	2.77	2.69	2.78	8.1	3.1
6R-1, 8–11	98.08	2.61	2.37	2.88	23.7	10.3
6R-1, 59–62	98.59	2.62	2.51	2.76	10.7	4.3
6R-1, 111–114	99.11	2.63	2.55	2.73	7.7	3.1
7R-1, 39–42	108.00	2.65	2.54	2.77	11.4	4.6
7R-2, 19–22	109.30	2.89	2.77	2.74	11.6	4.3
7R-2, 67–69	109.80	2.53	2.38	2.78	14.6	6.3
8R-1, 45–56	117.80	2.86	2.80	2.73	5.1	1.9
8R-1, 49–51	117.80	2.71	2.66	2.74	5.0	1.9
8R-1, 107–110	118.40	2.98	2.87	3.15	10.7	3.8
8R-1, 129–131	118.60	2.48	2.29	2.75	18.8	8.4
8R-2, 9–13	118.90	2.73	2.56	2.85	16.5	6.6
9R-1, 60–62	127.50	2.67	2.47	2.70	19.1	7.9
9R-1, 94–98	127.80	2.74	2.62	2.78	11.0	4.3
9R-1, 108–111	128.00	2.66	2.38	2.91	26.6	11.5
9R-1, 132–134	128.20	2.82	2.73	2.78	9.3	3.5
9R-2, 54–56	128.90	2.75	2.69	2.75	5.6	2.1
9R-2, 103–105	129.40	2.58	2.40	3.35	17.6	7.5
9R-2, 103–105	129.40	2.63	2.44	2.80	18.6	7.8
10R-1, 116–118	137.80	2.73	2.68	2.76	4.8	1.8
11R-1, 67–70	146.90	2.75	2.69	2.74	5.7	2.2
11R-1, 140–142	147.60	2.57	2.43	2.76	13.8	5.8
11R-2, 85–90	148.50	2.80	2.74	2.74	6.1	2.3
12R-1, 24–26	156.10	1.97	1.37	3.25	58.4	43.6
12R-1, 130–132	157.20	1.90	1.26	3.29	62.6	50.8
12R-2, 48–50	157.90	2.26	1.73	3.48	52.1	30.9
12R-3, 136–138	160.30	2.00	1.40	3.22	58.7	43.0
12R-5, 14–16	165.50	2.00	1.40	3.09	58.8	43.2
13R-1, 111–113	166.60	1.85	1.20	3.12	63.3	53.9
13R-2, 110–112	168.10	2.02	1.43	3.15	57.6	41.3
13R-3, 10–12	168.60	1.89	1.24	3.30	62.8	51.8
13R-4, 10–12	170.10	2.11	1.53	3.24	56.5	37.8
13R-5, 31–33	171.80	2.14	1.45	3.52	66.8	47.1
15R-1, 23–25	177.60	2.69	2.43	3.00	25.8	10.9
15R-1, 23–25	177.60	2.72	2.46	3.04	25.6	10.7
15R-1, 23–25	177.60	2.69	2.43	3.00	25.8	10.9
18R-1, 19–21	203.20	2.77	2.70	2.85	6.3	2.4
18R-1, 19–21	203.20	2.97	2.90	2.85	6.8	2.4
18R-1, 19–21	203.20	2.88	2.82	2.84	5.8	2.1
18R-1, 91–93	203.90	2.64	2.35	2.94	28.5	12.4
18R-1, 91–93	203.90	2.64	2.35	2.94	28.5	12.4
18R-1, 91–93	203.90	2.63	2.32	3.13	30.6	13.5
19R-2, 70–72	214.30	2.27	1.85	2.88	40.7	22.5
19R-2, 70–72	214.30	2.27	1.85	2.88	40.7	22.5
19R-2, 70–72	214.30	1.98	1.39	3.21	57.9	42.7
19R-4, 104–106	217.70	2.25	1.91	2.73	33.7	18.1
144-873-A						
19R-4, 104–106	217.70	2.25	1.91	2.73	33.7	18.1
19R-4, 104–106	217.70	2.26	1.88	2.94	37.3	20.4
20R-1, 6–8	221.80	2.64	2.53	2.74	11.2	4.5
21R-1, 126–128	229.50	2.23	1.90	2.72	32.1	17.3
21R-1, 126–128	229.50	2.23	1.90	2.73	32.1	17.3
21R-1, 126–128	229.50	2.20	1.89	2.74	30.5	16.5
144-873B-						
1H-1, 50–52	0.50	1.55	0.81	2.78	72.6	92.2
1H-2, 50–52	1.69	1.48	0.71	2.68	75.7	109.6
1H-3, 50–52	3.07	1.41	0.60	2.70	79.2	136.1
1H-4, 50–52	4.47	1.58	0.86	2.66	70.7	84.4
1H-5, 25–27	5.61	1.58	0.86	2.74	70.8	84.5
2H-1, 50–52	7.00	1.58	0.84	2.78	71.8	87.2
2H-2, 47–49	8.39	1.42	0.58	2.63	81.2	142.2
2H-3, 50–52	9.86	1.56	0.80	2.60	74.5	95.9
2H-4, 48–50	11.34	1.53	0.76	2.68	75.2	101.9
2H-5, 50–52	12.86	1.48	0.68	2.70	77.9	117.7
3H-1, 50–52	16.50	1.51	0.74	2.73	74.5	102.6
3H-2, 50–52	17.56	1.50	0.73	2.74	74.8	105.1
3H-3, 50–52	19.06	1.51	0.72	2.73	76.4	108.2
3H-4, 50–52	20.56	1.57	0.84	2.62	71.0	86.7
3H-5, 50–52	22.06	1.60	0.87	2.78	71.2	84.0
3H-7, 42–44	24.98	1.71	1.03	2.75	66.2	65.8
4H-1, 50–52	26.00	1.60	0.88	2.66	70.0	81.0
4H-2, 50–52	27.19	1.45	0.64	2.71	78.8	126.6
4H-3, 50–52	28.66	1.48	0.70	2.66	75.9	111.2
4H-4, 50–52	29.98	1.48	0.69	2.66	77.7	115.6
4H-5, 50–52	31.48	1.46	0.65	2.66	79.5	126.2
5H-1, 50–52	35.50	1.35	0.49	2.62	83.8	173.7
5H-2, 50–52	36.13	1.38	0.53	2.57	82.7	160.0
5H-3, 50–52	37.40	1.40	0.56	2.62	81.1	147.1
5H-4, 50–52	38.71	1.49	0.69	2.65	77.6	114.5
5H-5, 50–52	40.11	1.41	0.59	2.63	79.3	136.9
5H-6, 50–52	41.50	1.37	0.53	2.68	82.6	160.7
6H-1, 50–52	45.00	1.42	0.59	2.75	80.9	139.7
6H-2, 50–52	46.24	1.40	0.57	2.64	81.4	146.8
6H-3, 50–52	47.65	1.46	0.62	2.76	81.6	134.7
6H-4, 50–52	49.03	1.45	0.64	2.78	79.2	127.5
6H-5, 50–52	50.39	1.39	0.54	2.72	82.9	156.6
6H-6, 50–52	52.50	1.40	0.56	2.69	82.0	150.8
8N-1, 53–56	58.53	2.52	2.25	2.79	25.7	11.7
8N-1, 112–114	59.12	2.64	2.47	2.76	17.2	7.1
8N-2, 37–39	59.74	2.31	1.91	2.83	38.8	20.8
8N-2, 78–80	60.15	2.29	1.91	2.81	36.6	19.6
8N-2, 92–94	60.29	2.17	1.76	2.73	40.4	23.5
9N-1, 14–16	62.64	2.51	2.33	2.75	17.2	7.6
9N-1, 121–123	63.71	2.62	2.42	2.77	19.4	8.2
10N-1, 17–19	67.17	2.77	2.71	2.68	5.7	2.1
10N-1, 106–108	68.06	2.50	2.26	2.74	24.0	10.9

volcaniclastic units in an opposing direction to the present-day normal-polarity magnetic field. This is consistent with the reversed-polarity magnetization obtained for recovered core samples of these lithologies (see "Paleomagnetism" section, this chapter). The shallower inclination may be the result of the low southern paleolatitude setting of magnetization in these rocks. The fine-scale variations in the observed magnetic field with depth were duplicated during the two FMS passes, indicating that these variations probably correlate with distinct basaltic or weathering horizons.

Log-facies Comparisons

Lithologic units and subunits defined on the basis of the limited core recovery generally can be recognized in the composite logs. However, these logs indicate that the boundaries among facies often are demarcated by peaks in natural gamma-ray intensity peaks induced by uranium or thorium concentrations and that the lithologic units display considerable internal lithologic variation. The logging signatures of the different lithologic units can be used to set more precise boundaries among these facies (Fig. 51). The combined FMS resistivity maps of the borehole, coupled with the natural gamma-ray and medium-penetration resistivity signals, provide details of sedimentary structures on a meter to centimeter level. Some of the major features within the carbonate platform succession are summarized in terms of the shipboard-defined lithologic units.

Lithologic Unit I

Nature: foraminifer ooze
Interval: above Core 144-873A-1R
Assigned depth from coring: 54.3 mbsf
Age: Pleistocene to early Miocene

The pelagic cap on the carbonate platform consists of white, homogeneous foraminifer ooze. Only the lowermost 5 m of this facies was logged outside of the drill pipe, and, as expected, this ooze is characterized by very low bulk density (averaging approximately 1.5 g/cm^3), very low resistivity (averaging approximately 1 Ωm), and negligible natural gamma-ray intensity (approximately 5 API units). Logging measurements through the pipe confirm the homogeneous nature of this lithology; minor fluctuations in the geochemical logs of radiogenic and stable elements (Figs. 53–54) are near the noise levels.

Lithologic Unit II

Nature: manganese-coated, phosphatic rudstone with matrix of planktonic foraminifer packstone
Interval: Core 144-873A-1R
Assigned depth from coring: 54.3–58.1 mbsf
Age: middle Eocene to late Paleocene

The carbonate platform (Lithologic Unit III) is capped by a condensed layer (Lithologic Unit II) rich in manganese and phosphate (see "Lithostratigraphy" section, this chapter). The depth of this manganese crust was assigned as 54.3 mbsf, according to where the washing-down drilling process met significant resistance. In the first core drilled from this level to 59.8 mbsf, manganese crust was recovered. Unlike the phosphatic hardground at Site 871 on Limalok Guyot, which displayed a significant concentration in uranium and well-developed cementation of the underlying limestone, this Mn-crust interval in Hole 873A lacks a distinctive signature in the various logs (Fig. 51). A minor increase in uranium is distributed over about a 5-m interval, but no distinct peaks are seen. Geochemical logs (Fig. 54) suggest that this Mn-crust interval does not contain significant iron. The immediately underlying limestone, although slightly phosphatic (see "Lithostra-

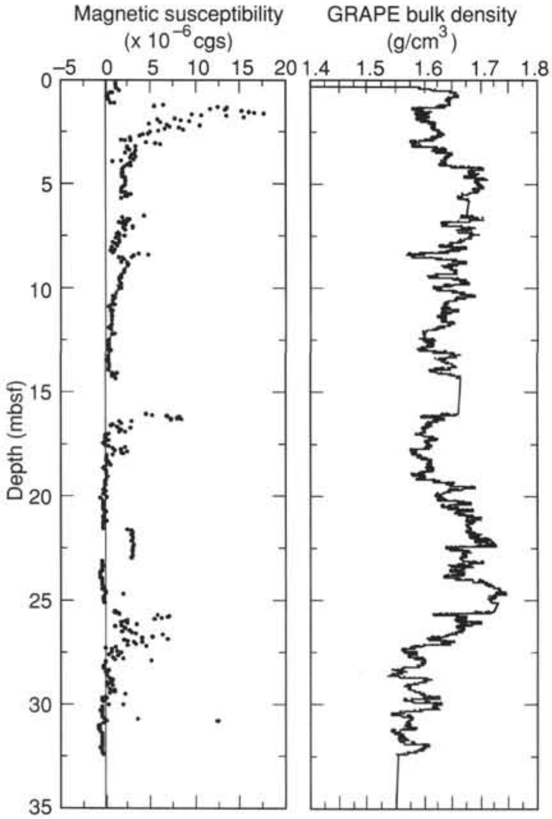

Figure 47. Magnetic susceptibility and GRAPE density vs. depth, Hole 873B. Data obtained from the multisensor track (MST). The GRAPE density data depicted have been digitally smoothed.

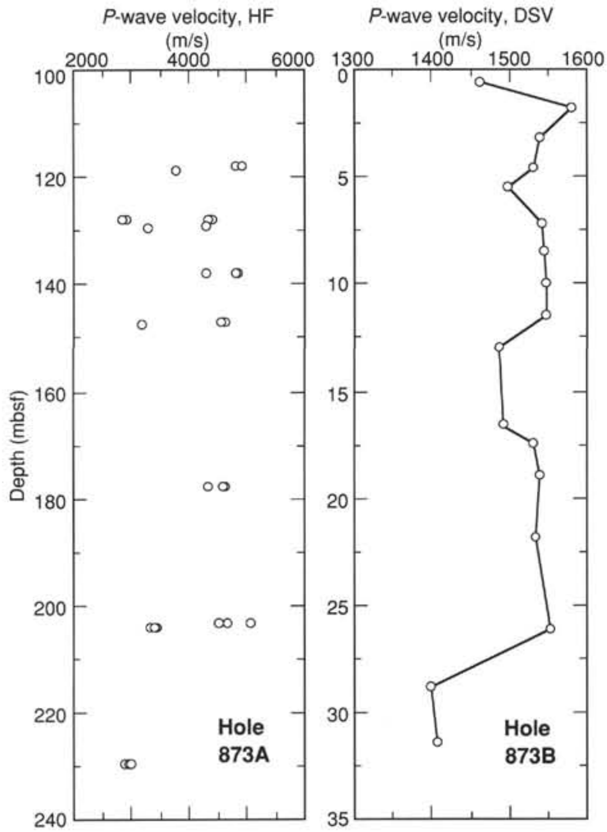

Figure 48. Hamilton Frame (HF) and digital sound velocimeter (DSV) measurements of compressional wave velocity vs. depth, Holes 873A and 873B. Note change in depth scale for DSV data taken on Hole 873B.

tigraphy" section, this chapter), has only a minor increase in uranium with respect to adjacent sediments (Fig. 53). In the FMS imagery, no apparent sedimentary structure can be seen above 58.4 mbsf, where a 10-cm-thick layer or lens of high-resistivity material was observed (see also Fig. 51). Therefore, it is possible that the main Mn-crust capping the carbonate platform facies is actually at 58.4 mbsf. The drilling of adjacent Hole 873B did not clarify the position of this Mn-crust, or whether more than a single Mn-crust is present.

Lithologic Unit III

Nature: carbonate platform
Interval: Cores 144-873A-1R through -11R
Assigned depth from logs: 58.4–151.5 mbsf
Age: Maastrichtian to Campanian

The 100-m-thick carbonate platform (Lithologic Unit III) has been divided into two facies or subunits on the basis of tan vs. gray coloration. In general, the upper, tan-colored facies has lower average resistivity (less cementation?) and lacks distinct bedding, whereas the lower, gray-colored facies has distinct interbedding of high- and low-resistivity lithologies. The log-response characteristics and internal features of these two subunits are discussed separately.

Lithologic Subunit IIIA

Nature: tan-colored skeletal packstone and wackestone
Interval: Cores 144-873A-1R through upper -8R
Assigned depth from logs: 58.4–117 mbsf
Age: Maastrichtian

The uppermost 16 m (54–70 mbsf) of the carbonate platform yields a bulk density of 1.5 g/cm^3 in the logs, in contrast to an average bulk density of 2.1 to 2.2 g/cm^3 for the underlying packstone-wackestone facies that comprise most of the platform facies (Figs. 51–52). Recovery of this upper interval in adjacent Hole 873B indicates that the low density is the result of high-porosity, poorly cemented grainstone and rudstone. The FMS imagery of this low-resistivity interval does not display any distinct sedimentary structures, other than rare, isolated, 1- to 3-cm diameter "clasts" of relatively high resistivity. This low-density facies has a sharp, irregular lower boundary to very high resistivity at 70.4 to 70.6 mbsf, corresponding to the top of Core 144-873A-3R.

The middle portion of the tan-colored skeletal limestone, corresponding to Cores 144-873A-4R and -5R, exhibits several peaks in uranium concentration. A major concentration of uranium is found at 83 mbsf, corresponding to the middle of the interval of Core 144-873A-4R, and lesser peaks can be seen at 76, 79, and 93 mbsf, respectively (Figs. 51 and 53). The recovered facies are bioclastic rudstone-grainstone to wackestone, with a pink-colored wackestone interval in Core 144-873A-5R. Only minor increases in density coincide with most of these uranium concentrations; therefore, variable degrees of cementation have not directly caused these anomalies. The sparse core recovery precludes a determination of whether these uranium concentrations correspond to hiatuses in sedimentation or to intervals having phosphate or organic carbon enrichments.

The FMS imagery of this middle portion of the tan-colored limestone indicates a progressive increase upward in average resistivity, from 74.0 to 70.5 mbsf, that is superimposed on thin (5–20 cm) alternations of higher and lower relative resistivity that display an apparent dip of 5° to the west. The underlying 8 m (74.0–82.5 mbsf) has much lower resistivity and no sedimentary structures, other than some rare 1- to 3-cm-diameter "clasts" of higher resistivity. At 83–

Table 13. DSV compressional wave velocity measurements, Hole 873B.

Core, section, interval (cm)	Depth (mbsf)	Temperature (°C)	Velocity (m/s)
144-873B-			
1H-1, 57–57	0.57	22.96	1462.4
1H-2, 60–60	1.79	22.36	1581.5
1H-3, 61–61	3.18	22.36	1540.8
1H-4, 59–59	4.56	22.36	1532.3
1H-5, 15–15	5.51	22.36	1497.3
2H-1, 64–64	7.14	22.76	1542.6
2H-2, 60–60	8.52	22.36	1546.0
2H-3, 60–60	9.96	22.36	1549.5
2H-4, 58–58	11.44	22.36	1549.5
2H-5, 60–60	12.96	22.36	1487.6
3H-1, 60–60	16.60	23.46	1494.1
3H-2, 36–36	17.42	22.36	1532.3
3H-3, 34–34	18.90	22.36	1539.1
3H-5, 24–24	21.80	22.36	1534.0
4H-1, 65–65	26.15	22.76	1553.0
4H-3, 66–66	28.82	22.36	1398.6
4H-5, 39–39	31.36	22.36	1407.2

Note: DSV = digital sound velocimeter.

82.5 mbsf, corresponding to the peak in uranium, a transition can be seen between underlying medium-bedded (30-cm average thickness) limestone and an overlying interval of relatively low-resistivity material. The medium-bedded unit extends to 117 mbsf and contains approximately 60 high-resistivity beds that alternate with low-resistivity interbeds within these 35 m. A few thicker beds, especially in the upper half of this bedded unit, display grading in resistivity, commonly from lower to higher resistivity. We interpret this resistivity grading as having been caused by an upward increase in cementation and/or decrease in grain size. For example, between 87.5 and 89.3 mbsf a 1.8-m-thick bed can be found that has an upward increase in resistivity and a sharp upper contact to low resistivity. Some of these "graded beds" may correspond to upward-fining and -coarsening sequences interpreted from the core recovery (see "Lithostratigraphy" section, this section), although some of these sequences may be an artifact of incomplete recovery juxtaposing limestones of different beds that have slight differences in average grain size. Most of the resistivity alternations do not display "grading" but have either sharp or gradational contacts with each other. We suggest that the lesser resistivity beds correspond to coarser and more porous grainstones and that higher relative resistivity intervals are finer-grained or contain more lime mud or cementation.

The lowermost 8 m of Subunit IIIA (109–117 mbsf) has a relatively lower density (1.7 g/cm^3) than the overlying and underlying limestone (2.1–2.3 g/cm^3), even though the average resistivity is similar. The corresponding recovery in Core 144-873A-7R suggests that shell-rich grainstone may contribute to this low bulk density.

Lithologic Subunit IIIB

Nature: gray-colored skeletal grainstone
Interval: lower part of Core 144-873A-8R through -11R
Assigned depth from logs: 117–151.5 mbsf
Age: Maastrichtian to Campanian

The uppermost 2 m (117–119 mbsf) of this subunit corresponds to a peak in intensity of natural gamma-ray intensity (45 API units) caused by uranium concentration (Figs. 51 and 53). This uranium-enrichment event is also associated with a significant increase in bulk density (2.3–2.4 g/cm^3) and a lesser peak in resistivity. The FMS imagery reveals a sharp upper surface to this resistivity high at 117.5 mbsf, underlain by five alternations of higher and lower resistivity beds in the following 2.5 m. This feature may be either (1) a diagenetic and cementation horizon associated with a redox front from the gray-colored, pyrite-bearing limestone to the overlying tan-colored

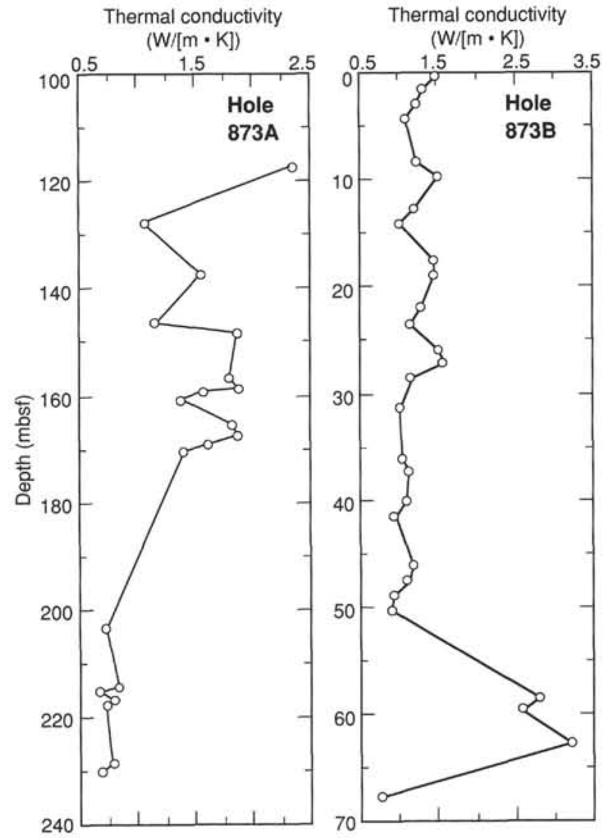

Figure 49. Thermal conductivity vs. depth, Holes 873A and 873B. Note change in depth scale for Hole 873B.

oxidized limestone or (2) a hiatus in sedimentation associated with a flooding surface, or both.

The next 6 m (120–126 mbsf) does not display any bedding features in the FMS imagery, but the underlying 25 m (126–151 mbsf) of gray skeletal limestone facies is medium to thin bedded by relatively high and lower resistivity. In particular, approximately 40 distinct high-resistivity beds, averaging 30 cm thick but as thin as 5 cm, were observed in a 17-m interval from 134.6 through 151.6 mbsf (Fig. 58). The interbedded low-resistivity intervals are of similar thicknesses, but the bedding is very irregular, having a range from 8 to 40 cm for individual beds. These beds generally display sharp upper and lower contacts, and no grading is apparent. The resistivity contrasts and implied cementation-composition differences of these alternations are much greater than those in the overlying tan-colored limestone (Subunit IIIA), where the textural and cementation contrasts are more subdued. Core recovery suggests that these features are caused by interbedded skeletal grainstone and wackestone textures with differential cementation. A possible interpretation for this distinctive bedding is deposition of storm beds of grainstone into a fine-grained lagoonal sediment. At Site 874 on Wodejebato Guyot, thick grainstone units were observed to correlate to low-resistivity intervals, in agreement with a general observation that an increasing amount of lime mud produces increasing resistivity (e.g., Asquith, 1979; Dorfman et al., 1990). Therefore, we tentatively assign the low-resistivity beds within Subunit IIIB to grainstone textures and the high-resistivity beds to packstone-wackestone textures. In addition to this bedding, there are superimposed meter-scale fluctuations in density and in resistivity.

A narrow peak in natural gamma-ray intensity at 139 mbsf is caused by thorium enrichment, not by uranium enrichment, as observed in most other peaks in natural gamma rays within the carbonate

Table 14. Thermal conductivity data, Holes 873A and 873B.

Core, section, interval (cm)	Depth (mbsf)	Thermal conductivity (W/[m · K])	Error range (W/[m · K])	Drift (K/min)
144-873A-				
8R-1, 44–54	117.74	2.35	0.01	0
9R-1, 98–109	127.88	1.07	0	–0.10
10R-1, 107–117	137.67	1.57	0.01	0.03
11R-1, 67–78	146.87	1.17	0	–0.07
11R-2, 92–102	148.58	1.86	0	–0.03
12R-1, 80–80	156.70	1.80	0	–0.01
12R-2, 125–125	158.65	1.86	0	0
12R-3, 60–60	159.50	1.57	0	0
12R-4, 60–60	161.00	1.37	0	0.01
13R-1, 20–20	165.70	1.82	0	0.02
13R-2, 60–60	167.60	1.85	0.01	0
13R-3, 60–60	169.10	1.60	0	0
13R-4, 60–60	170.60	1.40	0	0
18R-1, 72–80	203.72	0.76	0.01	–0.11
19R-2, 68–78	214.29	0.99	0.01	0.03
19R-3, 26–36	215.37	0.69	0	–0.09
19R-4, 30–40	216.91	0.92	0.01	–0.04
19R-4, 107–116	217.68	0.76	0.01	–0.08
21R-1, 19–27	228.39	0.90	0	–0.04
21R-2, 12–22	229.75	0.72	0	–0.10
144-873B-				
1H-1, 50–50	0.50	1.50	0.01	–0.04
1H-2, 50–50	1.69	1.31	0	–0.01
1H-3, 50–50	3.07	1.25	0.01	0.02
1H-4, 50–50	4.47	1.11	0	–0.01
2H-2, 50–50	8.42	1.24	0.01	–0.01
2H-3, 50–50	9.86	1.51	0.01	–0.01
2H-5, 50–50	12.86	1.21	0.01	0
2H-6, 50–50	14.28	1.03	0	–0.03
3H-2, 50–50	17.56	1.46	0	–0.02
3H-3, 50–50	19.06	1.46	0	0.01
3H-5, 50–50	22.06	1.30	0	–0.01
3H-6, 50–50	23.56	1.16	0	0
4H-1, 50–50	26.00	1.51	0	–0.03
4H-2, 50–50	27.19	1.59	0	0.02
4H-3, 50–50	28.66	1.17	0	–0.01
4H-5, 50–50	31.47	1.02	0	0
5H-2, 50–50	36.13	1.05	0.01	–0.08
5H-3, 50–50	37.40	1.13	0	0
5H-5, 50–50	40.11	1.10	0	–0.01
5H-6, 50–50	41.50	0.95	0	–0.01
6H-2, 50–50	46.24	1.19	0.01	–0.01
6H-3, 50–50	47.65	1.12	0.02	–0.03
6H-4, 50–50	49.03	0.94	0.01	–0.03
6H-5, 50–50	50.39	0.90	0.01	–0.01
8N-1, 52–52	58.52	2.81	0	0.02
8N-2, 28–28	59.65	2.59	0	0.02
9N-1, 23–23	62.73	3.23	0	0.01
10N-1, 68–68	67.68	0.77	0.01	–0.14

platform (Figs. 51 and 53). This unique horizon may be caused by a volcanic ash bed or a pulse of clay influx from a nearby emergent volcanic island, although no peak in aluminum was recorded. This feature was not recovered in Core 144-873A-10R at the corresponding sub-bottom depth range.

Small peaks in uranium are seen at 142 and 144.5 mbsf; the corresponding lower portion of Core 144-873A-10R has interbedded tan- and gray-colored limestone, suggesting that redox fronts may contribute to these uranium concentrations.

The base of the carbonate platform succession was observed by the FMS imagery as a 20-cm-thick layer of relatively high resistivity at 151.4–151.6 mbsf, sharply overlying a thick, featureless, very low-resistivity facies, which we interpret as being the reddish brown clay of Lithologic Unit IV.

Lithologic Unit IV

Nature: brownish red clay
Interval: Cores 144-873A-12R through -13R
Assigned depth from logs: 151.5–174 mbsf
Age: indeterminate

The clay facies is characterized by high concentrations of thorium, very low resistivity (0.6–0.7 Ωm), and wide borehole diameter.

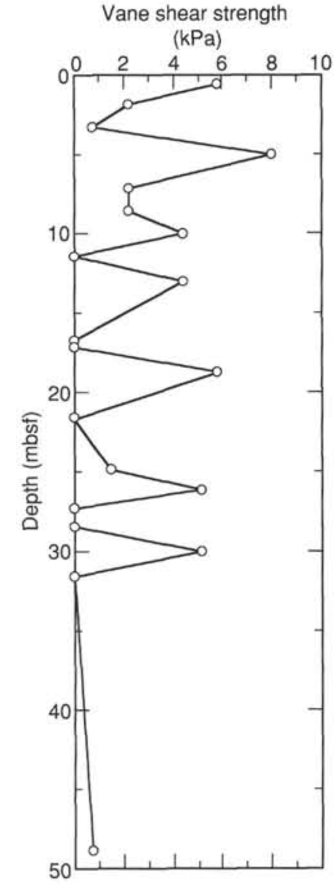

Figure 50. Wykeham-Farrance vane shear strength vs. depth in the pelagic sediments of Hole 873B.

Density is <2.0 g/cm^3, but exact values have been obscured by the widened hole. The high natural gamma-ray intensities are the result of thorium, rather than uranium, at lower concentrations than in the overlying carbonates (Fig. 53). The clays are very low in potassium and silicon relative to the underlying weathered basalts (Figs. 53–54). The aluminum/silicon ratio of the clays is twice that of the basalt, indicating that significant leaching of silica has taken place. Iron contents are also less than that in the underlying basalt. These characteristics are consistent with the sedimentologic interpretation that this clay is the byproduct of tropical subaerial weathering of basalts, during which potassium and silica were leached.

The FMS imagery within the clay interval is generally featureless, except for a zone of relatively moderate resistivity in the lower portion of this unit at 170.4–173.0 mbsf, which may represent an upward transition from the underlying altered basalts.

The top of the clay is well defined by a sharp decrease in thorium content at 151.5 mbsf (Fig. 51). The base of the clay is effectively at 174 mbsf (or at 173.8 mbsf in FMS images), overlying high-resistivity and increased bulk density material, which probably corresponds to the altered basalt recovered in Core 144-873A-14R. The lowermost clay has a peak in thorium/uranium ratio (Figs. 51 and 53). The clay/basalt contact within the borehole has an apparent dip of 27° to the west.

Lithologic Unit V

Nature: basalt with variable degrees of alteration
Interval: Cores 144-873A-14R to lower -18R
Assigned depth from logs: 174–200 mbsf
Age: indeterminate

Table 15. Wykeham-Farrance and Torvane shear strength data, Hole 873A and 873B.

Core, section, interval (cm)	Depth (mbsf)	Test type	Spring constant	Vane constant	Torsion angle (degrees)	Torsion (kg/cm^2)	Undrained shear strength (kPa)
144-873A-							
12R-1, 60	156.50	TV				0.14	34.32
12R-1, 117	157.07	TV				0.20	49.03
12R-CC, 13	161.30	TV				0.57	139.74
13R-2, 112	168.12	TV				0.28	67.42
144-873B-							
1H-1, 67	0.67	WF	32.72	0.23	8		5.83
1H-2, 73	1.92	WF	32.72	0.23	3		2.19
1H-3, 71	3.28	WF	32.72	0.23	1		0.73
1H-4, 103	5.00	WF	32.72	0.23	11		8.02
2H-1, 75	7.25	WF	32.72	0.23	3		2.19
2H-2, 70	8.62	WF	32.72	0.23	3		2.19
2H-3, 70	10.06	WF	32.72	0.23	6		4.37
2H-4, 68	11.54	WF	32.72	0.23	0		0
2H-5, 71	13.07	WF	32.72	0.23	6		4.37
3H-1, 71	16.71	WF	32.72	0.23	0		0
3H-2, 20	17.26	WF	32.72	0.23	0		0
3H-3, 21	18.77	WF	32.72	0.23	8		5.83
3H-5, 14	21.70	WF	32.72	0.23	0		0
3H-7, 34	24.90	WF	32.72	0.23	2		1.46
4H-1, 76	26.26	WF	32.72	0.23	7		5.10
4H-2, 66	27.35	WF	32.72	0.23	0		0
4H-3, 33	28.49	WF	32.72	0.23	0		0
4H-4, 63	30.11	WF	32.72	0.23	7		5.10
4H-5, 63	31.61	WF	32.72	0.23	0		0
6H-4, 36	48.89	WF	32.72	0.23	1		0.73

Notes: WF = Wykeham-Farrance vane, and TV = Soil-test Torvane.

Table 16. Hamilton Frame measurements of compressional wave velocity, Holes 873A and 873B.

Core, section, interval (cm)	Depth (mbsf)	Distance (mm)	Axes of measurement	Traveltime (μs)	Corrected traveltime (μs)	Measured velocity (m/s)	Velocity anisotropy index
144-873A-							
8R-1, 49–51	117.79	23.55	a	7.89	4.89	4820.88	
8R-1, 49–51	117.79	21.78	b	7.53	4.53	4813.26	
8R-1, 49–51	117.79	21.59	c	7.39	4.39	4923.60	–0.02
8R-1, 129–131	118.59	22.30	a	9.26	6.26	3562.30	
8R-1, 129–131	118.59	21.45	b	8.70	5.70	3764.48	
8R-1, 129–131	118.59	21.45	c	8.70	5.70	3764.48	–0.03
9R-1, 94–96	127.84	24.55	a	8.65	5.65	4345.13	
9R-1, 94–96	127.84	21.97	b	7.98	4.98	4416.08	
9R-1, 94–96	127.84	21.63	c	7.99	4.99	4339.02	0.01
9R-1, 108–110	127.98	22.18	a	10.63	7.63	2908.85	
9R-1, 108–110	127.98	21.59	b	10.55	7.55	2861.50	
9R-1, 108–110	127.98	21.86	c	10.66	7.66	2853.79	0.01
9R-2, 54–56	128.94	16.75	a	6.90	3.90	4300.39	
9R-2, 103–105	129.43	14.77	a	7.48	4.48	3296.88	
10R-1, 116–118	137.76	21.78	a	8.07	5.07	4295.86	
10R-1, 116–118	137.76	21.57	b	7.44	4.44	4858.11	
10R-1, 116–118	137.76	21.46	c	7.44	4.44	4833.33	–0.05
11R-1, 67–67	146.87	19.66	a	7.27	4.27	4609.61	
11R-1, 67–67	146.87	21.64	b	7.67	4.67	4638.80	
11R-1, 67–67	146.87	21.63	c	7.73	4.73	4572.94	0.01
11R-1, 140–142	147.60	21.35	a	9.72	6.72	3179.45	
15R-1, 23–26	177.63	25.78	a	8.94	5.94	4341.53	
15R-1, 23–26	177.63	21.53	b	7.64	4.64	4642.09	
15R-1, 23–26	177.63	21.42	c	7.66	4.66	4598.54	–0.02
18R-1, 19–22	203.19	19.74	a	7.36	4.36	4527.52	
18R-1, 19–22	203.19	21.33	b	7.19	4.19	5090.69	
18R-1, 19–22	203.19	21.55	c	7.63	4.63	4654.43	0.03
18R-1, 91–93	203.91	23.54	a	10.09	7.09	3320.17	
18R-1, 91–93	203.91	21.39	b	9.20	6.20	3450.00	
18R-1, 91–93	203.91	21.45	c	9.31	6.31	3399.37	0
21R-1, 126–128	229.46	23.83	a	11.24	8.24	2891.99	
21R-1, 126–128	229.46	21.38	b	10.21	7.21	2965.33	
21R-1, 126–128	229.46	21.39	c	10.13	7.13	3000.00	–0.02
144-873B-							
8N-2, 78–80	60.15	15.20	a	9.19	6.19	2455.57	
10N-1, 106–108	68.60	15.83	a	7.21	4.21	3760.10	

Notes: a = direction perpendicular to split core plane, b = direction transverse to split core plane, and c = core axis; all axes orthogonal.

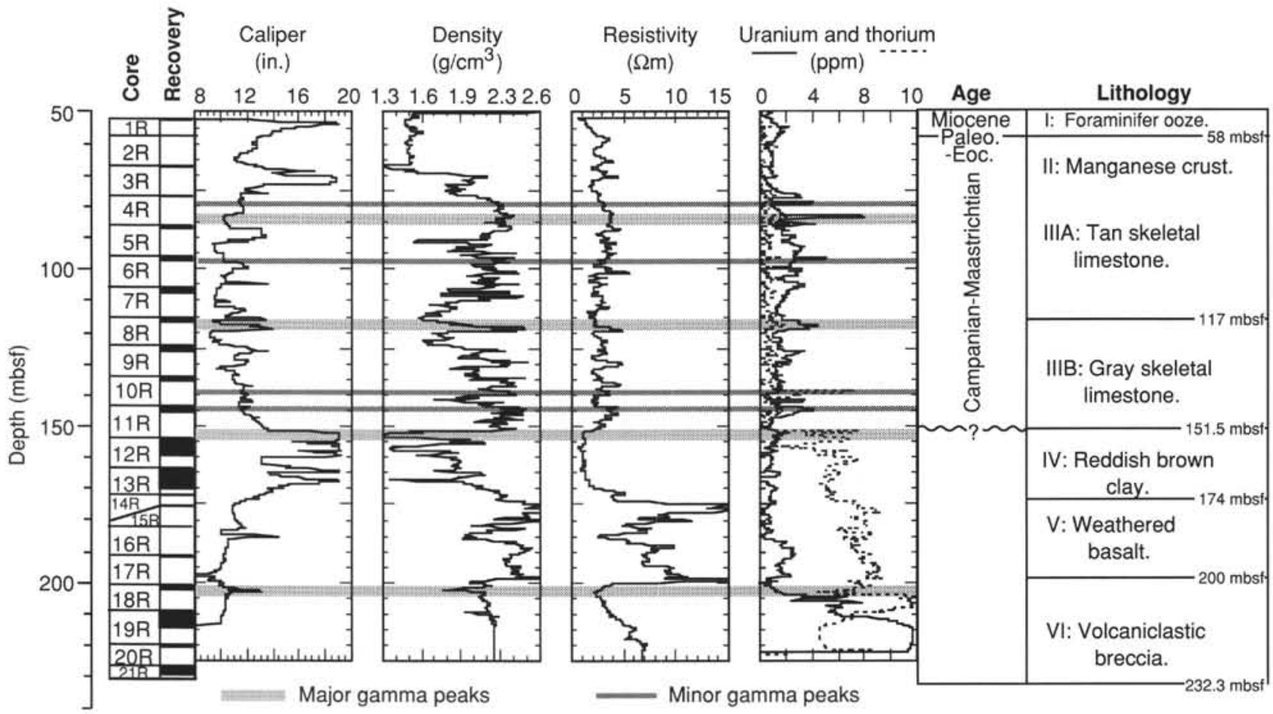

Figure 51. Stratigraphy of Hole 873A from selected geophysical logs compared to cored intervals, lithostratigraphy, and biostratigraphic ages. Resistivity is from the medium-penetration phasor-induction (IMPH) tool. Uranium and thorium concentrations are from the natural gamma tool on the geochemistry run. Caliper, or apparent hole diameter, does not record values greater than 19 in. (48 cm); drill-bit diameter is 9.9 in. (25 cm). Fluctuations in density and resistivity generally coincide within the carbonate platform; therefore, these variations provide a record of relative porosity of different limestone beds. Peaks in total natural gamma are marked by shaded lines. In the carbonate platform facies, these peaks are mainly a result of higher uranium concentrations and may be associated with hiatuses in sedimentation or exposure surfaces. In contrast, within the clay and volcanic facies, the natural gamma intensity variations are mainly caused by thorium concentrations in clay-rich zones.

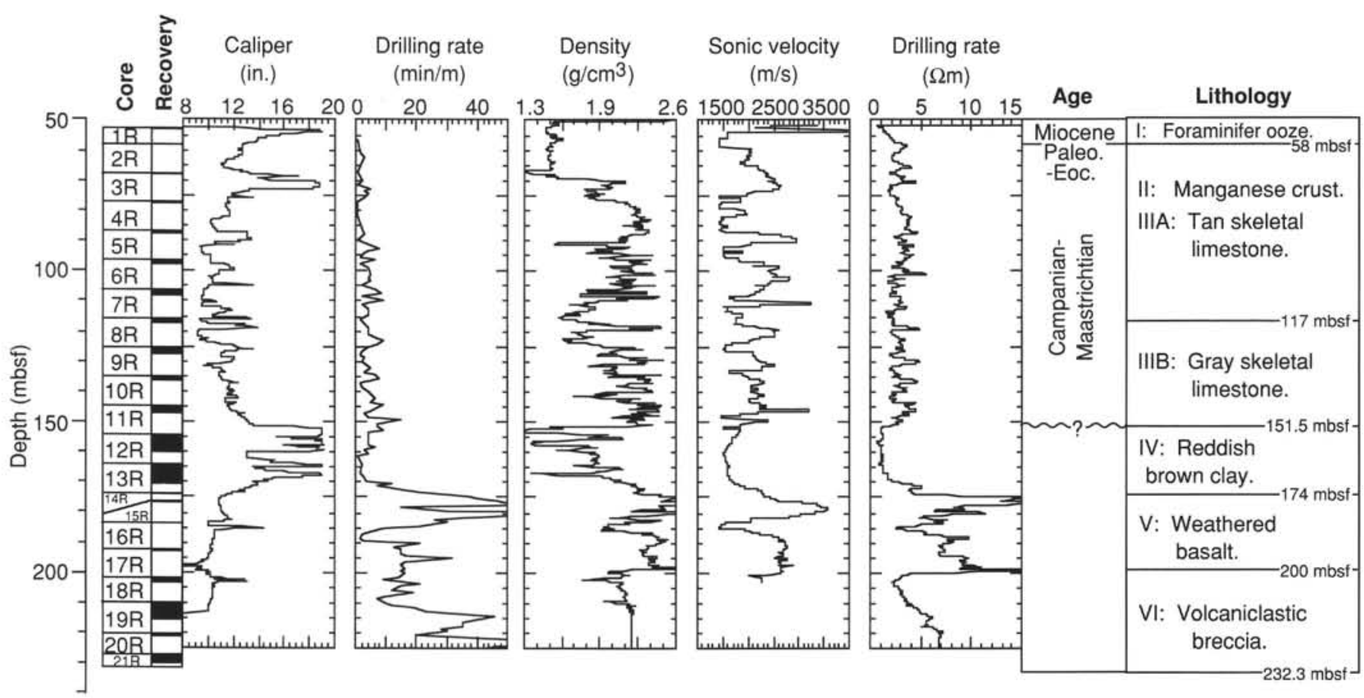

Figure 52. Geophysics logging measurements in the carbonate platform in Hole 873A. Individual peaks generally correlate among these logs and probably correspond to variations in porosity and cementation within the carbonate platform facies and to intervals of clay enrichment in the volcanic succession. Drilling or penetration rates were recorded at about 1-m intervals.

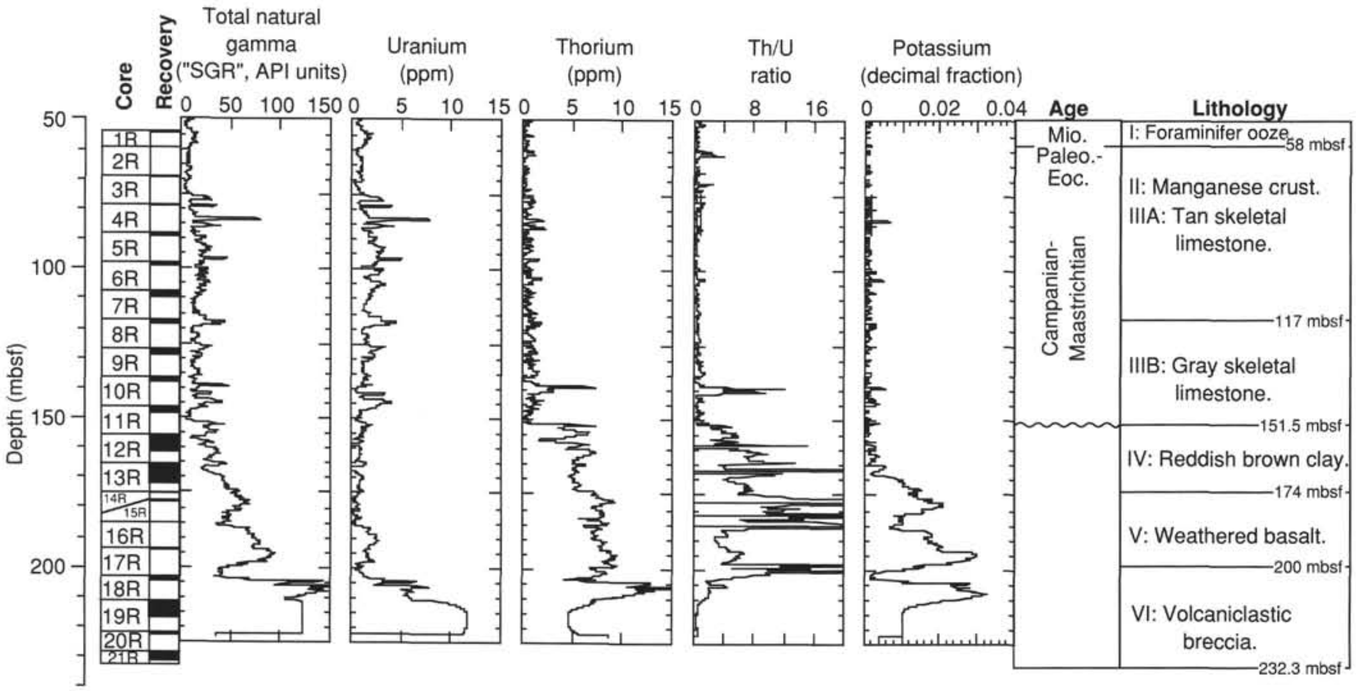

Figure 53. Radioactive element concentrations within the carbonate platform in Hole 873A. Total natural gamma, uranium, and potassium logs are from the geochemical tool-string run. The thorium/uranium ratio provides a gauge of the relative importance of clay (high Th/U) in the natural gamma signal. Potassium remains near the noise level of the measurements, except within the basalt layers.

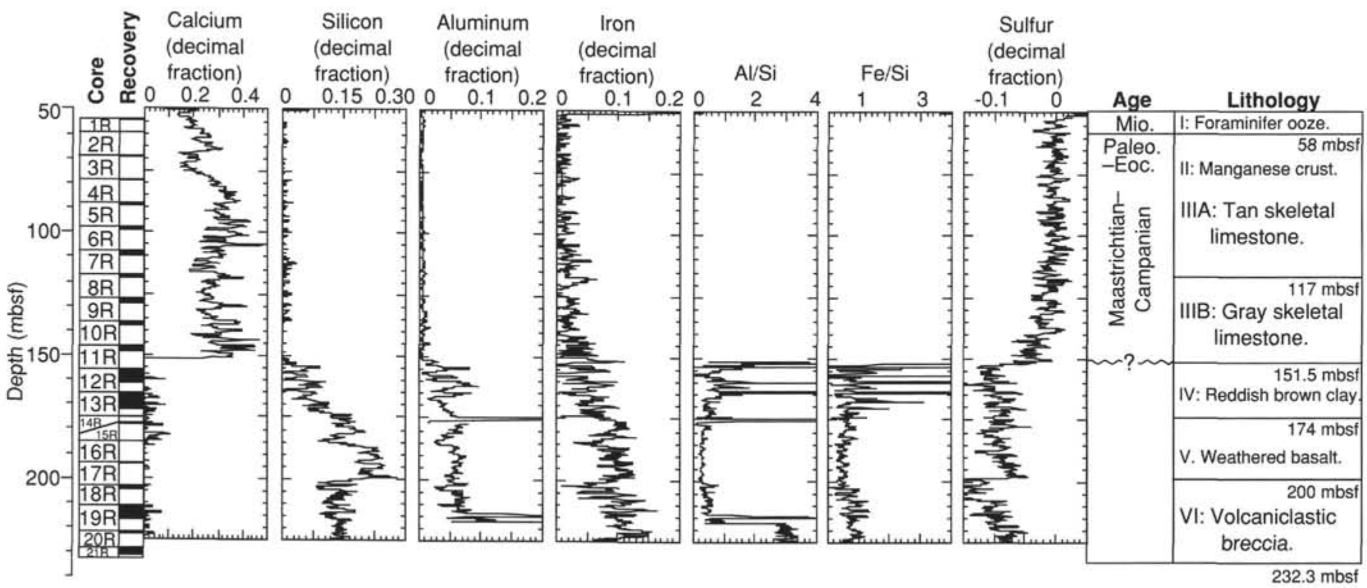

Figure 54. Relative stable elements (calcium, silicon, aluminum, iron, and sulfur) within the carbonate platform of Hole 873A. Values are given in relative proportions and have not been adjusted for porosity variations. Except for calcium, all other elements are in trace amounts within the platform carbonates. Iron, silica, and aluminum dominate within the clay and volcanic facies in the lower half of the hole, with the highest Al values occurring within clay-rich intervals. The Al/Si ratio is a partial indicator of the degree of silica leaching during tropical weathering.

The interbedded volcanics and weathering horizons of Lithologic Unit V are characterized by high bulk density (averaging 2.4–2.5 g/cm^3) and extreme fluctuations in both resistivity (from 1 to >3 Ωm) and thorium/uranium ratio (4 to 12). An interval of relatively low resistivity and density at about 184 mbsf corresponds to very low core recovery (Core 144-873A-16R) and may be caused by a clay layer between basalt flows. The FMS imagery indicates that this low-resistivity zone extends from 183 to 186 mbsf, but it is bordered by 2-m-thick medium-resistivity transitions.

The FMS imagery indicates that the highest resistivity intervals, which presumably represent the least-altered basaltic flows, are at 173.8–179.2, 188.0–189.1, and 198.7–199.8 mbsf. Between these layers are either intermediate resistivity zones or intervals containing 1- to 5-cm diameter "clasts" in a low-resistivity matrix.

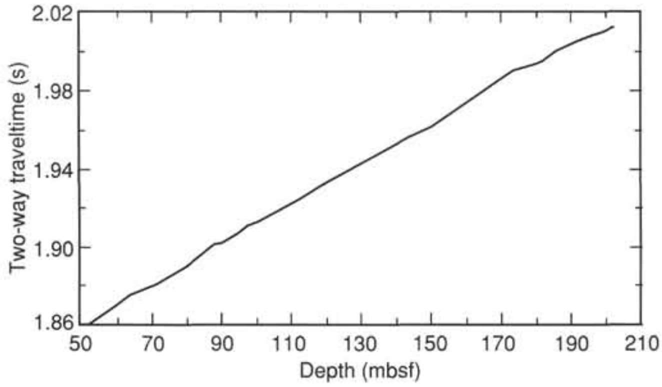

Figure 55. Integrated sonic traveltime vs. depth in the carbonate platform in Hole 873A. These interval velocities appear to have been biased to slower values because of the irregular borehole conditions.

Lithologic Unit VI

Nature: volcaniclastic breccia
Interval: lower part of Core 144-873A-18R through -21R
Assigned depth from logs and drilling: 200–232.3 mbsf
Age: indeterminate

At 200 mbsf, a sharp downward decrease occurs in silicon, density, and resistivity as well as a sharp increase in the Al/Si ratio (Figs. 51 and 54). This sharp boundary, located at 199.8 mbsf in the FMS imagery, probably corresponds to the clay-rich weathered top of the volcaniclastic breccia, overlain by a dense basalt flow of Lithologic Unit V. Only the upper volcaniclastic breccia could be logged, and this interval displays a progressive upward decrease in resistivity (7 Ωm near base, 2 Ωm at top) and to a lesser extent in density. An interval of very low relative resistivity from 199.8 to 204.5 mbsf coincides with a clay-rich interval at the top of this unit. This trend corresponds to the observed upward increase in clay content produced by surficial weathering of the volcaniclastic breccia. The FMS imagery also indicates that, above 213 mbsf, the resistivity contrast of the "pebble" texture decreases, and effectively disappears above 211.8 mbsf, accompanied by a trend to lower relative average resistivity and the occurrence of subvertical "fractures."

The FMS imagery of the underlying less altered volcanic breccia reveals a general "pebble" texture with relatively high- and low-resistivity "clasts" packed in an intermediate resistivity matrix. These "clasts" are 2 cm or less in diameter. At 216.4–218.4 mbsf, a 20-cm-thick irregular layer of low resistivity is present that could represent a clay-rich level or elongate lens; a similar feature is at 210.4 mbsf.

Seismic Stratigraphy Interpretation

Single-channel seismic profiles were obtained on two crossings of Hole 873A using a 200-in.^{3} water gun as a sound source. These data were recorded on a Masscomp computer, refiltered, and displayed; they were found to be inferior, however, to a seismic record collected on a previous survey across the Site 873 location with two 80-in.^{3} water guns shot to a six-channel seismic streamer. These multichannel data were processed up through migration and are displayed in Figure 56. Comparison with the coring results suggest that several internal reflectors can be correlated to the recovered lithologic section and the downhole measurements.

First, and most easily identified, is the base of the foraminifer ooze (pelagic cap) at ~54 mbsf from the drilling record, and 0.075 s TWT below the seafloor on the seismic record. This reflector is easily substantiated by the 3.5-kHz record that also shows a pronounced "hardground" reflector at the same two-way traveltime.

Below this distinct reflector that marks the limestone/pelagic cap boundary lie a series of discontinuous, "wavy" reflectors, none of which have any individual character. This package of reflectors marks the limestone section from ~54 to 151 mbsf, with a seismic section thickness of 0.08 s TWT. Like the seismic section, the geophysical logs and the caliper log (Fig. 52) show a ragged character, with no distinctive features at any particular level.

Below the package of discontinuous, homogeneous reflectors is an interval devoid of reflectors that seems to correspond to the clay section from 151 to 174 mbsf. The sonic log (Fig. 52) is remarkably constant at about 1.5 km/s through this interval, so a lack of reflections could be expected. However, as this interval occurs just above the distinct basement reflector, the lack of reflections may also be the result of the automatic gain control limiting the dynamic range of the underlying large event during post-acquisition processing.

The basement reflector occurs as a prominent event just above 2.0 s TWT on Figure 56. This corresponds to the top of the basalts in Lithologic Unit V. Within the logged interval from 174 to 200 mbsf within these basalts (Fig. 52), the sonic log shows a distinct velocity increase between 165 and 175 mbsf that also corresponds to downward increases in resistivity, density, and drilling rate. This interval is not apparent on the seismic record, but it may correspond to an unrecovered clay section that marks an older erosion surface within the basement platform.

Below the basement reflector between 2.1 and 2.3 s TWT, and therefore within the basement section, is another reflector with a pronounced dip, as shown on the left-hand side of Figure 56. This reflector flattens at its shallowest level (2.05 s TWT) just below Hole 873A. Hole 873A was positioned so that there would be the opportunity to reach this dipping reflector with the drill, if none of the overlying reflectors proved to be basement. Because basement was reached well above the level of the dipping reflector, the origin of this pronounced seismic event remains unknown.

The above correlations and formation velocities are reasonably confident statements of in-situ conditions at Hole 873A. As such, they can be used with regional seismic surveys to construct a seismic stratigraphic map of the entire Wodejebato Guyot platform.

In summary, the logging data and seismic stratigraphic succession at Site 873 on Wodejebato Guyot may be divided into four main parts:

1. A pelagic cap of Miocene through Pleistocene age indicating substantial subsidence of Wodejebato Guyot.
2. A succession of restricted to oxygenated lagoonal and back-reef facies from 58.4 to 151.5 mbsf. The sediments in this lagoonal environment changed at a depth of 117 mbsf from being pyrite-bearing skeletal limestone deposited under restricted conditions below to a more oxygenated facies above. In addition to this major surface, uranium-enrichment horizons indicate either levels of condensation or hiatuses that may be related to sea-level fluctuations, or changes in bottom-water oxygen levels in the lagoon. The carbonate platform is overlain by a Mn-crust (58.4–54.0 mbsf), with an apparent hiatus in sedimentation from the Latest Cretaceous to the Miocene.
3. A 22.5-m-thick clay layer (151.5–174.0 mbsf) developed from extensive chemical weathering of volcanic material.
4. An underlying volcanic edifice formed by interbedded volcaniclastics, basaltic flows, and weathering horizons, with its upper surface at 174 mbsf.

SUMMARY AND CONCLUSIONS

Initial interpretation of the cores obtained at Site 873 indicates that the upper portion of the igneous basement of Wodejebato Guyot is characterized by at least two volcanic events associated with the late-stage development of Wodejebato Guyot. Hyaloclastic breccias were formed during a phreatomagmatic, near-shore, or submarine basaltic eruption; these subsequently underwent deep oxidative weath-

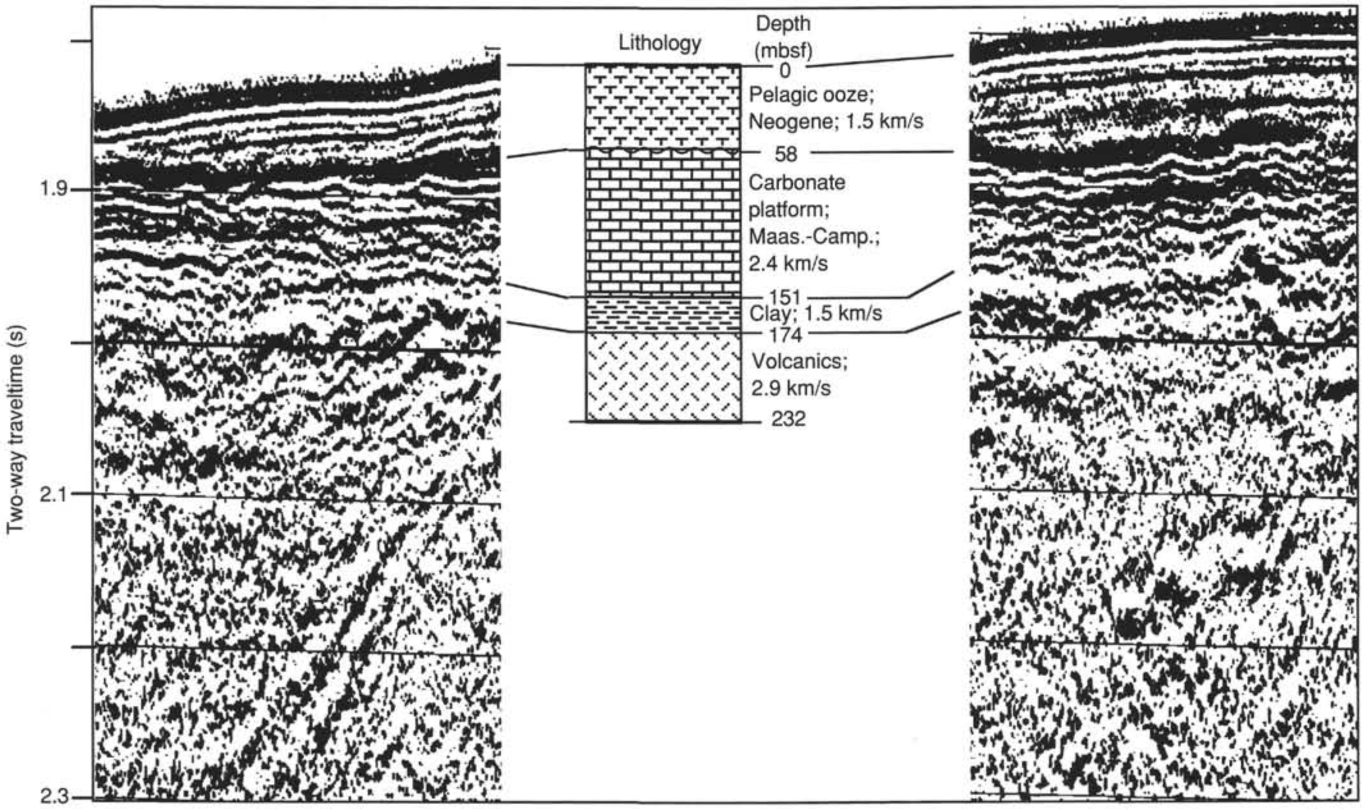

Figure 56. Lithostratigraphic correlations to the seismic stratigraphy section at Site 873. Major reflectors correspond to stratigraphic breaks in deposition or to major facies changes. Meter levels of key stratigraphic horizons are based upon the identification of the lithologic units in logs.

ering. After an unknown period of time, the second recorded event was the eruption of differentiated, olivine-poor, alkali basalt and hawaiite flows at Site 873. These are the last eruptions recorded at this site; they probably represent the final stages of constructional volcanism. These basalts, as well as the underlying hyaloclastite breccias, exhibit a reversed polarity with respect to the present geomagnetic field; this polarity was acquired at low latitude (~9° to 14°S) (+17° to +27°) in the Southern Hemisphere. After volcanism ceased, a second deep oxidative weathering profile developed and was preserved through apparently rapid submergence in a low-energy (lagoonal) environment or through rapid burial.

In the late Campanian, a transgression of the sea occurred over this complete or partially eroded weathering profile, and a shallow-water platform with open-marine circulation developed. Progressive and periodic flooding of the former island are documented as alternating phases of open-marine to more restricted conditions within a shallow lagoon. The presence of common plant remains at the beginning of shallow-water marine deposition documents the importance of a terrestrial influence at this site, and implies that a vegetated island was close to Site 873. The upward decrease of terrestrial influence, as suggested by the progressive decrease in the abundance of woody materials until they are virtually absent, parallels the establishment of gradually more open-marine conditions. Planktonic foraminifers are present in the middle of the lower carbonate platform sequence and record the period of maximum flooding. Evidence of restricted environments, such as a decrease in faunal and floral diversity, and the frequency of probable emergence surfaces increase upsection. The sequence recovered at Site 873 ends during the Maastrichtian under normal marine conditions, with the deposition of algal rudist rudstone as the only evidence of bioherm proximity.

The carbonate platform subsided into the pelagic realm before the late Paleocene, as indicated by the presence of upper Paleocene pelagic limestone and lithoclasts of Maastrichtian neritic limestone, which are reworked into the manganese-coated and phosphatized conglomerate. After submergence of the carbonate platform, and throughout the Paleogene, current activity prohibited sediment accumulation and aided the formation of the conglomerate. During early and middle Eocene times, Site 873 was under a zone of high productivity and intensive winnowing, and a manganese-encrusted and phosphatized hardground continued to develop.

The accumulation of pelagic sediments did not begin until the early Miocene. The pelagic deposition was never continuous; deposition was interrupted by a number of hiatuses of varying duration within the Miocene (the most conspicuous) and early Pliocene. Sedimentation rates increase from the Miocene (8 m/m.y.) to the Pliocene (20–25 m/m.y.). In the late Pliocene, between 2 and 3 Ma, sediment accumulation rates decrease again to around 3 m/m.y. As at the earlier sites farther to the south (Sites 871 and 872), the abundance of siliceous microfossils and their diagenetic products (zeolites) reach maximum values in the Pliocene, reflecting paleoproductivity patterns.

REFERENCES*

Asquith, G.D., 1979. *Subsurface Carbonate Depositional Models: A Concise Review:* Tulsa, OK (Petroleum Publ. Co.).

Bergersen, D.D., in press. Geology and geomorphology of Wodejebato (Sylvania) Guyot, Marshall Islands. *In* Pringle, M., Sager, W.W., Sliter, W.V., and Stein, S. (Eds.), *The Mesozoic Pacific:* Am. Geophys. Union.

Berggren, W.A., Kent, D.V., and Van Couvering, J.A., 1985. The Neogene: Pt. 2. Neogene geochronology and chronostratigraphy. *In* Snelling, N.J. (Ed.),

* Abbreviations for names of organizations and publication titles in ODP reference lists follow the style given in *Chemical Abstracts Service Source Index* (published by American Chemical Society).

The Chronology of the Geological Record. Geol. Soc. London Mem., 10:211–260.

Brewer, J.M., 1971. North Atlantic fluoride profiles. *Deep-Sea Res., Part A,* 18:237–241.

Cole, W.S., 1954. Larger foraminifera and smaller diagnostic foraminifera from Bikini drill holes. *Geol. Surv. Prof. Pap. U.S.,* 260-0:569–608.

Davis, A.S., Pringle, M.S., Pickthorn, L.B.G., Clague, D.A., and Schwab, W.C., 1989. Petrology and age of alkalic lava from the Ratak Chain of the Marshall Islands. *J. Geophys. Res.,* 94:5757–5774.

Deer, W.A., Howie, R.A., and Zussman, J., 1966. *An Introduction to the Rock-Forming Minerals:* London (Longman Group).

Detrick, R.S., and Crough, S.T., 1978. Island subsidence, hot spots, and lithospheric thinning. *J. Geophys. Res.,* 83:1236–1244.

Dorfman, M.H., Newey, J.-J., and Coates, G.R., 1990. New techniques in lithofacies determination and permeability prediction in carbonates using well logs. *In* Hurst, A., Lovell, M.A., and Morton, A.C. (Eds.), *Geological Applications of Wireline Logs.* Geol. Soc. Spec. Publ. London, 48:113–120.

Duncan, R.A., and Clague, D.A., 1985. Pacific plate motions recorded by linear volcanic chains. *In* Nairn, A.E.M., Stehli, F.G., and Uyeda, S. (Eds.), *The Ocean Basins and Margins* (Vol. 7A): *The Pacific Ocean:* New York (Plenum), 89–121.

Emery, K.O., Tracey, J.I., Jr., and Ladd, H.S., 1954. *Geology of Bikini and Nearby Atolls.* Geol. Surv. Prof. Pap. U.S., 260-A.

Hamilton, E.L., and Rex, R.W., 1959. Lower Eocene phosphatized *Globigerina* ooze from Sylvania Guyot. *Geol. Surv. Prof. Pap. U.S.,* 260-W:785–797.

Hein, J.R., Kang, J.K., et al., 1990. Geological, geochemical, geophysical, and oceanographic data and interpretations of seamounts and C-rich ferromanganese crusts from the Marshall Islands, KORDI-USGS R.V. *Faranella* cruise F10-89-CP. *Open-File Rep.—U.S. Geol. Surv.,* 90-407.

Hydrographer of the Navy, 1991. *Admiralty Tide Tables* (Vol. 3): *Pacific Ocean and Adjacent Seas:* London (Hydrographer of the Navy).

Lincoln, J.M., Pringle, M.S., and Premoli Silva, I., in press. Early and Late Cretaceous volcanism and reef-building in the Marshall Islands. *In* Pringle, M.S., Sager, W.W., Sliter, W.V., and Stein, S. (Eds.), *The Mesozoic Pacific.* Am. Geophys. Union, Geophys. Monogr. Ser.

Lovell, M.A., 1984. Thermal conductivity and permeability assessment by electrical resistivity measurements in marine sediments. *Mar. Geotechnol.,* 6:205–240.

Moore, J.G., Clague, D.A., Holcomb, R.T., Lipman, P.W., Normark, W.R., Torresan, M.E., 1989. Prodigious submarine landslides on the Hawaiian Ridge. *J. Geophys. Res.,* 94:17465–17484.

Nakanishi, M., Tamaki, K., and Kobayashi, K., 1992. A new Mesozoic isochron chart of the northwestern Pacific Ocean: paleomagnetic and tectonic implications. *Geophys. Res. Lett.,* 19:693–696.

O'Reilly, W., 1984. *Rock and Mineral Magnetism:* Glasgow (Blackie).

Premoli Silva, I., 1986. A new biostratigraphic interpretation of the sedimentary record recovered at Site 462, Leg 61, Nauru Basin, western equatorial Pacific. *In* Moberly, R., Schlanger, S.O., et al., *Init. Repts. DSDP,* 89: Washington (U.S. Govt. Printing Office), 311–319.

Premoli Silva, I., and Brusa, C., 1981. Shallow-water skeletal debris and larger foraminifers from Deep Sea Drilling Project Site 462, Nauru Basin, western equatorial Pacific. *In* Larson, R.L., Schlanger, S.O., et al., *Init. Repts. DSDP,* 61: Washington (U.S. Govt. Printing Office), 439–473.

Pringle, M.S., Jr., 1992. Geochronology and petrology of the Musicians Seamounts, and the search for hot spot volcanism in the Cretaceous Pacific [Ph.D. dissert.]. Univ. of Hawaii, Honolulu.

Schlanger, S.O., 1963. Subsurface geology of Eniwetok Atoll. *Geol. Surv. Prof. Pap. U.S.,* 260-BB:991–1066.

Vacquier, V., 1985. The measurement of thermal conductivity of solids with a transient linear heat source on the plane surface of a poorly conducting body. *Earth Planet. Sci. Lett.,* 74:275–279.

Von Herzen, R.P., and Maxwell, A.E., 1959. The measurement of thermal conductivity of deep-sea sediments by a needle probe method. *J. Geophys. Res.,* 65:1557–1563.

Ms 144IR-106

NOTE: For all sites drilled, core-description forms ("barrel sheets") and core photographs can be found in Section 3, beginning on page 453. Forms containing smear-slide data can be found in Section 4, beginning on page 1017. Thin-section data are given in Section 5, beginning on page 1037. Conventional log, FMS, dipmeter, and geochemical log (element and oxide weight %) data can be found in CD-ROM form (back pocket).

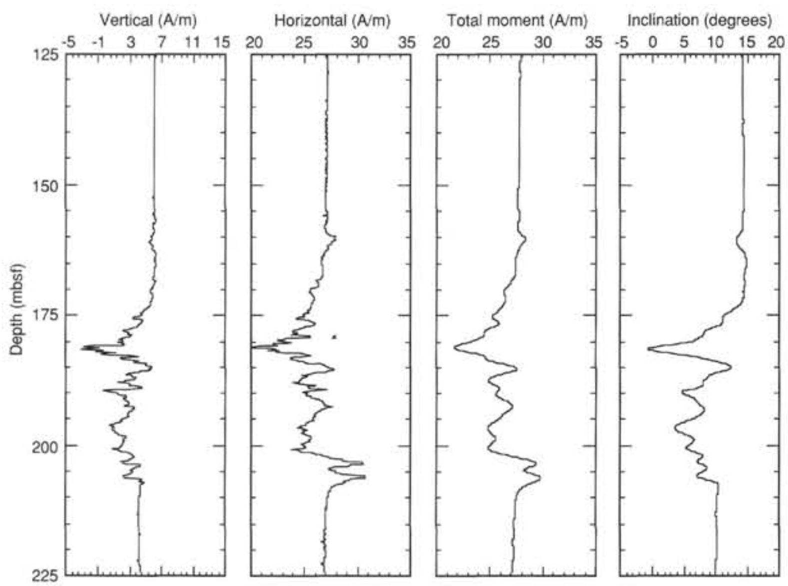

Figure 57. Downhole magnetic field measurements from the Formation MicroScanner (FMS) three-axis flux-gate magnetometer instrument. The three-component magnetic data (FX is the horizontal "*x*" component, parallel to the FMS Pad #1 direction; FY is the horizontal "*y*" component, perpendicular to the FMS Pad #1 direction; and FZ is the vertical "*z*" component) enable computation of horizontal intensity, total intensity, inclination, and relative declination. Within the carbonate section, the magnetometer appears to be recording only the ambient present-day field. At about 175 mbsf, coinciding with the clay/basalt boundary, sharp decreases occur in both the vertical and horizontal component of the downhole magnetic field. These decreases are caused by strong magnetization of the weathered basalt and underlying volcaniclastic units in an opposing direction to the present-day normal-polarity magnetic field. This is consistent with the reversed-polarity magnetization obtained for recovered core samples of these lithologies.

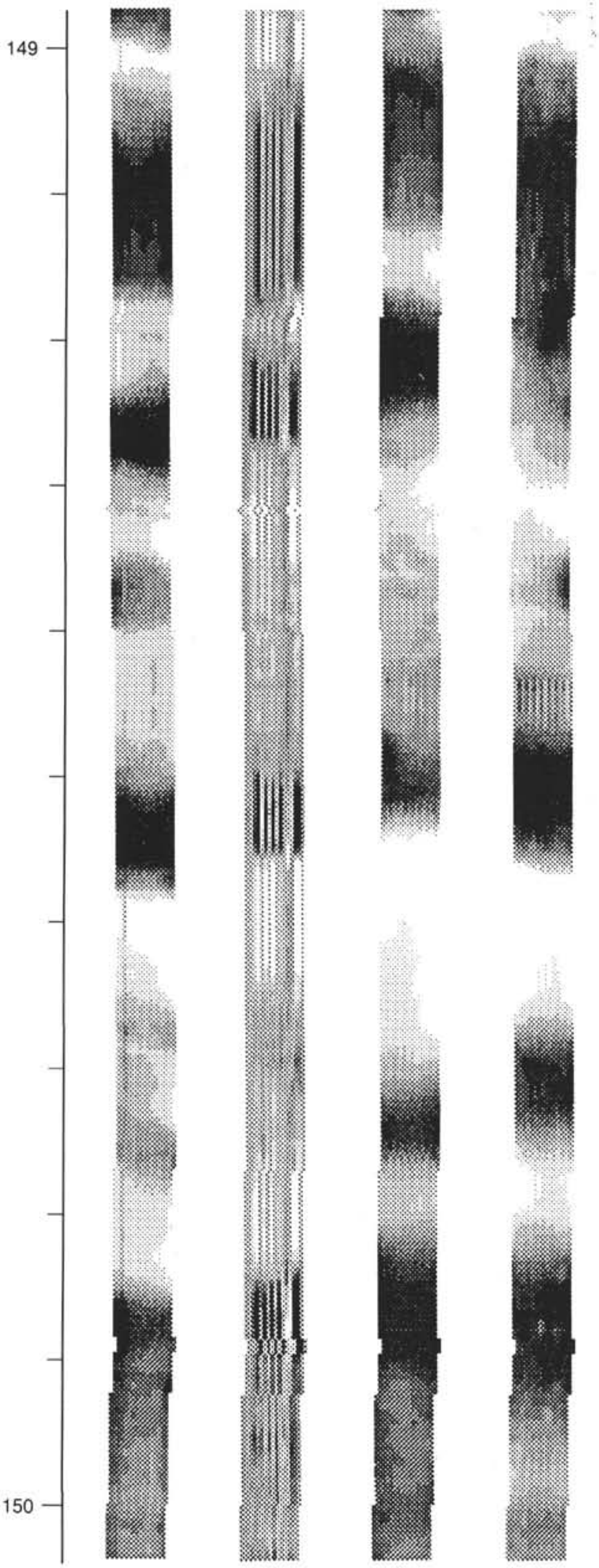

Figure 58. Formation MicroScanner (FMS) high-resolution, high-contrast, resistivity imagery of the borehole wall through a portion of the gray skeletal limestone in Lithologic Subunit IIIB, Hole 873A. The interbedded high-resistivity (light colored) and low-resistivity (dark colored) lithologies probably represent grainstone-packstone layers deposited within a wackestone, followed by differential cementation. An increase in the amount of lime mud generally produces an increase in resistivity (e.g., Asquith, 1979; Dorfman et al., 1990); therefore, the low-resistivity beds are tentatively interpreted as less-cemented grainstone textures and high-resistivity beds as packstone-wackestone textures. This layering may represent storm deposits carried into a restricted lagoon. The interval from 149 to 150 mbsf corresponds to the middle part of Core 144-873A-11R.

Hole 873A: Resistivity-Velocity-Natural Gamma Ray Log Summary

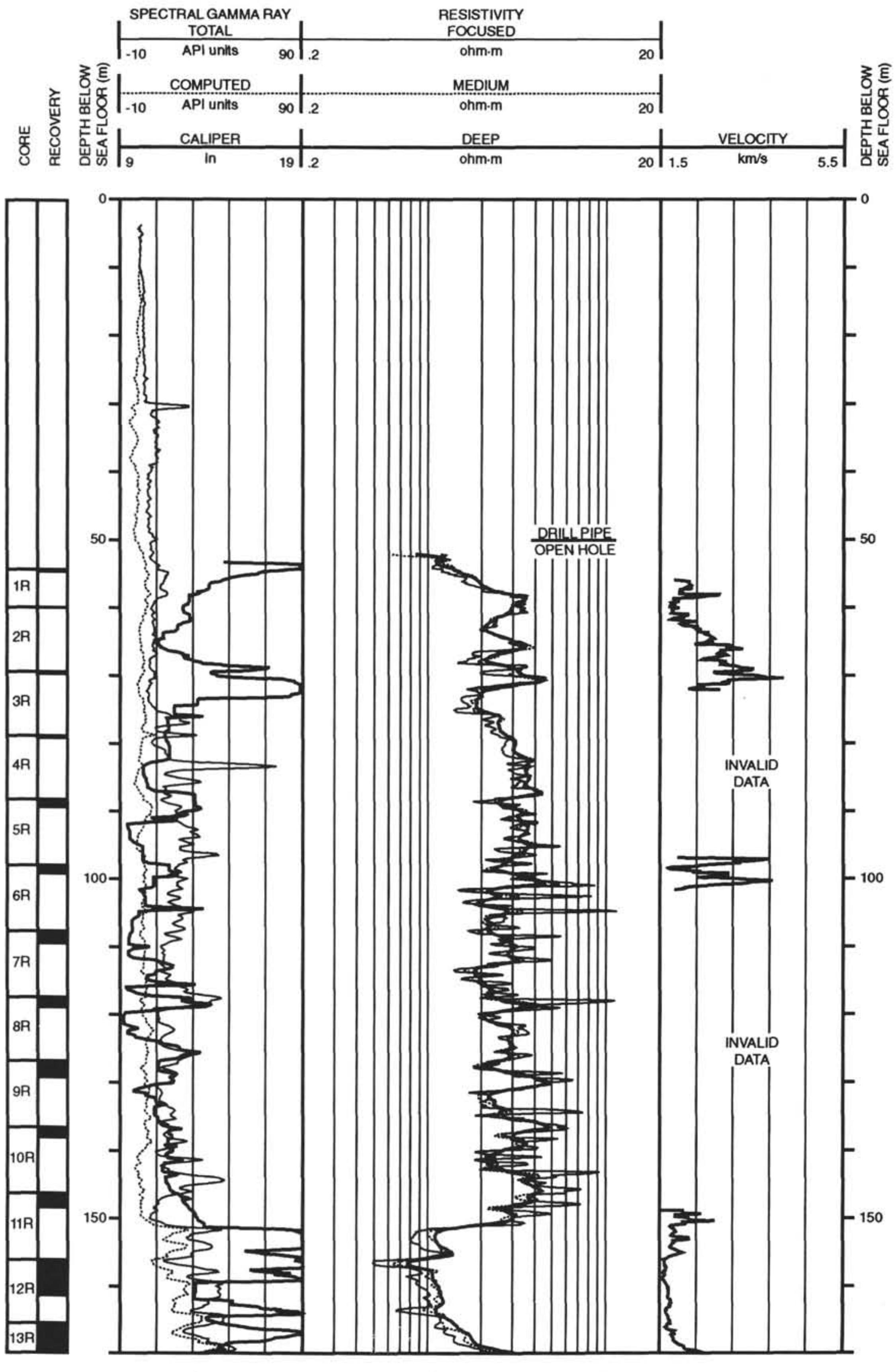

Hole 873A: Resistivity-Velocity-Natural Gamma Ray Log Summary (continued)

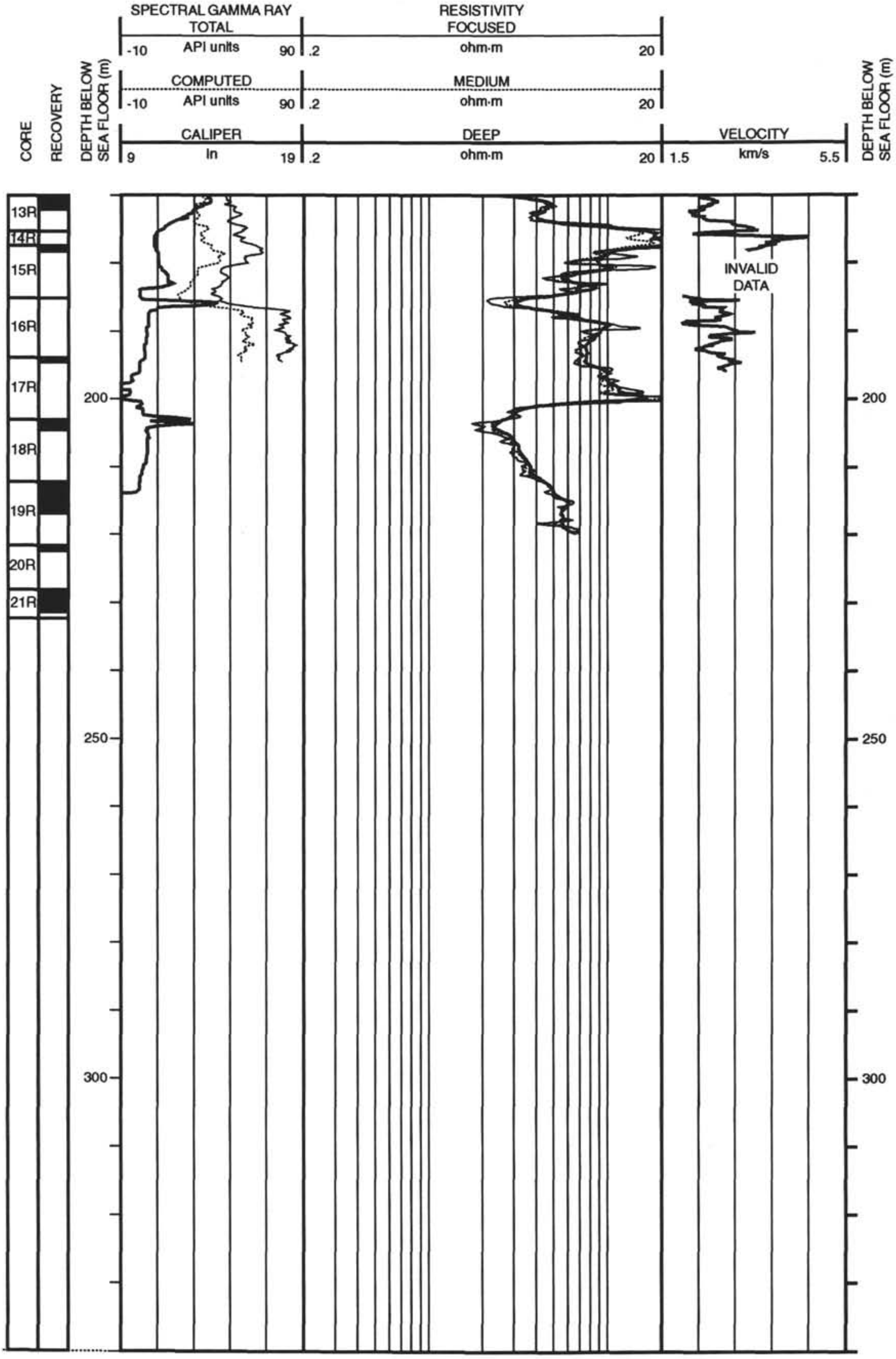

Hole 873A: Density-Porosity-Natural Gamma Ray Log Summary

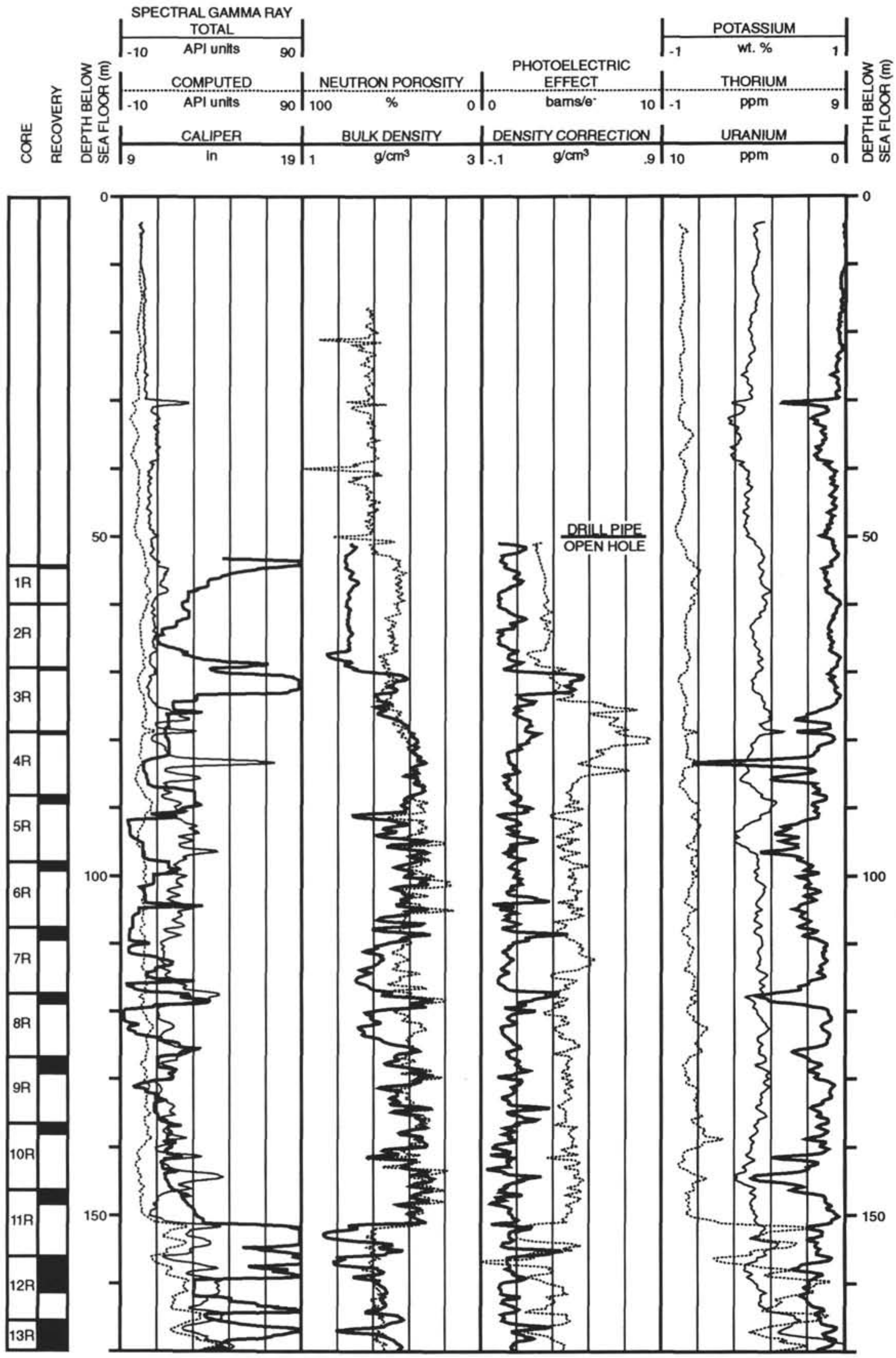

Hole 873A: Density-Porosity-Natural Gamma Ray Log Summary (continued)

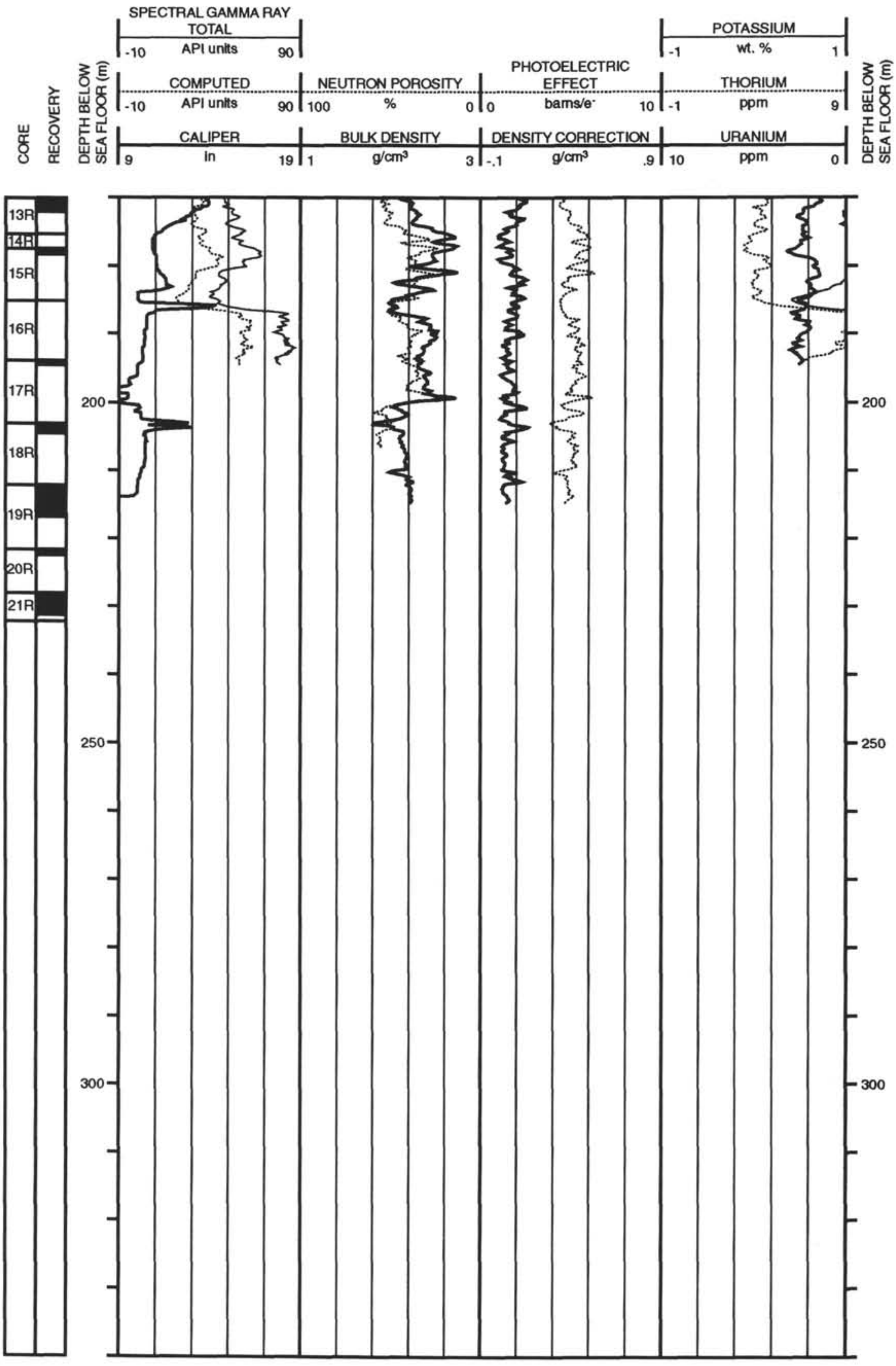

Hole 873A: Geochemical Log Summary

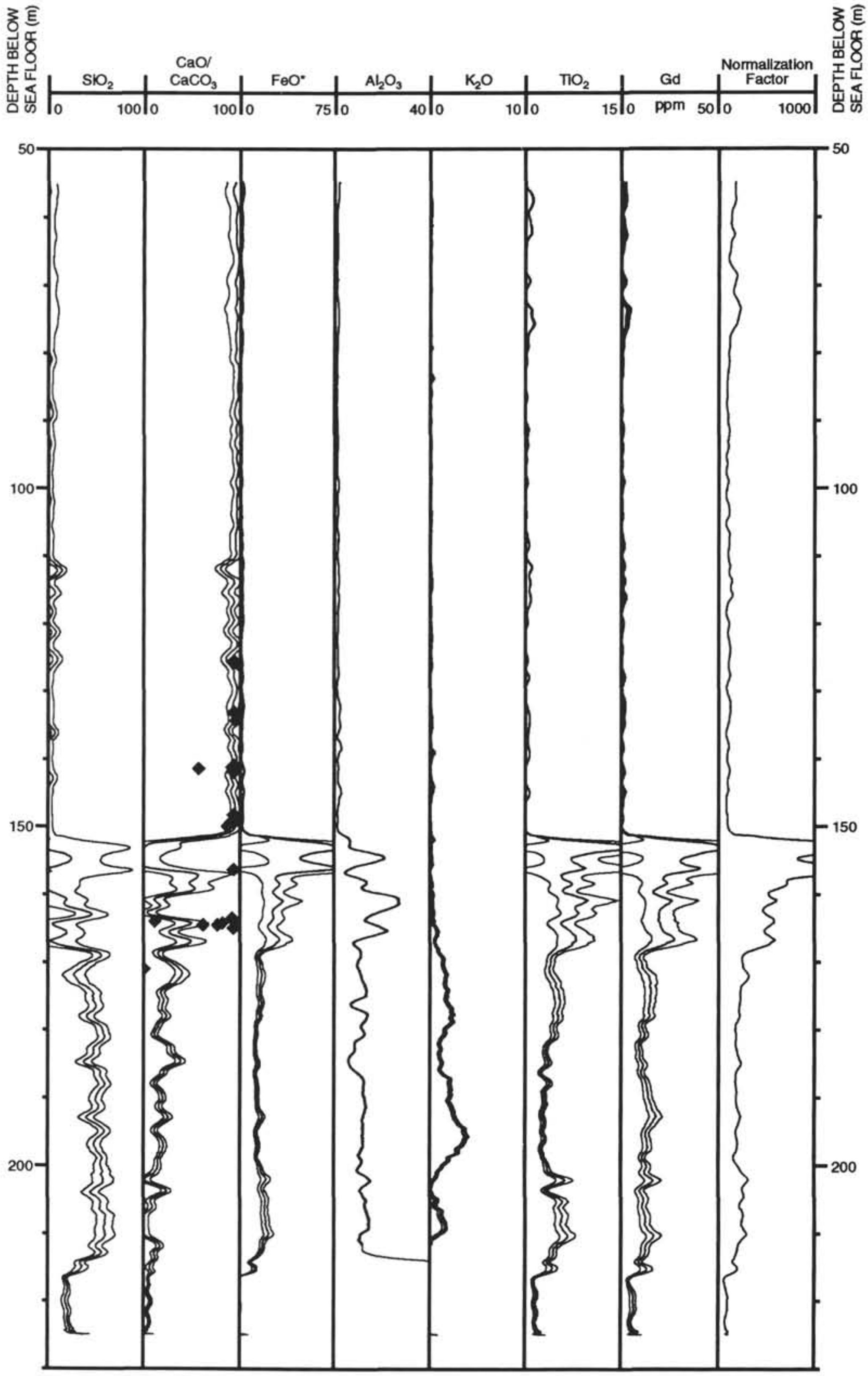

Hole 873A: Geochemical Log Summary